

# **Wind Turbine Condition Monitoring Based on SCADA Data**

Yue Wang

A thesis submitted for the degree of Doctor of Philosophy

Department of Electronic and Electrical Engineering

University of Strathclyde

2014

This thesis is the result of the author's original research. It has been composed by the author and has not been previously submitted for examination which has led to the award of a degree.

The copyright of this thesis belongs to the author under the terms of the United Kingdom Copyright Acts as qualified by the University of Strathclyde Regulation 3.50. Due acknowledgement must always be made of the use of any material contained in, or derived from, this thesis.

Signed:

Date:

# Abstract

Wind energy has an increasingly essential role in meeting electrical power demand and achieving environmental sustainability. The excellent offshore wind resource and the need to reduce carbon emissions from electricity generation are driving policy to increase offshore wind generation capacity in UK waters. Access and maintenance offshore can be difficult and will be more costly than onshore and availability correspondingly lower and as a result there is a growing interest in wind turbine condition monitoring allowing condition based, rather than responsive or scheduled, maintenance.

Existing wind turbine condition monitoring methods, such as vibration analysis and oil debris detection, require expensive sensors. The additional costs can be substantial considering the number of turbines typically deployed in offshore wind farms and in addition, costly expertise is generally required to interpret the results. In contrast, the potential to extend the Supervisory Control and Data Acquisition (SCADA) data based analysis approach is considerable and could add real value to the condition monitoring with little or no cost to the wind farm operator.

This thesis focuses on wind turbine condition monitoring that utilises exclusively data from SCADA systems. The aim is to detect incipient wind turbine operational faults or failures before they evolve to catastrophic failures, so that preventative maintenance or corrective action can be scheduled in time, hence reducing downtime and potentially preventing wider damage. Useful component condition indicators are derived by comparing incoming operational SCADA data with the results for relevant variables, like component temperature that reflect component condition, derived from relevant models trained on SCADA data from a healthy wind turbine. Incipient failures are identified through anomalous behaviour in the variables of interest manifest in the SCADA data. This approach is first applied to individual wind turbines, but then extended to include other wind turbines operating under similar conditions to derive

component condition indicators through inter-machine comparison. This is demonstrated to facilitate significant savings in computational effort and model complexity compared to the repetitive development of individual turbine models. In addition, a real time wind turbine power curve is implemented based on SCADA data, and compared with a reference power curve to identify anomalous behaviour, through minor changes in the power curve, in a timely manner.

# Acknowledgements

First of all I would like to express my greatest gratitude to Prof. David Infield for his thoughtful academic guidance and positive encouragement throughout the duration of my research. I also want to take this opportunity to give my special thanks to the researchers and academics in the department for their valuable and helpful suggestions to my work. Particular thanks are due to Dr. Julian Feuchtwang.

Thanks are also due to ETI FLOW project team (Moog-Insensys, EDF, E.ON, Romax and Seebyte) for providing me not only financial support, but also the experimental data to conduct this research and valuable feedbacks to improve the analyses. In addition, I would like to thank Scottish Power Renewables and also SgurrEnergy for making data available.

Finally I want to dedicate this work to my mum, dad and all my families for their unconditional love and support throughout this period of my life.

# Contents

<b>List of figures .....</b>	<b>V</b>
<b>List of tables.....</b>	<b>VIII</b>
<b>List of abbreviations .....</b>	<b>IX</b>
<b>List of variables .....</b>	<b>X</b>
<b>List of turbine types .....</b>	<b>XIII</b>
<b>1. Introduction.....</b>	<b>1</b>
1.1. Renewable energy drivers .....	2
1.2. The role of wind energy .....	2
1.3. Motivation for the research .....	3
1.3.1. Offshore wind deployment in the UK.....	4
1.3.2. Justification for wind turbine condition monitoring .....	5
1.3.3. Why SCADA data?.....	7
1.4. Wind turbine and its reliability.....	9
1.4.1. Wind turbine basics .....	9
1.4.2. Turbine components failure rates and downtime.....	11
1.5. Thesis overview.....	13
1.6. Research publications.....	14
1.7. Chapter references .....	16
<b>2. Wind turbine condition monitoring techniques.....</b>	<b>19</b>
2.1. System physics based techniques .....	19
2.1.1. Vibration signal analysis.....	20
2.1.2. Oil debris analysis.....	21
2.1.3. Blade strain measurement.....	23
2.1.4. Acoustic emission .....	23
2.2. SCADA data based modelling .....	24
2.2.1. Artificial neural networks .....	25

2.2.2.	Support vector machine .....	29
2.2.3.	Bayesian networks .....	33
2.2.4.	Nonlinear state estimation technique .....	36
2.2.5.	Operational power curve based techniques.....	38
2.3.	Chapter summary .....	41
2.4.	Chapter references .....	42
<b>3.</b>	<b>Power curve based wind turbine condition monitoring.....</b>	<b>49</b>
3.1.	Data pre-processing and power curve presentation.....	50
3.1.1.	Nacelle anemometer wind speed correction .....	51
3.1.2.	Air density correction .....	53
3.1.3.	Sources of uncertainty .....	54
3.2.	Reference power curve construction using Copulas based model .....	57
3.2.1.	Expressing Dependency through Copula Statistics .....	58
3.2.1.1.	The Frank Copula .....	58
3.2.1.2.	The Gaussian Mixture Copula Model (GMCM) .....	60
3.2.2.	Power curve density modelling with Copulas .....	61
3.2.2.1.	Model order selection .....	62
3.2.2.2.	Fitness analysis .....	64
3.2.3.	Power curve outlier rejection example using the GMCM .....	66
3.3.	Bin-by-bin based online power curve condition monitoring .....	69
3.3.1.	Rolling power curve realization.....	69
3.3.2.	Anomaly detection: the Welch’s hypothesis test.....	70
3.4.	General power curve fault logic .....	71
3.5.	Yaw misalignment case study .....	72
3.6.	Application of the proposed method to pitching performance condition monitoring .....	76
3.7.	Chapter summary .....	79
3.8.	Chapter references .....	81
<b>4.</b>	<b>NSET model applications to fault detection of subassemblies for individual turbine.....</b>	<b>84</b>
4.1.	Anomaly detection based on NSET model: Methodologies .....	84

4.1.1.	NSET algorithm.....	85
4.1.2.	State memory matrix construction.....	87
4.1.3.	Fault detection algorithm.....	89
4.1.4.	Discussion of the modified NSET algorithm.....	92
4.2.	Background information of wind farm SCADA data for NSET applications .....	93
4.3.	NSET application to wind turbine gearbox case study .....	95
4.3.1.	Memory matrix size decision.....	99
4.3.2.	Model validation.....	99
4.3.3.	Model testing and anomaly detection .....	101
4.3.4.	Comparison with a Neural Network model .....	104
4.3.5.	Justification for use of the augmented state memory matrix .....	107
4.3.6.	Comparison with the modified NSET model.....	110
4.3.7.	Impact of memory matrix normalisation on model performance .....	114
4.3.8.	Impact of weighted variables in the distance norm on model performance .....	119
4.3.9.	Discussions of the model performance by removing the parameter of Gearbox bearing temperature .....	119
4.3.10.	Discussions of the effect of time-lagged variable on model performance.....	124
4.3.11.	Discussions of other model performance metrics .....	125
4.4.	NSET application to wind turbine generator case study .....	128
4.5.	Chapter summary .....	133
4.6.	Chapter references.....	134

**5. Spatial application of NSET model for wind turbine gearbox fault detection ..... 135**

5.1.	Data usage for model training, validation and testing.....	136
5.2.	Model implementation within a sub-group .....	141
5.2.1.	Discussions of the necessity of nacelle temperature.....	145
5.2.2.	Impact of gearbox bearing temperature on model performance .....	147
5.2.3.	Impact of normalised memory matrix and weighted parameters on model performance .....	149
5.2.4.	Discussion of the modified model in spatial NSET application .....	149
5.3.	Effect of sub-group size on model performance .....	154

5.4. Discussion of the model’s capability of generalisation.....	157
5.5. Limitations of the spatial application of the NSET model.....	158
5.6. Comparison between the spatial and individual turbine NSET model .....	159
5.7. Chapter summary .....	160
<b>6. Conclusions and future works .....</b>	<b>161</b>
6.1. Conclusions .....	161
6.2. Future works.....	162
<b>Appendix I.....</b>	<b>165</b>
<b>Appendix II.....</b>	<b>170</b>
<b>Appendix III .....</b>	<b>173</b>

# List of figures

Figure 1-1: Global wind power cumulative capacity [1] .....	1
Figure 1-2: Growth in electricity generation (TWh) from renewable sources in the UK [9] .....	3
Figure 1-3: Offshore wind activity in the UK [12] .....	4
Figure 1-4: Evolution of component condition with deterioration [16].....	6
Figure 1-5: Simplified schematic for a 3-blade upwind turbine with gear drive [20] .....	10
Figure 1-6: Wind turbine operating strategy [21] .....	10
Figure 1-7: Wind turbine components failure rates and the corresponding downtime per failure for two surveys of European onshore wind turbines [24].....	12
Figure 2-1: Typical accelerometer layout in the drive train of wind turbine with a 3-stage gearbox [33] .....	21
Figure 2-2: Evolution of gearbox damage in terms of wear particle size [38] .....	22
Figure 2-3: Feed-forward neural network model architecture example [43].....	26
Figure 2-4: Inner structure of a general neuron with $R$ inputs [44] .....	26
Figure 2-5: A simple example of 2-dimensional linearly separable data separated by a line [63] .....	29
Figure 2-6: Data separation by transferring into feature space with higher dimension [63]31	
Figure 2-7: A discrete Bayesian network example [75].....	34
Figure 2-8: Schematic diagram for an auto-associative model.....	38
Figure 3-1: Typical manufacturer’s power curve.....	49
Figure 3-2: Relationship between Met mast and Nacelle anemometer wind speed for Turbine 1 .....	52
Figure 3-3: Comparison of power curves based on Met mast and Nacelle anemometer wind speed measurements for Turbine 1.....	52
Figure 3-4: Scatter plot of power curve measurements for Turbine 2 .....	55
Figure 3-5: Power curve with error bars showing data uncertainty for Turbine 2.....	56
Figure 3-6: Power curve with error bars showing data dispersion for Turbine 2 .....	56
Figure 3-7: The impact of $\delta$ value on variable dependency .....	60
Figure 3-8: SOM neighbour weight distances for Turbine 2 .....	63
Figure 3-9: Fitness comparison of three presented models for Turbine 2 .....	66
Figure 3-10: GMCM fitting to the power curve example from Turbine 1.....	67
Figure 3-11: Data exclusion for Turbine 1 using GMCM based density contour .....	68

Figure 3-12: Power curve for Turbine 1 after cleaning.....	68
Figure 3-13: Filtration of raw reference power curve data for Turbine 3.....	73
Figure 3-14: Constructed reference power curve vs. manufacturer’s curve for Turbine 373	
Figure 3-15: Absolute yaw error along with aggregate number of anomalous bins detected for Turbine 3 .....	75
Figure 3-16: Time series of wind direction and nacelle position for Turbine 3 .....	75
Figure 3-17: Pitch angle – wind speed reference with error bars for Turbine 3 .....	77
Figure 3-18: Power curve scatter for testing data from Turbine 3.....	77
Figure 3-19: Scatter of pitch angle vs. wind speed for testing data from Turbine 3.....	78
Figure 3-20: Pitching performance detection results for testing data with derated operation for Turbine 3 .....	79
Figure 4-1: Data selection flow chart for memory matrix construction.....	88
Figure 4-2: Pole and zero illustration of the selected low pass filtered in Z-plane.....	89
Figure 4-3: Magnitude of frequency response for the low pass filter within one period..	91
Figure 4-4: Wind farm layout .....	94
Figure 4-5: Memory matrix size decision .....	99
Figure 4-6: Validation results of T1 for standard NSET.....	100
Figure 4-7: Testing results and anomaly detection of T17 for standard NSET .....	101
Figure 4-8: Testing results and anomaly detection of T16 for standard NSET .....	103
Figure 4-9: Validation results of T1 for NN model .....	105
Figure 4-10: Testing results and anomaly detection of T17 for NN model .....	106
Figure 4-11: Testing results and anomaly detection of T16 for NN model .....	106
Figure 4-12: Testing results and anomaly detection of T17 for standard NSET with non- augmented state memory matrix .....	109
Figure 4-13: Testing results and anomaly detection of T16 for standard NSET with non- augmented state memory matrix .....	110
Figure 4-14: Validation results of T1 for modified NSET.....	111
Figure 4-15: Testing results and anomaly detection of T17 for modified NSET .....	113
Figure 4-16: Testing results and anomaly detection of T16 for modified NSET .....	113
Figure 4-17: Validation results of T1 for normalised NSET .....	114
Figure 4-18: Testing results and anomaly detection of T17 for normalised NSET .....	116
Figure 4-19: Testing results and anomaly detection of T16 for normalised NSET .....	116
Figure 4-20: Testing results of healthy T16 in testing case III for standard NSET .....	117
Figure 4-21: Testing results of healthy T16 in testing case III for normalised NSET....	117
Figure 4-22: Gearbox temperature vs. power output for T16 in testing case I.....	120

Figure 4-23: Gearbox temperature vs. power output for T17 in testing case II.....	121
Figure 4-24: Validation results of T1 for normalised NSET with reduced parameter and weighted variables.....	122
Figure 4-25: Testing results and anomaly detection of T17 for normalised NSET with reduced parameter and weighted variables .....	122
Figure 4-26: Testing results and anomaly detection of T16 for normalised NSET with reduced parameter and weighted variables .....	123
Figure 4-27: Testing results of healthy T16 in testing case III for normalised NSET with reduced parameter and weighted variables .....	123
Figure 4-28: Correlation coefficients between cooling oil temperature and turbine power output with different time delays .....	124
Figure 4-29: Illustration of auto-sensitivity performance using the validation data.....	127
Figure 5-1: Proportion of invalid data entries in different data usage for each turbine ..	137
Figure 5-2: New wind farm layout with disqualified turbines removed.....	138
Figure 5-3: Memory matrix size decision .....	142
Figure 5-4: Validation results of T16 for standard spatial NSET .....	143
Figure 5-5: Testing results and anomaly detection of T17 for standard spatial NSET...	143
Figure 5-6: Testing results and anomaly detection of T16 for standard spatial NSET...	144
Figure 5-7: Testing results of healthy T14 for false alarm testing with standard spatial NSET .....	144
Figure 5-8: Time series of the validation data for all of the sub-group candidates .....	145
Figure 5-9: Validation results of T16 for 2-inputs standard spatial NSET.....	146
Figure 5-10: Validation results of T16 for standard spatial NSET with bearing temperature.....	148
Figure 5-11: Testing results and anomaly detection of T17 for standard spatial NSET.	148
Figure 5-12: Validation results of T16 for modified spatial NSET .....	150
Figure 5-13: Testing results and anomaly detection of T17 for modified spatial NSET	151
Figure 5-14: Testing results and anomaly detection of T16 for modified spatial NSET	151
Figure 5-15: Testing results of healthy T14 for false alarm testing with modified spatial NSET .....	152
Figure 5-16: Spatial relationship for the available turbines in the wind farm with regards to turbine T16.....	155
Figure 5-17: Testing results of the modified spatial NSET for healthy T14 based on the anomalous T17 in testing case I.....	159

# List of tables

Table 1-1: The Crown Estate’s offshore wind leasing rounds [13] .....	5
Table 2-1: Three commonly used transfer functions in the neurons of NN models [47] .	27
Table 3-1: Goodness of fit for three models using BIC values.....	65
Table 4-1: List of events for analysis .....	94
Table 4-2: List of available SCADA data in 10-min format and intuitive input selection for the gearbox and generator model.....	95
Table 4-3: Pearson’s correlation coefficients between gearbox model input and output parameters .....	96
Table 4-4: Filtration criteria of the selected variables for gearbox case study and the corresponding results.....	98
Table 4-5: Model effectiveness comparison to justify the additional null and maximal vectors .....	108
Table 4-6: Model effectiveness comparison between standard model and modified model.....	112
Table 4-7: Further model effectiveness comparison under different situations for gearbox case study .....	118
Table 4-8: Pearson’s correlation coefficients between generator model input and output parameters .....	128
Table 4-9: Filtration criteria of the selected variables for generator case study and the corresponding results.....	131
Table 4-10: Model effectiveness comparison under different situations for generator case study .....	132
Table 5-1: Wind farm based data filtration (for 17 qualified turbines) and the corresponding results.....	140
Table 5-2: Effectiveness comparison for spatial models with different input combinations under standard and modified situations .....	153
Table 5-3: Correlation coefficients of wind speed between T16 and the available turbines in the wind farm .....	154
Table 5-4: Effectiveness comparison for the 3-inputs modified spatial model with different sub-group sizes .....	156
Table 5-5: Effectiveness comparison for spatial models constructed based on different turbines with sub-group size of 17 .....	157

# List of abbreviations

ANN/NN	Artificial Neural Network/ Neural Network
BIC	Bayesian Information Criterion
BN	Bayesian Network
CDF	Cumulative Distribution Function
CMS	Condition Monitoring Systems
DBN	Dynamic Bayesian Network
DFIG	Double-fed Induction Generator
DR	Detection Ratio
GMCM	Gaussian Mixture Copula Model
GMM	Gaussian Mixture Model
IIR	Infinite Impulse Response
kNN	k-Nearest Neighbour
NSET	Nonlinear State Estimation Technique
OEMs	Original Equipment Manufacturers
PDF	Probability Density Function
RMS	Root Mean Square
ROCs	Renewable Obligation Certificates
RR	Residual Ratio
RVs	Random Variables
SCADA	Supervisory Control and Data Acquisition
SOM	Self-organising map
SVM	Support Vector Machine

# List of variables

$a$	Output of neuron transfer function for NN model (Chapter 2) Axial flow induction factor (Chapter 3)
$B$	Barometric pressure
$b$	bias of neuron for NN model (Chapter 2, Section 2.2.1) bias of hyperplane for SVM (Chapter 2, Section 2.2.2)
$C$	Root cause for Bayesian networks (Chapter 2) Copula function (Chapter 3) Filter parameter (Chapter 4)
$C_p$	Power coefficient
$D$	State memory matrix
$\hat{D}$	Modified state memory matrix
$E$	Test results/observed evidence for Bayesian networks
$F$	Joint cumulative distribution function
$F_i, u_i$	$i^{\text{th}}$ marginal CDF
$f$	Neuron transfer function for NN model (Chapter 2) Joint probability density function (Chapter 3)
$f_i$	$i^{\text{th}}$ marginal PDF
$K_j$	Number of points in the $j^{\text{th}}$ wind speed bin
$k_j$	Weighting vector
$M$	Modality number for GMM (Chapter 3) Number of state vectors in the training data (Chapter 4)
$m$	Number of state vectors in memory matrix for NSET model
$N$	Number of samples
$N_{ref}$	Sample size of reference data
$N_{test}$	Sample size of testing data
$n$	Output of neuron transfer function for NN model (Chapter 2) Data dimension (Chapter 3)

	Number of variables for NSET model (Chapter 4)
$P$	Wind turbine power output
$p$	Input vector for NN model
$p$	Number of parameters
$R$	Number of elements in neuron input vector for NN model (Chapter 2)
	Radius of wind turbine rotor (Chapter 3)
$S_j$	Power output uncertainty in category A for $j^{\text{th}}$ wind speed bin
$S_{Ai}$	Auto-sensitivity for variable $i$
$S_{Ci}$	Cross-sensitivity for variable $i$
$S_{ref}$	Sample standard deviation of reference data
$S_{test}$	Sample standard deviation of testing data
$T$	Ambient temperature
$t$	t statistics for Welch's hypothesis test
$V_C$	Air density corrected wind speed
$V_M$	Turbine anemometer based wind speed measurement
$v$	Wind speed experienced by wind turbine rotor
$W$	Weight vector
$\widehat{W}$	Modified weight vector
$X_k$	Row vector recording sensor readings
$X_{obs}$	Observation vector
$\widehat{X}_{obs}$	Modified observation vector
$X_{est}$	Estimation vector
$\overline{X}_{ref}$	Averaged value of reference data/validation data
$\overline{X}_{test}$	Averaged value of testing data
$x_i$	Input vector for SVM
$x_{ki}$	The $k^{\text{th}}$ original measurement for variable $i$
$x_{ki}^{drift}$	The $k^{\text{th}}$ modified measurement for variable $i$
$x_{kj}$	The $k^{\text{th}}$ original measurement for variable $j$
$x_{kj}^{drift}$	The $k^{\text{th}}$ modified measurement for variable $j$

$\hat{x}_{ki}$	Estimation of the $k^{\text{th}}$ original measurement for variable $i$
$\hat{x}_{ki}^{drift}$	Estimation of the $k^{\text{th}}$ modified measurement for variable $i$
$y_j$	Classified output for SVM
$z$	Z domain variable
$\alpha$	Significance level
$\alpha_k$	Weight for the $k^{\text{th}}$ component of GMM
$\delta$	Parameter for Frank Copula model (Chapter 3)
	Vicinity criterion parameter: a small positive value close to zero (Chapter 4)
$\varepsilon$	Residual vector
$\eta$	Parameter for Frank Copula model
$\theta$	Aggregated parameter set for all components of GMM
$\theta_k$	Parameter set for the $k^{\text{th}}$ component of GMM including $\mu_k$ and $\Sigma_k$
$\mu_k$	Mean vector for the $k^{\text{th}}$ component of GMM
$\nu$	Number of degrees of freedom
$\xi, \xi^+, \xi^-$	Slack variables for SVM
$\rho$	Ambient air density
$\Sigma_k$	Covariance matrix for the $k^{\text{th}}$ component of GMM
$\sigma_j$	Standard deviation of power measurement in the $j^{\text{th}}$ wind speed bin
$\Phi_i^{-1}$	Inverse marginal CDF for the $i^{\text{th}}$ dimension of GMM
$\varphi_i$	Marginal PDF for the $i^{\text{th}}$ dimension of GMM
$\Omega$	Signal frequency

# List of turbine types

		Operating strategy	Rated wind speed (m/s)	Rated power (kW)
Chapter 3	Turbine 1	Pitch regulated variable speed	13-14	2300
	Turbine 2	Pitch regulated variable speed	13-14	2000
	Turbine 3	Pitch regulated variable speed	14-15	2500
Chapters 4 & 5	26 turbines	Stall regulated fixed speed	16-17	600

# 1. Introduction

Wind energy has developed rapidly as a significant green power source in recent decades, facilitated by innovative and cost effective technology. As is illustrated by Figure 1-1, global wind power installed capacity has been increasing over the last few decades and by the end of 2012 the cumulative capacity reached 282GW, a 18.7% increase on the installed capacity at the end of 2011 [1]. At time same time the turbine size has exhibited a steady increase with commercial wind turbines having power ratings of up to 7.5MW for offshore applications [2]. Some innovative offshore turbine models under development are expected to generate more than 15MW in the coming years [3].

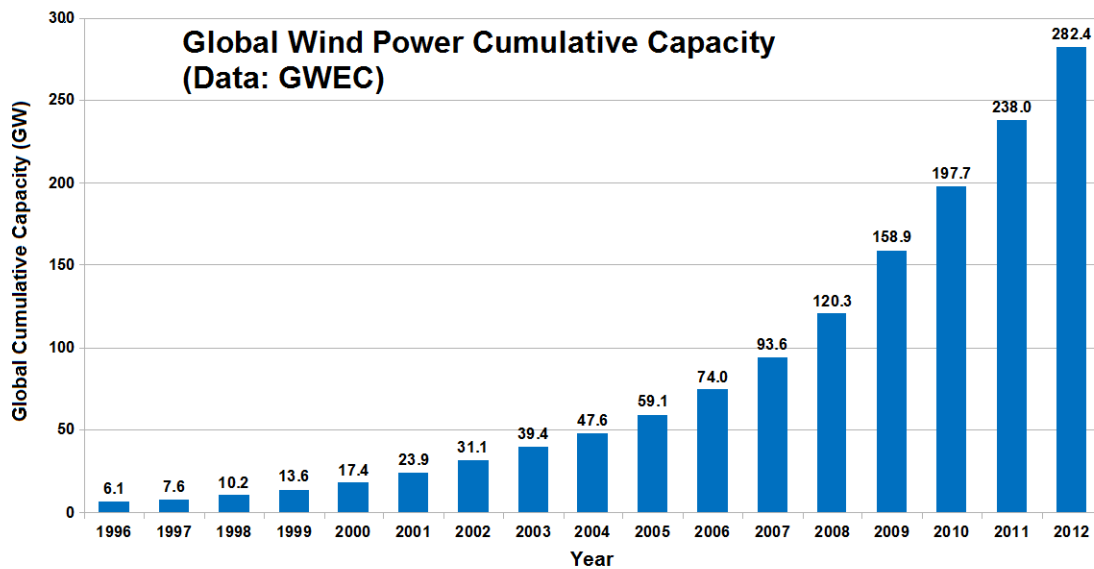


Figure 1-1: Global wind power cumulative capacity [1]

The motivation for renewable energy development will be briefly outlined in this chapter, followed by the discussions of the important role played by wind energy in terms of government policies and industrial deployment in the UK. Particular attention will then be paid to research justification. The basics for wind turbine operation will then be briefly introduced, followed by a presentation of failure rates for turbine sub-assemblies and associated downtime as these motivate condition monitoring, which is

the subject of this thesis. The thesis structure will then be outlined in the following section and my research related publications will be listed at the end of this chapter.

## **1.1. Renewable energy drivers**

The major scale-up of the renewable energy market in recent years is fuelled by the depletion of fossil fuel reserves as well as the global agreement to reduce the carbon emission in order to tackle climate change. The main target set by the Copenhagen Accord, [4] of 2009 was to limit the global temperature increase to below 2 °C. Following this, the EU enacted the climate and energy package policy, which is also known as the '20-20-20' directive, [5], aiming at a 20% reduction in EU greenhouse gas emissions from 1990 levels, a 20% share of EU energy consumption generated from renewable resources and a 20% improvement in the EU's energy efficiency by 2020. As part of the EU plan, the UK government has also made clear its commitment to increasing the deployment of renewable energy by endorsing the Renewable Energy Directive and the UK's objective, [6], agreed in 2009, to deliver 15% of energy consumption from renewable sources by 2020.

Another main driver for the deployment of renewable energy is energy security which refers to the uninterrupted availability of energy sources at an affordable price [7]. The growing penetration of renewable power will help to reduce the dependence on the conventional energy and protect domestic consumers from fossil fuel price fluctuations, contributing to a more stable and reliable national energy supply market.

## **1.2. The role of wind energy**

In order to provide national energy security and meet the agreed decarbonisation targets, Ofgem (the UK regulator) introduced the Renewables Obligation, [8], as a main support mechanism to promote the growth of large-scale renewable deployment. This obligation came into effect in 2002. It places an obligation on eligible UK electricity suppliers via Renewable Obligation Certificates (ROCs) to generate a rising share of electricity from renewable resources. According to reference [8], wind farms in the UK, including both onshore and offshore, were issued with more ROCs than generating stations based on

other renewable technologies; wind based generation also contributed to a greater proportion of new generating capacity that is accredited by Ofgem than other technologies.

Department of Energy and Climate Change (DECC) statistics for the UK electricity generation growth from renewable resources is illustrated in Figure 1-2, which clearly shows the rapid expansion of wind energy over the past decade and also confirms its increasingly important role in contributing to the total renewable power generation and realising the national energy security goal. It can also be observed from this figure that the offshore contribution has made an impact during recent years. Details of the UK offshore wind energy deployment plan will be presented in the following section.

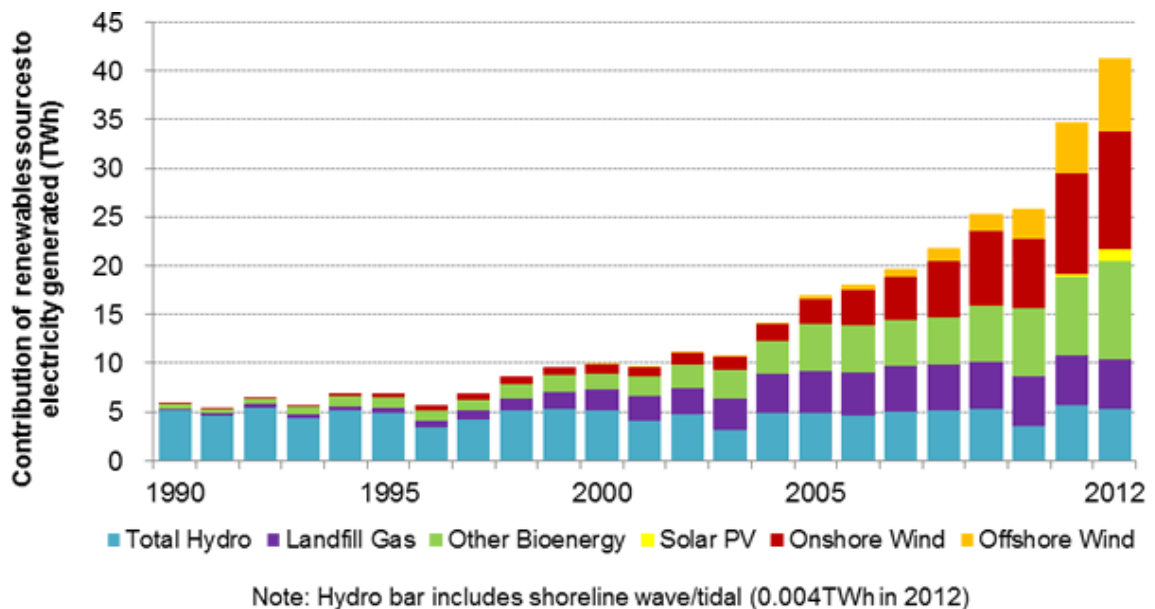


Figure 1-2: Growth in electricity generation (TWh) from renewable sources in the UK [9]

### 1.3. Motivation for the research

UK offshore deployment will be briefly introduced in the next section and this then leads on to discussion of the motivation for wind turbine condition monitoring and in particular the utilisation of the Supervisory Control and Data Acquisition (SCADA) data to determine the state of health of wind turbines.

### 1.3.1. Offshore wind deployment in the UK

With an excellent offshore wind resource, the UK has now become the largest offshore wind energy market in the world with a total installed capacity of 4.6GW across 24 wind farms installed by May 2013 [10]. Offshore deployment in the UK has been structured into a series of rounds, 1 to 3. [11]. Figure 1-3 presents the locations of planned offshore wind activities with the various rounds coloured differently and the associated development plan is summarised in Table 1-1.



Figure 1-3: Offshore wind activity in the UK [12]

Installations involved in Round 1 are now completed with site locations typically close to shore. Round 2 two sites are generally larger and further from shore and some are still

under construction [11]. Round 3 sites are far more ambitious and challenging than Rounds 1 and 2 with considerably larger deployment zones, most of which are in deeper water and further offshore [11], as is shown in Figure 1-3. On completion of the construction of all three rounds, together with their extensions, the UK offshore capacity will total 49GW as summarised in Table 1-1.

Round	Year announced	Original capacity (GW) (from public announcements)
Round 1	2000	1.5
Round 2	2003	7.2
Round 3	2008	32.2
Scottish territorial waters	2008	6.4
Round 1 and Round 2 extensions	2009	1.7
<b>Total</b>		<b>49</b>

Table 1-1: The Crown Estate’s offshore wind leasing rounds [13]

### 1.3.2. Justification for wind turbine condition monitoring

The apparent benefit of moving offshore is the better wind profiles above sea. A larger capacity factor is expected offshore due to higher wind speeds. Offshore wind turbines tend to be larger than those used onshore due to the way foundation and installation costs scale. Also, the absence of obstacles above sea water leads to less turbulence offshore than at the onshore sites. In addition, the noise and visual intrusion from offshore turbines are much less significant and this leads to greater public acceptance compared to onshore turbines.

However, there is a price to pay and the largest downside of offshore wind is the remarkably high costs for installing and accessing the offshore turbines during turbine installation and maintenance. The total costs involved in hiring the maintenance vessel and associated personnel will be considerable, and a crane vessel is generally required for installation in the worst case scenario where component replacement is necessary.

The analysis in reference [14] indicates a trend of increasing failure rate as turbine capacity rises, which would also be a potential concern for the offshore turbines since high-rating machines are preferable for the reason mentioned above.

A number of aspects, including turbine reliability, maintenance strategy and accessibility of the site, contribute to the turbine availability, which is defined as the percentage of time that the system is operating properly when there is available wind [15]. Apart from the environmental wind condition, the generated revenue is directly related to turbine availability. The availability for onshore turbines can reach as high as 98% since the service organisation and the regular maintenance actions (around 4 times in a year) can be performed promptly due to the ease of access [15], as can unplanned repairs following faults or component failures. In contrast, offshore availability is much lower since the regular maintenance actions are less affordable due to the high costs involved and there can be substantial delays to unplanned repairs due to lack of access resulting from adverse weather conditions. Moreover, severe sea states can hamper repairs due to the higher average winds and lead to more revenue lost than for onshore turbines during the downtime when faulty turbines are inaccessible for repair.

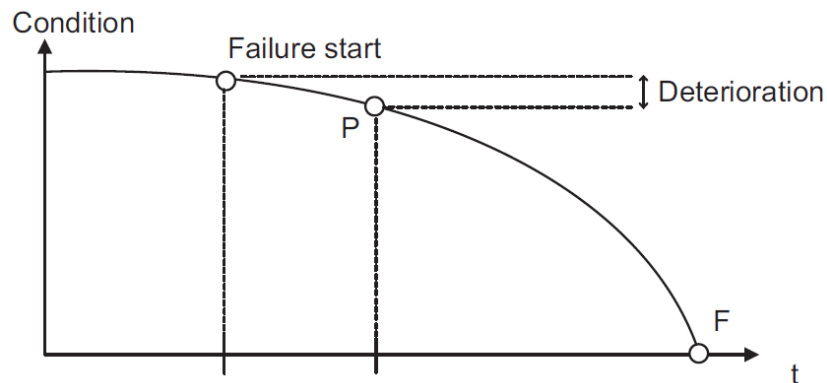


Figure 1-4: Evolution of component condition with deterioration [16]

The increasing trend for offshore deployment plus the poor offshore availability and accessibility suggest the need for an effective and reliable condition based maintenance scheme for wind turbines rather than the traditional combination of responsive repair and scheduled maintenance strategy. Reference [16] utilises a so called P–F curve, as

shown in Figure 1-4, to present the evolution of component deterioration. Point ‘P’ with a specific level of deterioration as given by the curve refers to the first time at which this deterioration can be detected, ahead of complete failure at time ‘F’. The time interval between P and F is crucial for the effective deployment of condition based maintenance, since it allows for improved maintenance scheduling. From an economic perspective, the earlier the potential anomaly can be detected, the lower will be the downtime associated with failure, and also the subsequent damage to other parts of the turbine. For example, lack of attention to a worn bearing can result in a catastrophic failure of an entire gearbox involving considerable cost and downtime.

Approaches that are able to identify faults at an early stage and thus leave sufficient time for the turbine operator to make decisions regarding maintenance scheduling before the incipient anomalies evolve into catastrophic failures, would therefore be beneficial for reducing turbine downtime and improving the availability.

This thesis presents two effective condition monitoring methods including a historical states based prediction approach for turbine key drive train components and an operational power curve based scheme to provide an overview of the turbine performance. Both approaches are supported by 10-minute SCADA data analysis.

### **1.3.3. Why SCADA data?**

Most modern wind farms are built with a Supervisory Control and Data Acquisition (SCADA) system, which logs general turbine operational and meteorological data usually in a 10-minute averaged form for each individual wind turbine and any meteorological masts within the wind farm, and then sends these measurements in real-time to a remote central computer via a communication system [17]. SCADA data has been used by the power generation industries for more than 35 years, and for wind turbine applications its role is to supervise basic turbine operation such as the turbine cut-in, cut-out and emergency stop [18]. A remarkable advantage of SCADA data is that it provides an overview of the turbine from the rotor, such as the rotational speed and pitch angle, to the drive train such as the gearbox oil and bearing temperatures and

power output from the generator. Environmental factors such as the wind speed and ambient temperature are also recorded in the SCADA system. This extensive data provides a valuable source of information on the operational health of the turbines that can be used as part of a holistic turbine condition monitoring system.

The survey of commercially available wind turbine condition monitoring systems (CMS) available in reference [19] shows a clear trend towards vibration signals based techniques. The vibration monitoring mainly covers the turbine drive train where rotating machinery is involved. Other techniques such as oil debris analyses for gearbox and fibre optic based strain measurement for blades also play important roles in monitoring key components. These techniques will be introduced in the next chapter.

An advantage of the SCADA based condition monitoring over traditional CMS is the significantly lower cost due to the lack of need of expensive sensors that are required such as the accelerometers to acquire the vibration signals and metal particle sensors for oil analysis. The SCADA data is already there so no additional costs are involved. Moreover, there is a significantly greater volume of data to be analysed with a traditional CMS than the SCADA system and also a greater requirement of data storage due to the difference in their sampling rates. According to reference [19], the sampling frequency for a vibration monitoring system exceeds 10kHz while the normal SCADA system samples at a rate of less than 0.002Hz. The SCADA data used in this thesis is the 10-minute averaged value.

However, accurate diagnosis is not always achievable using the SCADA data due to its low sampling rate. This weakness in analysis depth could be compensated by the width of information that is provided by the SCADA data across the key components [18]. With effective and reliable approaches, SCADA data should add confidence to the indicated results from the existing CMS, and add considerable value to wind turbine condition monitoring with little or no cost.

## **1.4. Wind turbine and its reliability**

Wind turbines can be categorized into 4 types according to their operating and control strategy: stall regulated fixed speed turbines; stall regulated variable speed turbines; pitching regulated fixed speed turbines; and the pitch regulated variable speed turbines. Of these the pitch regulated variable speed operation is the most popular option for commercial turbine application. The basics for wind turbine operation will be briefly introduced in this section, followed by a review of failure rates for turbine sub-assemblies and associated downtime.

### **1.4.1. Wind turbine basics**

The majority of modern wind turbines adopt the 3-blade upwind horizontal axis concept with pitch regulated variable speed operation. The rotor with an upwind configuration is preferred mainly due to noise and fatigue considerations. The key components within a gearbox driven turbine are illustrated in Figure 1-5. The kinetic energy in the incident wind is converted to mechanical energy by the rotor as the wind passes through it, and this mechanical energy is then transmitted to the turbine drive train, where the rotational speed is stepped up by the gearbox to an appropriate level to drive the generator which converts the energy into its final electrical form.

The operating strategy for a typical pitch regulated variable speed wind turbine is illustrated by the blue solid line in Figure 1-6, where the bunch of curved dash lines represent the torque – rotor speed characteristics under various constant wind speeds and the group of point lines depicts the performance for different constant turbine efficiencies, with the 100% efficiency corresponding to the maximal  $C_p$ . For the low wind speed region just above the cut-in speed, the rotor speed is constant while the torque builds up. The rotational speed is then varied to track the maximal  $C_p$  (i.e. the 100% efficiency line) for the various wind speeds below rated level, ensuring maximum energy capture from the wind. The rotational speed is maintained constant once it reaches its maximum value, and the torque keeps growing to increase the generated power until rated power is reached, beyond which blade pitching commences to prevent the torque value from further increase, limiting the turbine output to its rated power.

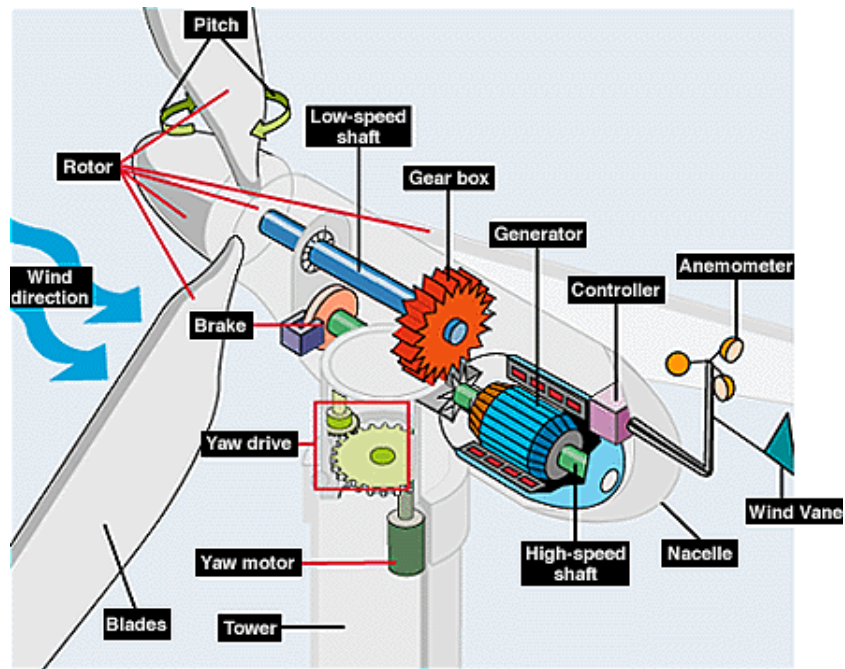


Figure 1-5: Simplified schematic for a 3-blade upwind turbine with gear drive [20]

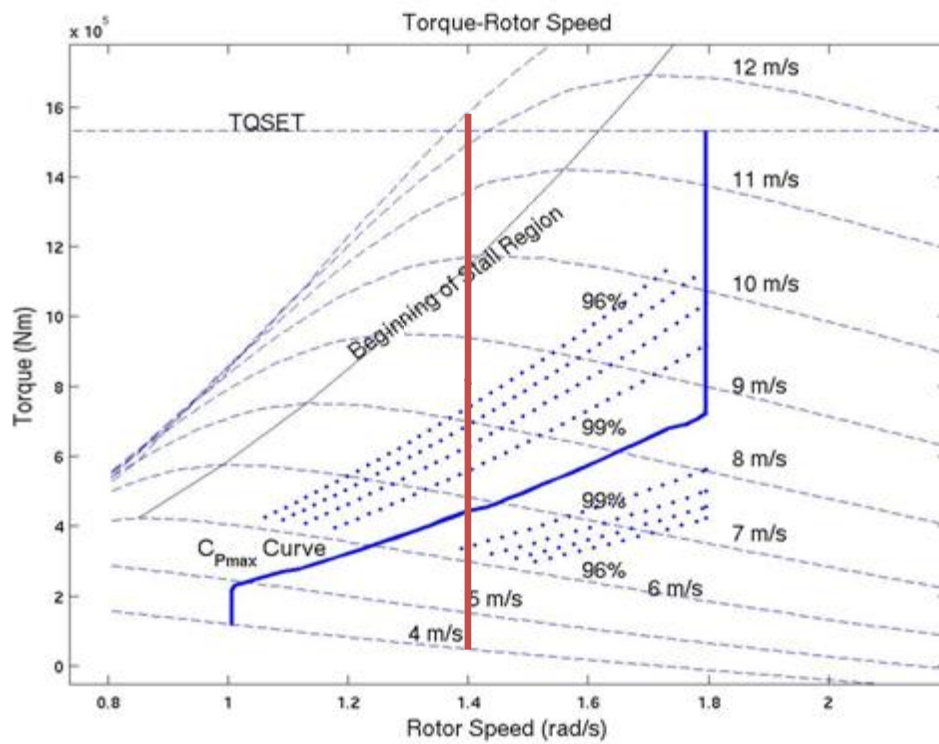


Figure 1-6: Wind turbine operating strategy [21]

The red straight line in Figure 1-6 shows the operating strategy for a stall regulated constant speed turbine. Unlike the variable speed turbines which operate optimally over a wide wind speed range, turbines with constant speed stay mainly sub-optimal along its operating line, indicating a lower overall efficiency. The power generation for stall regulated turbines at high wind speeds is limited by aerodynamic stall. As is shown in this figure, the turbine becomes insensitive to wind speed changes once it enters the stall region. During stall the blade will experience extremely high loading (mainly thrust), requiring more stiffness and of course more mass and thus higher cost, which will become a serious issue as the turbine size gets larger. For this reason, pitch regulation is more favourable than stall based power limitation.

The discussion above explains why variable speed operation provides the turbine with more flexibility under different wind conditions than the fixed speed operation and allows maximal turbine power generation with minimised loading [22]. The double-fed induction generator (DFIG) has become a popular choice to realise the variable speed operation since the late 1990s. The variable slip in DFIG allows the variations in rotational speed while the generated power is maintained at synchronous frequency by feeding the generator rotor winding an AC signal with frequency equal to the difference between the synchronous and rotational frequency. This extra power loop is achieved using power electronics and accounts for up to 30% of the rated power of the turbine, [23], giving a 30% speed range for the turbine.

Synchronous generators followed by fully-rated power converters offer another variable speed solution. By completely decoupling the generators from the grid, the fully rated converters allow more flexibility in terms of speed variation and fault isolation.

#### **1.4.2. Turbine components failure rates and downtime**

Most of the work on the quantitative analysis of wind turbine reliability published so far, such as references [24] and [25], are based on statistics from onshore turbines. The reliability analysis carried out by Crabtree et al. in reference [24] covers data from 2 large surveys of European onshore wind turbines over 13 years including over 13800

turbine years. The failure rate for different turbine components and the corresponding downtime per failure are illustrated in Figure 1-7. It can be seen from this figure that the gearbox plays the most problematic role in both surveys in terms of downtime which can be up to 2 weeks, followed by generator and turbine blade, even though its failure rate is not as high as the electrical system and electronic control.

The direct-drive wind turbines were proposed in recent years in order to eliminate the gearbox related troubles. Such a type of turbine requires a large-dimension generator with multi-poles to cope with the low rotor rotational speed. However, the configuration of the low-speed, high-torque generator together with the fully rated converters is rather expensive [23], and it is also claimed by reference [26] that the aggregate failure rate of electrical related subassemblies for the direct-drive turbines is much higher than that for the conventional gearbox driven turbines.

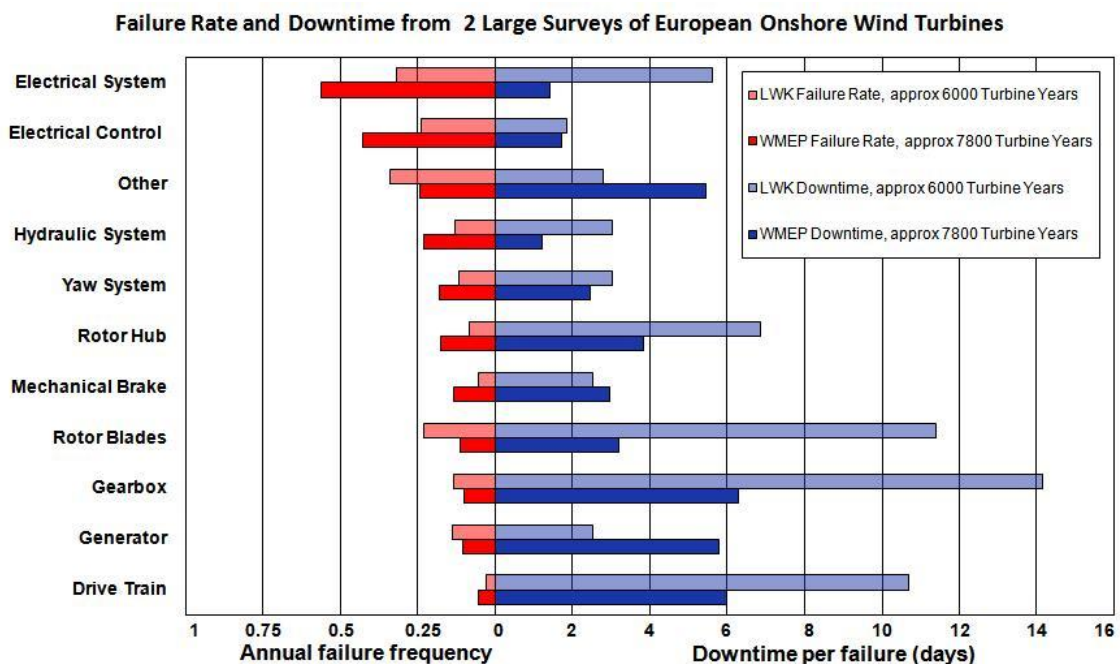


Figure 1-7: Wind turbine components failure rates and the corresponding downtime per failure for two surveys of European onshore wind turbines [24]

Similar results to reference [24] are obtained in reference [25], where the failure statistics are further divided into minor failure which occurs frequently with downtime

shorter than 1 day, and major failure which occurs less frequently with downtime longer than 1 day for all turbine sub-assemblies. This study finds that the minor and major failures account for 75% and 25% of the onshore wind turbine failure rates respectively, leading to a respective downtime percentage of 5% and 95%.

The downtime for both failure types will increase for offshore wind turbines since timely maintenance will not be achieved due to the difficulties and higher costs for offshore access. The corresponding availability is also expected to decline. According to reference [27], the averaged technical availability for Barrow offshore wind farm in its first year of operation was as poor as 67.4%. Effective condition monitoring approaches can therefore play an important role in improving offshore availability and reducing downtime by allowing maintenance work to be scheduled ahead of anticipated failure. Maintenance strategies such as those proposed in references [28] and [29] can be employed to ensure the maximal turbine availability and optimal management of the available equipment taking account of the weather and the sea state.

## **1.5. Thesis overview**

This thesis is organised to present the progress made and results obtained throughout the PhD study. There are 6 chapters in total, each of which will be briefly covered as follows.

This chapter briefly introduces readers to background information including the current status of the wind energy development and the wind turbine reliability. And importantly the research emphasis on condition monitoring is justified.

Chapter 2 reviews in some detail the various techniques that are commonly used for wind turbine condition monitoring. Here particular attention is paid to techniques that are applicable to SCADA data based analyses.

Chapter 3 proposes a real-time condition monitoring approach based on the wind turbine operational power curve. This includes the reference power curve construction and a real-time comparison with a running operational power curve that is updated every ten

minutes with the latest power curve measurement pair (wind speed and power). The proposed method has also been applied to pitch system condition monitoring.

Chapter 4 applies a nonlinear state estimation technique (NSET) to the condition monitoring of individual turbine components. Case studies for two key components in the drive train including the gearbox and generator are presented. The performance of the technique under different conditions are compared and discussed.

Chapter 5 extends the method described in Chapter 4 to multi-machine application and uses it for wind farm condition monitoring. The effect of model size on the performance is investigated. A modified model is identified that delivers more reliable results.

Finally, Chapter 6 draws conclusions on the presented research including both the effectiveness of the proposed methods and their potential for improvement.

In addition, a number of appendices are attached at the end of this thesis that include NSET model results that are omitted in the main chapters for the individual turbine and multi-machine applications.

## **1.6. Research publications**

Much of the research undertaken for this thesis was supported by the Energy Technologies Institute (ETI) FLOW project to develop a holistic wind turbine condition monitoring system. The project was led by Moog-Insensys and also included EDF, E.ON, Romax and Seebyte. ETI encouraged dissemination and publication of the research results and throughout the period of research a fair amount of effort has been dedicated to this. A number of journal publications and conference papers (including peer reviewed) resulted. They are listed below with the most recent publications presented first.

### **Journals**

Wang, Y., Infield, D. G., Stephen, B., Galloway, S. J., *Copula-based model for wind turbine power curve outlier rejection*, Wind Energy, doi: 10.1002/we.1661, 2013.

Wang, Y., Infield, D., *Supervisory control and data acquisition data-based non-linear state estimation technique for wind turbine gearbox condition monitoring*, Renewable Power Generation, IET, vol.7, no.4, pp.350-358, July 2013.

**Conference proceedings**

Wang, Y., Infield, D., *Multi-machine Based Wind Turbine Gearbox Condition Monitoring Using Nonlinear State Estimation Technique*, EWEA Barcelona 2014.

Wang, Y., Infield, D. G., Stephen, B., and Galloway, S. J., *Power Curve Based Online Condition Monitoring for Wind Turbines*, COMADEM Helsinki 2013.

Stephen, B., Gill, S., Galloway, S., Wang, Y., McMillan, D., Infield, D., *Wind turbine operation anomaly detection using copula statistics*, EWEA Vienna 2013.

Wang, Y., Infield, D., *Neural Network Modelling with Autoregressive Inputs for Wind Turbine Condition Monitoring*, SuperGen 2nd international Conference, Hangzhou 2012.

Wang, Y., Infield, D., *SCADA data based nonlinear state estimation technique for wind turbine gearbox condition monitoring*, EWEA Copenhagen 2012.

## 1.7. Chapter references

1. *Global Wind Statistics 2012*, Global Wind Energy Council (GWEC), Brussels, Belgium.
2. [Online]. Available: <http://www.windpowermonthly.com/10-biggest-turbines> (Accessed 21st October 2013), 2013.
3. [Online]. Available: <http://www.c2es.org/energy/source/renewables> (Accessed 22nd October 2013), 2013.
4. *Copenhagen Accord*, UN Framework Convention on Climate Change, Conference of the parties, 15<sup>th</sup> session, Copenhagen, Dec. 2009.
5. Bohringer, C., Rutherford, T. F., Tol, R. S., *The EU 20/20/2020 targets: An overview of the EMF22 assessment*, Energy Economics, vol. 31, 2009.
6. *National Renewable Energy Action Plan for the United Kingdom*, Article 4 of the Renewable Energy Directive, 2009.
7. *Energy Security*, International Energy Agency, [Online]. Available: <http://www.iea.org/topics/energysecurity/> (Accessed 22nd October 2013), 2013.
8. *Renewable Obligation Annual Report 2011-12*, Ofgem, 2012.
9. *Electricity growth*, Department of Energy and Climate Change (DECC), [Online]. Available: <https://restats.decc.gov.uk/cms/electricity-growth/> (Accessed 23rd October 2013), 2013.
10. *Offshore wind operational report 2013*, The Crown Estate, [Online]. Available: <http://www.thecrownestate.co.uk/media/418869/offshore-wind-operational-report-2013.pdf> (Accessed 2<sup>nd</sup> April 2014), 2014.
11. *UK Renewable Energy Roadmap*, DECC, 2011.
12. *Map of Rounds 1, 2 and 3 for offshore wind development in the UK*, [Online]. Available: <http://www.renewbl.com/wp-content/uploads/2009/11/rounds123-offshore-wind-UK.jpg> (Accessed 28th November 2013), 2013.

13. BVG associates, *Towards Round 3: Progress in building the offshore wind supply chain*, Feb. 2011.
14. Spinato, F., Tavner, P. J., van Bussel, G. J. W., Koutoulakos, E., *Reliability of wind turbine subassemblies*, IET Renewable Power Generation, Vol. 3, Iss. 4, pp. 1-15, 2009.
15. van Bussel, G.J.W., Zaaijer, M.B., *Reliability, Availability and Maintenance aspects of large-scale offshore wind farms, a concepts study*, ImarE Conference In MAREC 2001 Marine Renewable Energies Conference, Vol. 113, No. 1, pp. 119-126, March 2001.
16. Van Horenbeek, A., Van Ostaeyen, J., Duflou, J. R., Pintelon, L., *Quantifying the added value of an imperfectly performing condition monitoring system—application to a wind turbine gearbox*, Reliability Engineering & System Safety, vol. 111, pp. 45-57, 2013.
17. Young, W. F., Stamp, J. E., Dillinger J. D., *Communication Vulnerabilities and Mitigations in Wind Power SCADA Systems*, American Wind Energy Association WINDPOWER 2003 Conference, Texas, May 2003.
18. Tavner, P., *Offshore Wind Turbines: Reliability, availability and maintenance*, IET Renewable Energy Series 13, 2012.
19. Crabtree, C.J., *Survey of Commercially Available Condition Monitoring Systems for Wind Turbines*, SuperGen Report, Nov. 2010.
20. [Online]. Available: <http://www.energybc.ca/profiles/wind/hawt.html>, (Accessed 30th October 2013), 2013.
21. Leithead, W.E., *Wind turbine control*, Lecture notes for Wind Energy CDT, University of Strathclyde.
22. Muljadi, E., Butterfield, C.P., *Pitch-Controlled Variable-Speed Wind Turbine Generation*, IEEE Industry Applications Society Annual Meeting, Feb.2000.

23. Polinder, H., van der Pijl, F.F.A., de Vilder, G.-J., Tavner, P., *Comparison of direct-drive and geared generator concepts for wind turbines*, IEEE Trans. Energy Conversion, vol. 21, no. 3, pp. 725-733, 2006.
24. Crabtree, C.J., Feng, Y., Tavner, P.J., *Detecting Incipient Wind Turbine Gearbox Failure: A Signal Analysis Method for Online Condition Monitoring*, Scientific Track Proceedings, European Wind Energy Conference 2010, Warsaw, Poland, 2010.
25. Faulstich, S., Hahn, B., Tavner, P. J., *Wind turbine downtime and its importance for offshore deployment*, Wind Energy, vol.14, no. 3, pp. 327-337, 2011.
26. Tavner, P. J., van Bussel, G. J. W., Spinato, F., *Machine and Converter Reliabilities in Wind Turbines*, IEE 2<sup>nd</sup> International Conference on Power Electronics, Machine & Drives, Dublin, April 2006.
27. Feng, Y., Tavner, P.J., Long, H., *Early experiences with UK Round 1 offshore wind farms*, Proceedings of the Institution of Civil Engineers : energy., vol. 163, (4), pp. 167-181., 2010.
28. Karyotakis, A., *On the optimisation of operation and maintenance strategies for offshore wind farms*, Doctoral thesis, UCL (University College London), 2011.
29. Dinwoodie, I. A., McMillan, D., Quail, F., *Analysis of offshore wind turbine operation & maintenance using a novel time domain meteo-ocean modeling approach*, ASME Turbo Expo 2012.

## **2. Wind turbine condition monitoring techniques**

Significant effort has been made in the field of wind turbine condition monitoring because of its potential to improve turbine availability and reduce downtime. A common feature of robust condition monitoring techniques is their capability of effectively detecting deviations from expected system performance. This chapter provides an overview of the techniques that are commonly used for wind turbine condition monitoring including the approaches based on turbine physics and data based modelling that can be implemented using SCADA data.

Physical models require substantial and detailed knowledge of the engineering science of the relevant system, or a sub-assembly, to generate an accurate engineering model that can be used for condition monitoring. Exact anomaly signatures required for the purpose of diagnosis can be extracted from such physics of failure models, [30]. In contrast, data based modelling makes use of system operational measurements, and does not rely on precise physical knowledge of the system, although a general engineering knowledge may well guide the choice of data parameters and their acceptable range. Most wind turbines record extensive SCADA data, most commonly every ten minutes, so that useful data are available in principle at no cost. With an appropriate selection of variables, data based modelling is capable of learning the complex inter-relationships among the variables including any nonlinearities and embedding the main system features in the model architecture, sometimes with the aid of artificial intelligence or machine learning techniques.

Both of these distinct approaches will be reviewed in the context of application to wind turbine condition monitoring. They will be introduced and discussed in the following sections, with particular attention to SCADA data based modelling.

### **2.1. System physics based techniques**

Conventional physics-based, sometimes called physics of failure, models are usually constructed based on equations expressing the relevant physics, such as in reference

[31], which presents a physics-based model of a gearbox and applies this to wind turbine gearbox fault detection. The physics that can represent the evolution of damage for a specific component needs to be thoroughly understood in order to construct a physically accurate damage model that relates the applied loads to the expected fatigue damage, and thus remaining fatigue life, of the component, [31]. This knowledge, however, can be difficult to obtain in some circumstances, [30].

The concept of the physics-based modelling is extended here to include techniques based on physical system information and measurements that are obtained using additional sensors and equipment. According to the survey carried out and reported in reference [19], vibration signal analysis, oil debris analysis, blade strain measurement and acoustic emission could all play important roles in the condition monitoring of commercial wind turbines. The realisation of these techniques relies on both the sensors that collect relevant measurements and an accurate specification of the system, such as the component design and fatigue life. The following sections will introduce and discuss each of the approaches in turn.

### **2.1.1. Vibration signal analysis**

Vibration analysis is the most commonly used technique for the condition monitoring of rotating equipment, and this is true of wind turbines in particular. In the context of wind turbine application, vibration monitoring covers the overall turbine drive train where rotating machinery is involved and the vibration signals are acquired from accelerometers that are installed on or near key components such as high and low speed bearings. Figure 2-1 illustrates a typical accelerometer layout for vibration monitoring purposes in the drive train of a wind turbine with a 3-stage gearbox.

The collected vibration measurements usually undergo frequency based analysis and the spectrum obtained provides an explicit indication of the component condition that facilitates the fault diagnosis for specific components. In case of degrading quality within the component, large harmonics could appear in the spectrum or the energy contained in the sideband of the spectrum will increase. Very detailed knowledge about

the parameters of drive train, including the dimensions for each sub-assembly within the gearbox and the number of gear teeth for all stages of the gearbox, is required in order to gain better understanding of which part of the spectral signal corresponds to the normal operation and which part is caused by the deterioration of the component [32].

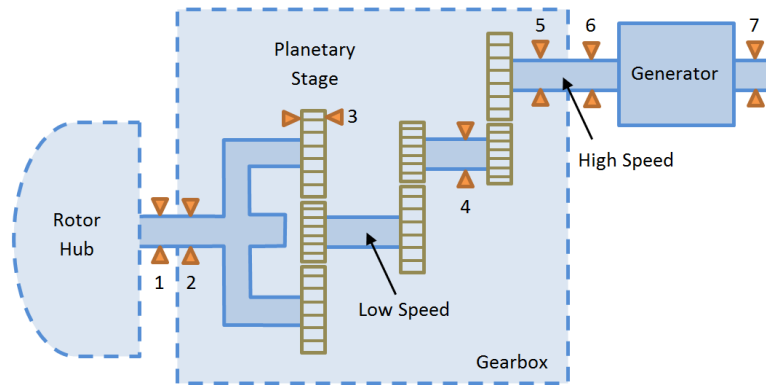


Figure 2-1: Typical accelerometer layout in the drive train of wind turbine with a 3-stage gearbox [33]

Reference [34] presents a comprehensive evaluation of vibration techniques for wind turbine drive train condition monitoring including the Fast Fourier Transform, Cepstrum processing (that involves the inverse Fourier Transform), bearing envelope analysis, and wavelet transforms, which are capable of tracking specific frequency components under varying rotor speed due to their inherent ability to provide better frequency resolution at low frequencies and better time resolution at high frequencies [35].

Apart from frequency domain based techniques, anomaly detection can also be undertaken using time series analyses of the vibration signals, such as those presented in reference [36], where the development of an impending gearbox bearing failure is indicated by an increasing trend of the time series representing the enveloped high speed shaft axial vibration amplitude signal.

### 2.1.2. Oil debris analysis

Oil debris analysis is also a potentially useful method for monitoring gearbox condition. It is sometimes integrated together with vibration analysis to provide a complete gearbox

condition monitoring system that can achieve a better and more accurate detection of gearbox faults [36]. Debris found in the gearbox lubricant oil can be considered an indication for wear or damage of gearbox components, where particles of different size and material imply different types and position of damage. A commonly used device, the induction sensor, is employed to check the size and amount of the ferrous and non-ferrous debris in the lubricating oil [37]. Following particle counting, the oil is usually pumped to the filtration system to remove the debris, before being returned to the gearbox.

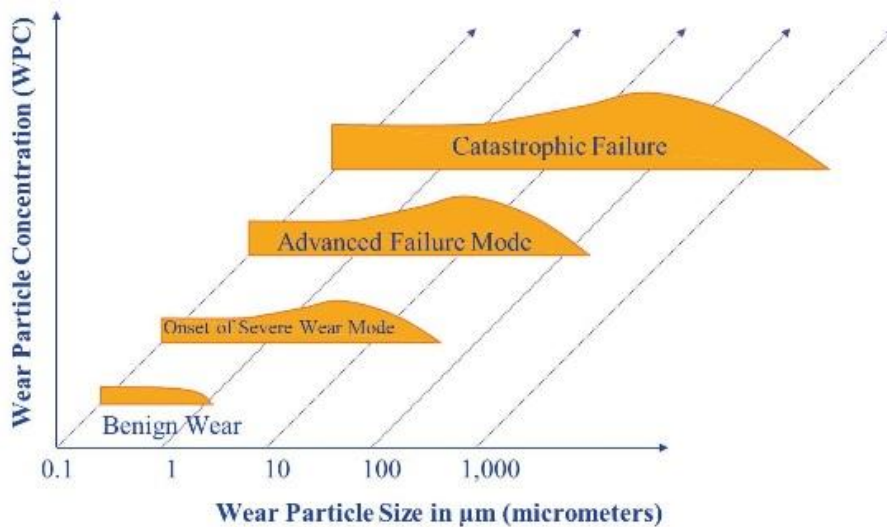


Figure 2-2: Evolution of gearbox damage in terms of wear particle size [38]

The evolution of gearbox damage in terms of wear particle size is illustrated in Figure 2-2, from which it can be seen that the detection of large ferrous wear particles (with size more than 100 microns) can provide an early indication of potential gearbox sub-assembly wear. For medium and small particle size ranges, however, the increment rate of the oil counting particles will be more informative than the absolute value of cumulant. Reference [24] presents an example of gearbox intermediate shaft failure, where the increase in the particle (ferrous 50-100 microns) count increment rate prior to the final failure indicates the deterioration of the intermediate shaft.

### **2.1.3. Blade strain measurement**

Strain measurement provides a simple and effective way to investigate blade loads and to thus predict their remaining fatigue life. Relevant sensors can be placed on the tension side, the compression side, the blade edge or most commonly around the blade root to measure the blade bending moment in response to either the blade weight or the incident wind (in plane and out of plane respectively).

A common and traditional technique for blade strain measurement is to use conventional strain gauges. These output an electrical signal corresponding to local strain and determined by the shape of the sensor. For a typical foil strain gauge, the conducting element in vertical direction is designed to be much longer than in the horizontal direction, which results in more sensitivity to conductor geometry change in the vertical direction than the horizontal direction. The ambient temperature also acts as a very significant error source for the strain gauge measurement since the resistance within the strain gauge is prone to temperature changes. For isotropic materials with uniform temperature distributions, the temperature effect can in principle be eliminated through proper selection of half- or full-bridge strain gauge configurations. These are not however applicable to composite blades [39]. It is also claimed in reference [32] that strain gauges are not robust in the long term. In contrast, the fibre optic based sensor technology offers a longer life time and more accurate measurements. However, their high present cost limits the current application of such strain gauges [32]. Prices are expected to drop as the technology further matures, and optical fibre sensors are likely to be of considerable importance for condition monitoring of wind turbine blades, particular in independent blade pitch control.

### **2.1.4. Acoustic emission**

Acoustic emission is sound emitted by an object that undergoes fatigue or stress. Acoustic monitoring consists of two types: passive, where the excitation is produced by the component itself; and a second type where the excitation is externally applied [32]. Condition monitoring for wind turbine blades would most likely be of the passive type, and the acoustic sensors are attached to the turbine components under investigation

using a material that acts as excellent acoustic coupler, such as flexible glue with low sound attenuation.

Acoustic emission monitoring is strongly related to vibration monitoring [32], and some recent systems combine the two techniques to obtain a more accurate condition indicator. For example, reference [40] uses the combination of these two techniques for condition monitoring of wind turbine gearbox and generator shaft. Acoustic emission signals are also used to identify possible blade fatigue in critical areas such as the blade root, [41].

## **2.2. SCADA data based modelling**

Compared to vibration analysis, oil debris analysis, strain gauge measurement and acoustic emission that all require detailed engineering knowledge and knowledge of the operating characteristics of the monitored component, SCADA data based modelling is relatively easy to construct and generalize. As already mentioned, SCADA data based techniques require no new sensors and thus are cheap to implement. The increasing application of machine learning techniques in recent years and the diverse choices of artificial intelligence approaches have facilitated SCADA data based modelling for the condition monitoring of wind turbines, [42].

The inter-relationships between key operational parameters represented by the SCADA data have to be identified (or learned) in order to produce effective models and anomaly detection. For parametric models, such as Artificial Neural Networks (ANNs), the interrelationship among key variables are represented by the weight and bias parameters of each neuron, and these are determined by training on historical data. For non-parametric models, such as the Nonlinear State Estimation Technique (NSET), the model output is computed by calculating the similarity between each new input and the stored historical exemplars taken from a healthy unit, in this context the wind turbine.

Numerous techniques have been successfully applied to the area of SCADA based wind turbine condition monitoring, some of which will be introduced in the following sections including the ANN, Support Vector Machine (SVM), Bayesian network (BN) and the

NSET. All of these techniques were originally developed for other applications but are readily applicable to wind turbine SCADA data. Relevant research results and potential issues will also be discussed in more detail for each technique below. Finally, there are condition monitoring approaches based on operational power curves. Actually these are a special form of SCADA data analysis. They cannot always directly identify the faulty component but they can flag up a range of issues that impact on power generation performance. Such approaches provide a simple and effective means to monitor the overall turbine status in general and will be presented at the end of this chapter.

### **2.2.1. Artificial neural networks**

Artificial Neural Network or Neural Network (NN) models, being biologically inspired by the mechanism of human brains, are parametric models designed to capture data interrelationships between input parameters and outputs using weight and bias parameters for individual neurons. NN models can be used for both data classification where the output variables take values of class labels and data regression where the outputs take continuous values. In either case, the neuron parameters are established through a training process, often using the back propagation algorithm.

Figure 2-3 shows an example of multilayer feed-forward neural network consisting of input layer, hidden layer and output layer, each of which comprises a group of neurons [43]. Sometimes the hidden layer could consist of more than one layer. Figure 2-4 illustrates the inner structure of an elementary neuron where  $R$  represents the number of elements in input vector;  $W$  and  $b$  are weight vector and bias of the neuron, respectively. The weighted sum is then input into a transfer function,  $f$ , to generate neuron output  $a$ , which is fed as input to the neurons in next layer until reaching the output layer [44]. The most commonly used three transfer functions for multilayer neural network model are log-sigmoid transfer function, the tan-sigmoid transfer function and linear transfer function, the algebraic algorithms and corresponding graphs of which are tabulated in Table 2-1.

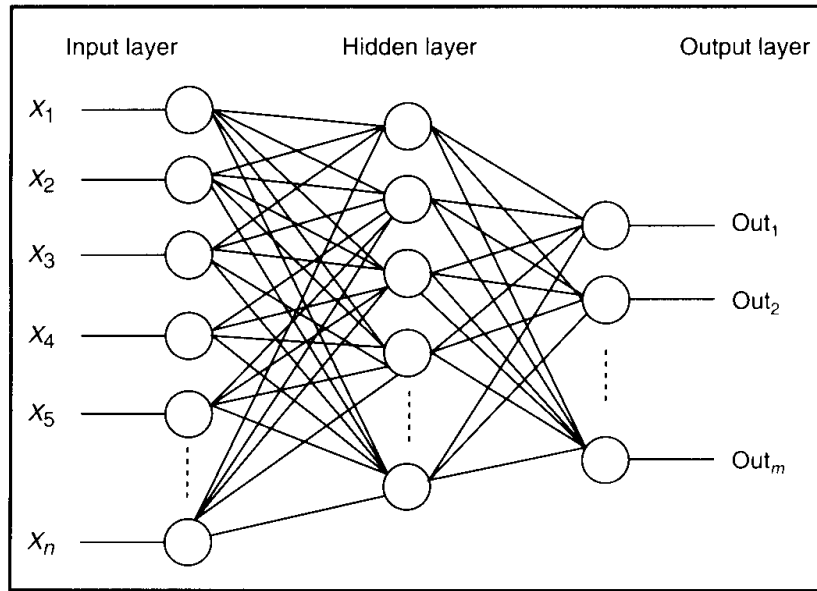


Figure 2-3: Feed-forward neural network model architecture example [43]

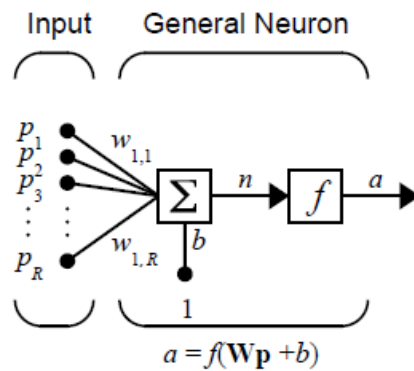


Figure 2-4: Inner structure of a general neuron with  $R$  inputs [44]

Unlike the feed-forward neural network where all concurrent information flow transmits uni-directionally from inputs nodes to outputs, the recurrent neural network enables dynamic temporal processing by utilizing an internal state with memory to take into account the historical inputs through feedback loops [45]. And the NN models have achieved a significant breakthrough in model accuracy by employing back propagation techniques, which iteratively adjust the weights and biases in each neuron in order to minimise the output error [46]. A list of either gradient or Jacobin based back propagation algorithms with their detailed descriptions for NN model training is presented in [44]. Among all the training functions provided, the Levenberg-Marquardt

algorithm is claimed to be the fastest algorithm for small networks, but not so appropriate for large networks due to its requirement of more memory and computation time.

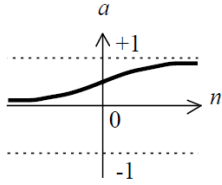
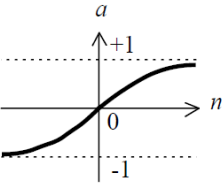
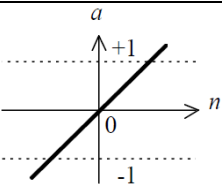
	Transfer function algorithm	Transfer function illustration
Log-sigmoid	$a = \text{logsig}(n) = \frac{1}{1 + e^{-n}}$	
Tan-sigmoid	$a = \text{tansig}(n) = \frac{2}{1 + e^{-2n}} - 1$	
Linear	$a = \text{purelin}(n) = n$	

Table 2-1: Three commonly used transfer functions in the neurons of NN models [47]

As is shown in Figure 2-3, the number of neurons in the input and output layers is determined by the number of input and output variables that are relevant for a given problem, hence these are treated as fixed in model construction. As for how many neurons should be chosen for the hidden layer, the general rule is that the neuron number should not be too large as this can lead to over-fitting of the model and cause failure to model generalization, and also not too small as this will result in model under-fitting. Reference [48] suggests the hidden layer size should to be between one-half and three times the inputs size, and reference [49] proposes an optimal hidden neuron of 75% of the input variables number, neither of which is commonly accepted due to insufficient theoretical foundation. In practice, the choice of the number of hidden layer neurons involves experience and experiment [50].

NN models have been widely employed in wind turbine condition monitoring research due to their ability to model nonlinear dynamic process and efficiently resolve pattern recognition issues [51, 52]. References [53] and [54] both present successful wind turbine gearbox fault diagnosis examples using NN models with a three-layer structure. The former identifies gearbox anomalies through model learning and comparison with turbine performance data based on gearbox cooling oil temperature taken from SCADA data, and the latter employs 9 vibration signals from a gearbox, in vertical, horizontal and axial directions, as model inputs.

Despite of its robustness in nonlinear statistical identification and relationship learning, care is required during model construction and training. Issues such as local minima in gradient descent algorithm and extrapolation limitations in model estimation have already gained awareness for different neural network model applications. Reference [55] investigates the local minima issue of neural networks in using the back propagation algorithm and proposes some sufficient conditions for robust solutions. Reference [56] provides an insight into the neural network model structure and gives an explanation of its limited extrapolation capability.

Apart from the common issues mentioned above, neural network models may also suffer from performance limitation with specific reference to models including autoregressive inputs. The main purpose for introducing autoregressive lag terms of a variable in a time series is to feed information to current or future value estimation from recently past values [57]. The success of Markov modelling underpins this approach. Successful identifications of incipient turbine anomalies are demonstrated in both [58] and [59], both of which employ autoregressive inputs. The effect of including autoregressive inputs on model performance is investigated in reference [60], based on the identical NN model presented in reference [58]. A potential but not conclusive issue of unreliability has been pointed out in reference [60] for such models due to the heavily weighted autoregressive terms, requiring a more cautious approach to model construction and training.

### 2.2.2. Support vector machine

The support vector machine (SVM) is a relatively new machine learning technique proposed by Vapnik in 1995. It is capable of data pattern recognition, such as classification, and regression for nonlinear and high dimensional data, similar to the NN model. However, unlike the NN model whose architecture and various associated parameters need to be found, the SVM requires few parameters and is not prone to identification of false (local) minima due to optimization using a convex function during training, [61]. The basic idea of the SVM is to map the input vectors that are not fully linearly separable into a feature space with a higher dimension where optimal separation of the mapped data can be achieved using hyperplanes, [62].

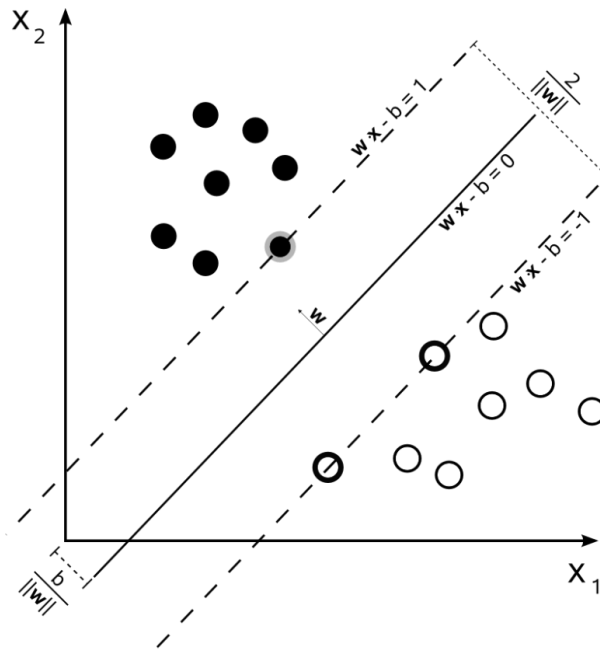


Figure 2-5: A simple example of 2-dimensional linearly separable data separated by a line [63]

An example of 2-dimensional linearly separable data is illustrated in Figure 2-5, where the empty and filled circles represent two different data classes. There are infinite choices of lines that could be used to separate the two classes and SVM uses the maximum-margin line, as shown in Figure 2-5, which allows for noise and has greatest tolerance to errors in the data on either side. The data points closest to the separating line

are the support vectors, as shown by the boldly circled points, which define the upper and lower decision boundaries for each data class. The generalized separating hyperplane and associated regions for different classes in higher dimensions are expressed by Equations (2-1), (2-2) and (2-3).

$$\mathbf{W} \cdot \mathbf{x}_i + b = 0 \quad (2-1)$$

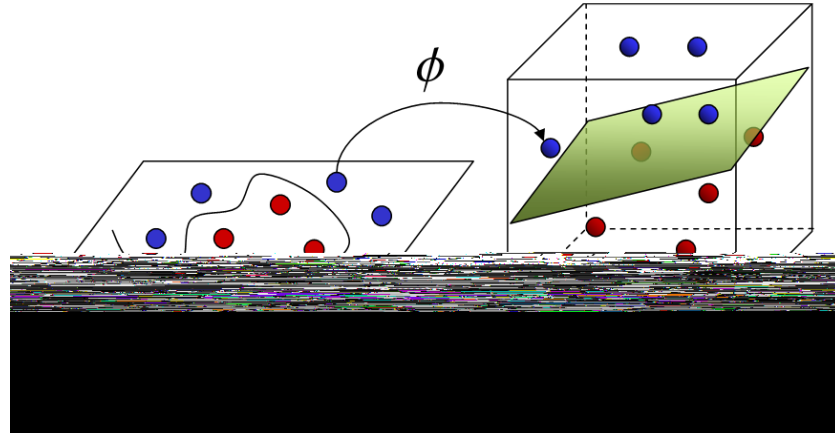
$$\mathbf{W} \cdot \mathbf{x}_i + b \geq 1 \quad (2-2)$$

$$\mathbf{W} \cdot \mathbf{x}_i + b \leq -1 \quad (2-3)$$

where  $\mathbf{W}$  and  $b$  are the parameters that define the hyperplane, and vector  $\mathbf{w}$  is normal to the plane. For each input  $\mathbf{x}_i$ , there is a corresponding output  $y_i$  that belongs to one of the two classes, i.e.  $y_i = 1$  for Equations (2-2) or  $-1$  for Equations (2-3). Therefore Equations (2-2) and (2-3) can be combined into Equation (2-4) below.

$$y_i(\mathbf{W} \cdot \mathbf{x}_i + b) - 1 \geq 0 \quad (2-4)$$

The margin is defined to be the distance between the upper and lower boundaries, which is  $\frac{2}{\|\mathbf{W}\|}$  according to vector geometry.  $\|\mathbf{W}\|$  need to be minimised in order to achieve the maximal margin, which is equivalent to minimising  $\frac{1}{2}\|\mathbf{W}\|^2$ , [64]. This use of this term provides a quadratic optimisation with unambiguous global minimum and no local minima, due to its convex form. The parameters are conventionally solved using a Lagrange algorithm based on the training data, and can then be used to classify further testing data.



(a) Non-linear data in original space (b) Linearly separable data in feature space

Figure 2-6: Data separation by transferring into feature space with higher dimension [63]

In reality most of the training data are usually not completely linearly separable, such as the case shown in Figure 2-6(a), where the red hollow points and the blue solid points represent two different classes. In this case no straight lines can be used in the two dimensional space to perfectly separate these two groups. However, the data would become linearly separable by being transferred into a higher dimensionality space, which is known as the feature space, using a proper nonlinear kernel function  $\mathbf{x} \rightarrow \phi(\mathbf{x})$ , and a separating hyperplane can be found to achieve the separation task as illustrated in Figure 2-6(b). Some common choices for kernel functions include the Gaussian radial basis kernel, the polynomial kernel and the sigmoid kernel [64].

In the cases where misclassifications exist for a very small population randomly distributed in the training data, the kernel approach to exact separation of data would probably lead to over-fitting and hence lack of general applicability, and a soft margin is employed in such situations by introducing a positive slack variable,  $\xi$ , to relax the constraints of the decision boundaries as shown in Equations (2-5) and (2-6). The associated objective function is also modified to Equations (2-7), where the second term is a regularization term which constrains the model complexity and hence prevent over-fitting and parameter  $C$  indicates the compromise between the slack variable penalty and the margin size [64].

$$\mathbf{W} \cdot \mathbf{x}_i + b \geq 1 - \xi \quad \text{for } y_i = 1 \quad (2-5)$$

$$\mathbf{W} \cdot \mathbf{x}_i + b \leq -1 + \xi \quad \text{for } y_i = -1 \quad (2-6)$$

$$\min \frac{1}{2} \|\mathbf{W}\|^2 + C \sum \xi_i \quad \text{s.t. } y_i(\mathbf{W} \cdot \mathbf{x}_i + b) - 1 + \xi_i \geq 0 \quad \forall_i \quad (2-7)$$

For SVM to perform regression, a real-valued and continuous output is obtained using Equation (2-8) based on the training data. Two slack variable penalties,  $\xi^+$  and  $\xi^-$ , are used to indicate the position of the observations, i.e. whether above or below the hyperplane respectively, and the corresponding objective is expressed by Equation (2-9) [64]:

$$y_i = \mathbf{W} \cdot \mathbf{x}_i + b \quad (2-8)$$

$$\min \frac{1}{2} \|\mathbf{W}\|^2 + C \sum (\xi_i^+ + \xi_i^-) \quad \text{s.t. } \xi_i^+ \geq 0, \xi_i^- \geq 0 \quad (2-9)$$

SVMs have been extensively applied to many domains ranging from image and text detection and categorization [65] to astronomy [66]. The use of SVM for fault detection started in 1999 and the associated detection accuracy was found to be improved, [67]. Widodo et al. present a review of the SVM applications to the diagnosis for roller bearings, induction machines, turbo pump and a number of other mechanical machinery in reference [68].

A successful SVM based fault diagnosis for a direct-drive wind turbine is presented in reference [69], in which the time-domain vibration signals from turbine main shaft under five different failure modes are used as model inputs. The SVM model is trained by establishing a mapping relation between the characteristic input vectors and the corresponding failure types. Reference [70] presents a study of gear fault detection to compare the model performance of ANN and SVM based on the time-domain vibration signals. The comparisons are implemented under different load conditions and model configurations, and the results for most of the cases demonstrate a better classification

accuracy using SVM. It is also claimed that for all the cases considered the training time for SVM is much reduced compared to ANN models.

Until now not much research has been done using SVM analysis of SCADA data for condition monitoring. Considering the excellent performance reviewed above and its capability of data feature extraction without too much background knowledge due to its artificial intelligence nature, SVMs should be readily applicable to wind turbine condition monitoring using SCADA data. Of course there are other techniques such as k-nearest neighbour and random forest modelling that have found successful applications to wind turbine condition monitoring as presented in references [71, 72].

### **2.2.3. Bayesian networks**

Bayesian networks (BNs) can be used to construct probabilistic graphical models that represent the causal relationships among a set of random variables (RVs). A directed acyclic diagram is utilised, where each variable is represented by a node [73]. In diagnostic models the nodes can be categorized into root causes or faults, evidences or tests, [74], and directed arrows are used to indicate the cause and effect relationship between these nodes, pointing from the root cause (parent node) to its effect (child node) [75]. For diagnosis purpose a conditional probability table (or conditional probability function in the case of continuous RVs), obtained by either learning from the existing data or from expert knowledge, is required for each node, where all the possibilities for all of its parent nodes (if they exist) should be included. Based on these statistics the probability of a root cause, denoted  $C$ , conditional upon test results/evidence observed,  $E$ , is  $P(C|E)$ , which is also known as the posterior. It can be inferred from the prior,  $P(C)$ , and the likelihood ratio,  $P(E|C)/P(E)$ , using Bayes' rule, which is expressed in Equation (2-10),

$$P(C|E) = \frac{P(C) \times P(E|C)}{P(E)} \quad (2-10)$$

A simple example of a discrete BN with binary valued RVs is presented in Figure 2-7, in which the causalities relating four variables, including cloudy, sprinkler, rain and wet

grass, are illustrated together with the associated (conditional) probability tables. The event ‘being cloudy’ has an effect on the status of sprinkler and rain, both of which directly determine whether the grass would be wet or not. As mentioned above, all the possible outcomes from the parent nodes should be considered in the conditional probability tables for their children nodes, which results in  $2^1 = 2$  conditions for the nodes ‘sprinkler’ and ‘rain’, and  $2^2 = 4$  conditions for node ‘wet grass’. Applications of Bayes’ rule to calculate the probability of specific events, such as ‘being cloudy given the grass is wet’, based on observed evidence, are presented in detail in reference [76].



Figure 2-7: A discrete Bayesian network example [75]

The Bayesian network model is capable of dealing with missing data, thus allowing it to be widely applied [75]. A successful application of the BN model to detect and locate an anomaly of the electrical pitching system of wind turbine blade is presented in reference [77], where a combination of 10-minute SCADA data and 1-second alarm signals are used in the BN model reasoning and the dependencies among different variables are established using the binary valued conditional probability table as shown in Figure 2-7. Additionally, the BN model has been extended to wind resource estimation. Carta et al. propose a BN based probabilistic model in reference [78] for prediction of long-term

wind speed histogram and the associated power generation, which is an essential prerequisite to wind farm site assessment. The wind speed histogram is estimated based on the wind speed and wind direction measurements from three reference sites nearby.

Unlike the Bayesian network which presents the causality of random variables under the concurrent state, a dynamic Bayesian network (DBN) also takes account of the effect from historical states of a variable on its concurrent state as in the Markov modelling with memory. By including dynamic nodes in the extended state space, the DBN is able to integrate the degradation mechanisms of a specific system to its probabilistic model, thus enabling prognosis of system anomalies [79]. The dependencies on the historical states in a DBN can be obtained by either learning from the existing data or expert knowledge as in a Bayesian network.

Reference [80] presents the application of both BN and DBN to condition monitoring of wind turbine gearbox, with supporting evidence from both the ice sensing and oil debris information. The Bayesian network is implemented in Labview for online diagnosis by importing the real-time signals from the ice sensor and particle sensor that are installed on the physical test rig. The DBN is used for further prognosis of gearbox anomalies by including historical states for different variables and the associated dependencies in the directed acyclic graph.

The construction of the conditional probability table (or function) for the child node is based on the combination of each single state from all of its parent nodes, which results in an exponential scaling up of the model complexity with the associated number of parent variables. Another problem is that the observations required for fault reasoning are sometimes indirect or costly [74]. The exponential scaling pattern and difficulties in implementing the diagnostic tests limit the application of the BN and DBN as diagnostic and prognostic tools to complex problems, therefore the BN and DBN variables based on which the diagnostic tests are performed must be selected efficiently and effectively.

#### **2.2.4. Nonlinear state estimation technique**

The Nonlinear State Estimation Technique (NSET) was originally proposed and has been successfully applied for nuclear power plant condition monitoring [81]. It provides a state based vector recognition technique in which the state vectors consist of historical sensor readings at a specific time stamp for variables that are closely related to the model.

Unlike parametric models, such as the ANN and SVM, whose model parameters need to be fitted through the training process, NSET is a non-parametric model that learns data relationships by directly computing the similarity between the input signals and the historical state vectors that model the behaviour of the relevant system. A so called training data are used to select the representative state vectors which are then stored in a memory matrix, usually a subset of the training set, for further use and model estimation. For both the parametric and non-parametric models, the available data are divided into three parts, namely: the training data; validating data; and testing data. The former two are both chosen from operational data where the wind turbine is known to be healthy, whilst the latter contains potential turbine anomalies/incipient faults that the condition monitoring system is seeking to identify.

Despite of the fact that parametric models require relatively less computational effort for output estimation than non-parametric models since the model architecture has been defined up-front, a big advantage of the non-parametric models over the parametric ones is the ease of modification of the embedded functional relationship in case of changes in operating region. Retraining is required if parametric models are to take into account any changes in the functional relationship between variables corresponding to a new operating state. For example a NN model may require extensive computational effort to be retrained and may produce inconsistent results due to random initialization and the issue of inherent local minima, [82]. In contrast, non-parametric models, such as the NSET, can easily adapt continuously to changes in operating region by the simple addition of associated state vectors into the memory matrix, [82].

The ease of use and the enormous potential of NSET for wind turbine condition monitoring, based on the successful application to health monitoring of the nuclear plants, [81], and rotational machinery, [83], are reflected in its selection to monitor the key turbine components in the research presented in later chapters.

The NSET is used for SCADA data based anomaly detection of a wind turbine generator in reference [84], using the generator winding temperature as the condition indicator. The memory matrix in this work was constructed using a proposed state vector selection algorithm and although the selected candidate vectors are limited to a small proportion of the available training set, they cover most effectively the complete operating region of the turbine. A variety of nonlinear functions can be used as the nonlinear operator for the model output estimation, but the Euclidean distance is most commonly used, as it is in reference [84], due to its excellent performance as presented in reference [85]. Hines et al. take the nonlinear operator in reference [86] in the form of a Gaussian kernel function which requires an extra bandwidth parameter to be optimized during model output estimation. It is also claimed by reference [86] that the impact of operator choice on the algorithm performance is insignificant. For this reason the Euclidean distance is most often retained as the nonlinear operator due to its simplicity, see for example reference [87], which presents a successful NSET application to turbine gearbox anomaly identification using the SCADA data. The threshold for anomaly detection in reference [84] is set to an arbitrary multiple of the maximal validating residual, whereas reference [87] uses the more rigorous Welch's hypothesis test to identify any significant performance deviations based on the NSET model estimation. Reference [40] utilizes a Gaussian error function to measure the probability of detecting an actual anomaly in the context of false alarms.

It should be noted that NSET has been proposed and presented in the form of an auto-associative model in all the relevant works mentioned above. It can be seen from the schematic diagram for an auto-associative model in Figure 2-8 that the outputs are designed to emulate its inputs over an appropriate dynamic range, [82]. State vectors that represent the dynamic system in normal operation are selected during the memory

matrix construction. Based on the learned relationship, the model is capable of denoising the inputs/observations which may contain noise or reflect a system anomaly and producing the true values of parameters that correspond to system operation under normal conditions. These fault-free model outputs can then be used to detect anomalous behaviour through their deviation from operational data (observations) with incipient faults.

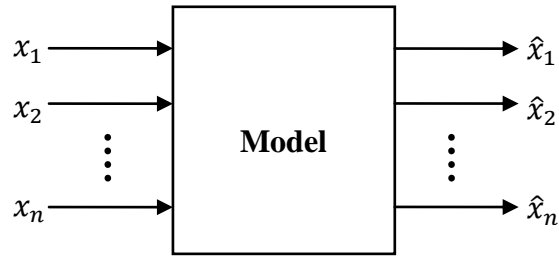


Figure 2-8: Schematic diagram for an auto-associative model

The research carried out in this thesis takes reference [79] as its starting point. Early thesis work was reported in reference [87], and this will be presented in Chapter 4, where NSET based condition monitoring methodologies and associated algorithms will be detailed. Model performance under different situations, and also the impact of additional state vectors and reduced input variables, will also be discussed in the context of applications to anomaly detection for a wind turbine gearbox and generator, using the 10-minute SCADA data. The individual turbine condition monitoring method based on NSET will then be extended to a multi-machine application in Chapter 5 using the same case studies.

### 2.2.5. Operational power curve based techniques

The relationship between wind turbine power output and the corresponding wind speed experienced by the turbine rotor defines a wind turbine power curve, and this provides a fundamental but important metric with which to identify the operational health of a wind turbine. A key attraction for condition monitoring purposes is that power curves can be calculated with an acceptable degree of accuracy using the already available wind farm SCADA data. SCADA data is normally collected at 10 minute intervals and thus is

compatible in this important regard with IEC Standards, [88], for power curve calculation.

To date, power curves have mainly been used by developers (the purchasers of the turbines) to ensure that the turbines supplied by the original equipment manufacturers (OEMs) conform to their specification, of which the manufacturer's power curve is an essential part. With the aid of proper techniques, regularly updated power curves can also provide a convenient means by which to identify whether operational wind turbines continue to function well.

The nonparametric k-nearest neighbour (kNN) algorithm is utilized in reference [71] to construct the reference power curve for further anomaly identification based on exemplar training data from individual turbine. The same algorithm has been extended in reference [89] to construct a wind farm level reference in order to monitor the general operational status for the complete site. In this extended use, principal component analysis, [90], was used in combination with the kNN algorithm to reduce the dimension of the input data by selecting only the most informative wind speed components. The drawback of the kNN approach is not only the computational burden involved, which becomes significant for large training data sets, as implied in [89], but also the fact that the original data is transformed by the k-averaging process, which replaces the original data with the averaged value from the k nearest points.

Reference [91] treats the relationship between wind speed and power output across the wind farm as stochastic and develops a probability distribution of wind farm power generation in terms of wind speed and wind direction, based on conditional kernel density estimation. The resulting distribution could be used by power system operators to model expected power production.

Identification of blade and yaw system faults based on the monitoring of power curves are documented in reference [92], where a Copula model based method is employed for reference power curve construction due to its excellent performance in characterising nonlinear relationships such as that between wind speed and the power output as

represented by the power curve, and a sequential probability ratio test is used for anomaly identification.

A similar approach is followed in reference [93], where the ‘method of bins’ as specified by the IEC standard is used to form the power curve, and a Copula based model is used to clean the power curve measurements by automatically removing outliers in order to achieve a more precise reference curve. A bin by bin statistical comparison through hypothesis testing is undertaken to facilitate the identification of anomalies and these are interpreted using a proposed power curve fault logic. Unlike reference [92], which transfers the power curve measurement data into the Copula domain, this work analyses the power curve performance data in the original measurement domain, thus providing a more meaningful and straightforward interpretation. This research has been further extended and will be presented in Chapter 3.

Schlechtingen et al. present a comparative study of four techniques for turbine power curve based monitoring in reference [94], including cluster centre fuzzy logic, an ANN model, a kNN model and an adaptive neuro-fuzzy interference system. This highlights the adaptive neuro-fuzzy interference system to be the most effective of the four techniques. The model based on the selected technique is then improved by introducing two additional parameters: ambient temperature; and wind direction.

One of the potential issues of power curve based analyses is that the wind speed measurements available in the SCADA data sets will not in general comply with the IEC standard for power curve determination. For instance, the standard specifies a preferred meteorological mast position at a distance of 2.5 rotor diameters upwind of the wind turbine, whereas the SCADA wind speed data is recorded using a nacelle mounted anemometer which is located immediately behind the rotor and suffers from wind speed loss, and added turbulence, due to the turbine wake. The correction of such wind speed measurements, and corresponding data pre-processing, will be discussed in the next chapter. The authors in reference [94] have pointed out the significance of ambient temperature on model performance due to its impact on power output through air density.

It is preferable to follow the IEC performance standard and incorporate the effect of ambient temperature by making an air density correction. This will also be presented in the next chapter.

### **2.3. Chapter summary**

This chapter has provided an overview of the commonly used physics based techniques and also machine learning/artificial intelligence based data mining methods. In order to be effective, wind turbine condition monitoring must be based on robust techniques capable of producing accurate and reliable results, thus facilitating timely detection of anomalies that can be interpreted as incipient fault. Different techniques are available and the correct choice for condition monitoring purposes will depend on the nature of the available data and expert domain knowledge.

It should be noted though, that although much research has been published on SCADA based condition monitoring, there are few commercial applications. Wind farm operators remain rather sceptical about the benefits of SCADA based condition monitoring and worry about a propensity of such systems to flag up numerous false alarms. The following chapters will demonstrate the effectiveness of SCADA based techniques and hence show the potential for SCADA based condition monitoring.

The NSET technique has been identified as promising early on in this research and will be further explored in Chapters 4 and 5. It requires less domain knowledge than the physics based techniques during application due to its data mining nature, and it requires much less effort for modifications to reflect time dependent changes in the functional relationship between key variables, associated for example with changes in operating regime, compared to the effort to retrain parametric models. Power curve based condition monitoring for wind turbines has been introduced, and will be taken up in more detail in Chapter 3.

## 2.4. Chapter references

30. Hyers, R. W., McGowan, J.G., Sullivan, K.L., Manwell, J.F., Syrett, B.C., *Condition Monitoring and Prognosis of Utility Scale Wind Turbines*, Energy Materials, vol. 1, no. 3. pp. 187-203, Sep. 2006.
31. Gray, C.S., Watson, S.J., *Physics of Failure Approach to Wind Turbine Condition Based Maintenance*, Wind Energy, 13: 395–405, 2010.
32. Hameed, Z., Hong, Y.S., Cho, Y.M., Ahn, S.H., Song, C.K., *Condition Monitoring and Fault Detection of Wind Turbines and Related Algorithms: A Review*, Renewable and Sustainable Energy Reviews, Vol.13, pp. 1-39, 2009.
33. May, A.F., McMillan, D., *A Review of Commercially Available Condition Monitoring Systems*, Poster, University of Strathclyde, 2013.
34. Sheng, S., *Wind Turbine Gearbox Condition Monitoring Round Robin Study–Vibration Analysis*, NREL technical report, 2012.
35. Watson, S. J., Xiang, B. J., Yang, W., Tavner, P. J., Crabtree, C. J., *Condition monitoring of the power output of wind turbine generators using wavelets*, IEEE Transactions on Energy Conversion, 25(3), pp. 715-721, 2010.
36. Feng, Y., Qiu, Y., Crabtree, C. J., Long, H., Tavner, P. J., *Monitoring wind turbine gearboxes*. Wind Energy, vol. 16, (5), pp. 728-740, July 2013.
37. Hamilton, A., Quail, F., *Detailed State of the Art Review for the Different Online/Inline Oil Analysis Techniques in Context of Wind Turbine Gearboxes*, Journal of Tribology, 133(4), 044001, 2011.
38. *Combining Particle Count Data And Elemental Analysis Information To Detect Failures*, [online]. Available: <http://www.azom.com/article.aspx?ArticleID=10293> (accessed 28th Nov, 2013), 2013.
39. Papadopoulos, K., Morfiadakis, E., Philippidis, T. P., Lekou, D. J., *Assessment of the strain gauge technique for measurement of wind turbine blade loads*, Wind Energy, 3(1), 35-65, 2000.

40. Soua, S., Van Lieshout, P., Perera, A., Gan, T. H., Bridge, B., *Determination of the combined vibrational and acoustic emission signature of a wind turbine gearbox and generator shaft in service as a pre-requisite for effective condition monitoring*, Renewable Energy, vol. 51, pp. 175-18, 2013.
41. Beattie, A. G., *Acoustic emission monitoring of a wind turbine blade during a fatigue test*, In AIAA Aerospace Sciences Meeting, RENO, Nevada, January, 1997.
42. Wang, K.S., Sharma, V.S., Zhang, Z.Y., *SCADA data based condition monitoring of wind turbines*. Advances in Manufacturing, 2(1), 61-69, 2014.
43. Venugopal, V., Baets, W., *Neural networks and statistical techniques in marketing research: A conceptual comparison*, Marketing Intelligence & Planning, 12(7), 30-38, 1994.
44. Beale, M.H., Hagan, M.T., Demuth, H.B., *Neural Network Toolbox™ User's Guide*, The Math Works, Version 7, Sep 2010.
45. Bullinaria, J.A., *Recurrent Neural Networks*, Neural Computation: Lecture 12, 2013.
46. Zaher, A., *Automated Fault Detection for Wind Farm Condition Monitoring*, A thesis submitted for the degree of Doctor of Philosophy, University of Strathclyde, Sep. 2010.
47. Dorofki, M., Elshafie, A. H., Jaafar, O., Karim, O. A., Mastura, S., *Comparison of Artificial Neural Network Transfer Functions Abilities to Simulate Extreme Runoff Data*, International Proceedings of Chemical, Biological & Environmental Engineering, 33, 2012.
48. Katz, J.O., *Developing Neural Network Forecasters for Trading*, Technical Analysis of Stocks and Commodities, pp. 58-70, Apr. 1992.
49. Baily, D., Thompson, D.M., *Developing Neural Network Applications*, AI Expert, Sep. 1990.
50. Kaastra, I., Boyd, M., *Designing A Neural Network for Forecasting Financial and Economic Time Series*, Neurocomputing, Vol. 10, pp. 215 -236, 1996.

51. Haykin, S., *Neural Networks: A Comprehensive Foundation*, IEEE Press, 1994.
52. Munoz, A., Sanz-Bobi, M.A., *An Incipient Fault Detection System Based on the Probabilistic Radial Basis Function Network: Application to the diagnosis of the condenser of a coal power plant*, *Neurocomputing* 23, pp. 177–194, 1988.
53. Mesquita Brandão, R. F., Beleza Carvalho J. A., Maciel Barbosa, F. P., *Neural Networks for Condition Monitoring of Wind Turbines*, Modern Electric Power Systems, Poland, 2010.
54. Yang, S., Li, W., Wang, C., *The intelligent fault diagnosis of wind turbine gearbox based on artificial neural network*, International Conference on Condition Monitoring and Diagnosis, pp. 1327-1330, 2008.
55. Bianchini, M., Gori M., Maggini, M., *On the Problem of Local Minima in Recurrent Neural Networks*, IEEE Transactions on Neural Networks, Vol. 5, No. 2, pp. 167-177, Mar. 1994.
56. Haley, P.J., Soloway, D., *Extrapolation Limitations of Multilayer Feedforward Neural Networks*, International Joint Conference on Neural Network, Vol. 4, pp. 25-30, 1992.
57. Cabedo, J.D., Moya, I., *Estimating Oil Price 'Value at Risk' Using the Historical Simulation Approach*, Energy Economics, Vol. 25, Issue 3, May 2003.
58. Zaher, A., McArther, S.D.J., Infield, D.G., Patel, Y., *Online Wind Turbine Fault Detection through Automated SCADA Data Analysis*, Wind Energy, Vol. 12, pp. 574-593, Sep. 2009.
59. Garcia, M.C., Sanz-Bobi, M.A., Pico, J.D., *SIMAP: Intelligent System for Predictive Maintenance: Application to Health Condition Monitoring of a Wind Turbine Gearbox*, Computers in Industry, Vol. 57, pp.552-568, Aug, 2006.
60. Wang, Y., Infield, D., *Neural Network Modelling with Autoregressive Inputs for Wind Turbine Condition Monitoring*, SuperGen 2nd international Conference, Hangzhou 2012.

61. Campbell, C., *Lecture Note: Introduction to Support Vector Machine*, University of Bristol, 2008.
62. Vapnik, V.N., *The Nature of Statistical Learning Theory*, Springer-Verlag, New York, 1995.
63. [online]. Available: <http://www.quora.com/Support-Vector-Machines/What-does-support-vector-machine-SVM-mean-in-laymans-terms> (accessed 2nd Dec 2013), 2013.
64. Fletcher, T., *Support vector machines explained*, Tutorial paper, University College London, Mar. 2009.
65. Joachims, T., *Text categorization with support vector machines: Learning with many relevant features*, Springer Berlin Heidelberg, pp. 137-142, 1998.
66. Ball, N. M., Brunner, R. J., *Data mining and machine learning in astronomy*, International Journal of Modern Physics, Vol. 19(07), 1049-1106, 2010.
67. Nassim, L., Sheibat-Othman, N., Othman, S., *Support vector machines for fault detection in wind turbines*, In Proceedings of IFAC World Congress, vol. 2011, pp. 7067-7072. 2011.
68. Widodo, A., Yang, B. S., *Support vector machine in machine condition monitoring and fault diagnosis*, Mechanical Systems and Signal Processing, Vol. 21, 2560-2574, 2007.
69. An, X. L., Jiang, D. X., Li, S. H., Chen., J., *Fault diagnosis of direct-drive wind turbine based on support vector machine*, In Journal of Physics: Conference Series, vol. 305, no. 1, IOP Publishing, 2011.
70. Samanta, B., *Gear fault detection using artificial neural networks and support vector machines with genetic algorithms*, Mechanical Systems and Signal Processing 18, no. 3, pp. 625-644, 2004.
71. Kusiak, A., Zheng, H., Song., Z., *On-line monitoring of power curves*, Renewable Energy 34, no. 6, pp. 1487-1493, 2009.

72. Kusiak, A., Verma, A., *A Data-Mining Approach to Monitoring Wind Turbines*, Sustainable Energy, IEEE Transactions on , vol.3, no.1, pp.150,157, Jan. 2012
73. Kollar, D., Friedman., N., *Probabilistic graphical models: principles and techniques*, The MIT Press, 2009.
74. Agosta, J. M., Gardos, T., *Bayes network smart diagnostics*, Intel. Technol. J., vol. 8, no. 4, pp. 361 -372, 2004.
75. Hujer, T., *Design and Development of a Compound DSS for Laboratory Research*, 2011.
76. Murphy, K., *A brief introduction to graphical models and Bayesian networks*, Oct, 2001.
77. Chen, B., Tavner, P. J., Feng, Y., Song, W., Qiu, Y., *Bayesian Networks for Wind Turbine Fault Diagnosis*, EWEA Copenhagen 2012.
78. Carta, J.A., Velázquez, S., Mat ás, J.M., *Use of Bayesian networks classifiers for long-term mean wind turbine energy output estimation at a potential wind energy conversion site*, Energy Conversion and Management, Vol.52, Issue 2, pp. 1137-1149, February 2011.
79. Muller, A., Weber, P., Salem, A. B., *Process model-based dynamic Bayesian networks for prognostic*, In Fourth International Conference on Intelligent Systems Design and Applications, ISDA 2004, August, 2004.
80. Lian, Y., Pattison, D., Kenyon, A., Segovia-Garcia, M., Quail, F., *Wind Turbine Gearbox Ice Sensing and Condition Monitoring for Fault Prognosis and Diagnosis*, COMADEM Helsinki 2013.
81. Bockhorst, F.K., Gross, K.C., Herzog, J.P., Wegerich, S.W., *MSET Modeling of Crystal River-3 Venturi Flow Meters*, International Conference on Nuclear Engineering, San Diego, 1998.

82. Hines, J.W., Garvey, D., Seibert, R., Usynin, A., *Technical Review of On-Line Monitoring Techniques for Performance Assessment*, Volume 2: Theoretical Issues, United State Nuclear Regulatory Commission, May 2008.
83. Wegerich, S.W., *Similarity based modeling of time synchronous averaged vibration signals for machinery health monitoring*, Proceedings in Aerospace Conference, vol. 6, pp. 3654-3662. IEEE, 2004.
84. Guo, P., Infield, D., Yang, X., *Wind Turbine Generator Condition-Monitoring Using Temperature Trend Analysis*, IEEE Transactions on Sustainable Energy, Jan. 2012, vol. 1, (3), pp.124-133.
85. Black, C.L., Uhrig R.E., Hines J.W., *System Modeling and Instrument Calibration Verification with a Nonlinear State Estimation Technique*, Maintenance and Reliable Conference, Knoxville, TN, May 1998.
86. Hines, J.W., Usynin., A., *MSET performance optimization through regularization*, Nuclear Engineering and Technology, vol. 37, no. 2, 2005.
87. Wang, Y., Infield, D., *Supervisory control and data acquisition data-based non-linear state estimation technique for wind turbine gearbox condition monitoring*, Renewable Power Generation, IET, vol.7, no.4, pp.350-358, July 2013.
88. *Wind Turbines—Part 12-1: Power Performance Measurements of Electricity Producing Wind Turbines*, British Standard, IEC 61400-12-1, 2006.
89. Kusiak, A., Zheng H.Y., Song, Z., *Models for Monitoring Wind Farm Power*, Renewable Energy, vol. 34, pp. 583-590, 2009.
90. Jolliffe, I.T., *Principal Components Analysis*, 2nd Edition. Springer Series in Statistics, 2002.
91. Jeon, J., Taylor, J., *Using Conditional Kernel Density Estimation for Wind Power Density Forecasting*, Journal of the American Statistical Association, vol. 107, no. 497, pp. 66-79, 2012.

92. Gill, S., Stephen, B., Galloway, S., *Wind Turbine Condition Assessment Through Power Curve Copula Modelling*, IEEE Transactions on Sustainable Energy, vol. 3, no. 1, pp. 94-101, Jan. 2012.
93. Wang, Y., Infield, D.G., Stephen, B., Galloway, S. J., *Power Curve Based Online Condition Monitoring for Wind Turbines*, COMADEM Helsinki 2013.
94. Schlechtingen, M., Santos I.F., Achiche, S., *Using Data-Mining Approaches for Wind Turbine Power Curve Monitoring: A Comparative Study*, IEEE Transactions on Sustainable Energy, vol. 4, no. 3, pp. 671-679, July 2013.

### 3. Power curve based wind turbine condition monitoring

Power curve measurements from the SCADA system provide a conventional and effective means of assessing the performance of a wind turbine, both commercially and technically. Increasingly high wind penetration in power systems and offshore accessibility issues make it even more important to monitor the condition and performance of wind turbines based on timely and accurate wind speed and power measurements.

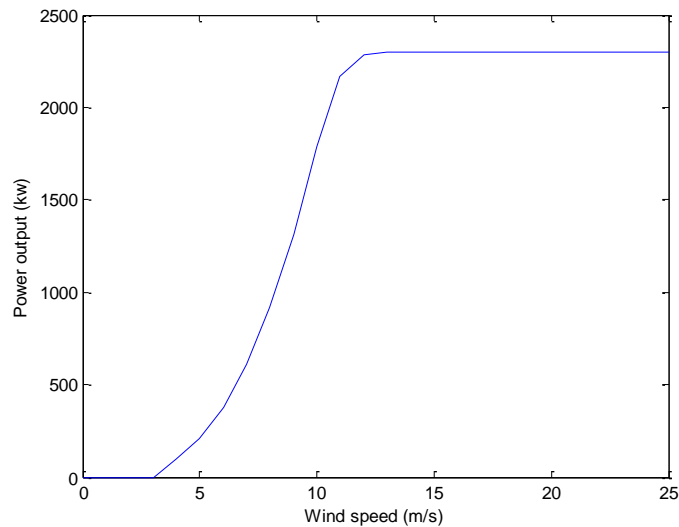


Figure 3-1: Typical manufacturer's power curve

An example of manufacturer's power curve for a pitch regulated commercial wind turbine with rated power of 2.3MW is shown in Figure 3-1, where the cut-in and cut-out wind speeds of this specific wind turbine are 3m/s and 25m/s respectively, and the relationship between wind speed and output power shows the usual nonlinear features. No power production from the turbine is available for wind speed below the cut-in and above the cut-out values. For wind speed in the range between the cut-in and rated wind speed level, the central controller maintains the turbine operation at an optimal power coefficient by controlling the generator torque, and the turbine output power is limited to rated power above the rated wind speed by adjusting the blade pitch angle [95].

This chapter will first introduce the power curve basics and the associated data correction and uncertainty presentation. A Copula-based joint probability model, which is capable of capturing the complex nonlinear relationship between the power output and wind speed, will then be employed to exclude the outliers in the reference data. This will lead to more reliable subsequent fault detection, which involves a bin-by-bin based real-time power curve comparison method. A general fault logic will be outlined for interpreting aspects of power curve deviations, followed by a case study of successful detection of yaw misalignment to demonstrate the effectiveness of the proposed method. Finally the application of the proposed method to pitch performance condition monitoring will also be briefly discussed.

### **3.1. Data pre-processing and power curve presentation**

Measurements retrieved from the SCADA system consist of 10-minute averaged values of nacelle anemometer wind speed, turbine power output, ambient temperature and atmospheric pressure. The latter two measurements determine the air density,  $\rho$ , to which the power in the wind is proportional, and to which the turbine power output,  $P$ , can be assumed to be proportional for below-rated operation:

$$P = \frac{1}{2} \rho \pi R^2 v^3 C_p \quad (3-1)$$

where  $R$  represents the radius of turbine rotor;  $v$  is the free wind speed experienced by the rotor which is different from the nacelle anemometer measurement and  $C_p$  indicates the power coefficient.

The wind speed measurement from the nacelle anemometer needs to be corrected to the free-stream rotor wind speed in order to reflect the actual relationship with the turbine output power as expressed in Equation (3-1). In order to make fair comparisons between operational power curves, the acquired power curve measurements are also required to be corrected to standard air density conditions (15°C and 101.325kPa). The details for both of these corrections will be shown in following sub-sections. And the bin-averaged

power curve based on the corrected data will be presented in Section 3.1.3 with the error bars indicating the uncertainty associated with the data.

### **3.1.1. Nacelle anemometer wind speed correction**

The accurate measurement of wind speed is essential for the reliability of both the annual energy production estimation and power curve performance tests. The IEC standard [88] specifies that the meteorological mast position should be between 2 and 4 rotor diameters upwind of the testing turbine, with a preferable distance of 2.5 rotor diameters and at approximately the hub height. However, these specifications are mainly used for initial contractual obligation verification of the power performance performed by turbine manufacturers [89], and are rarely met for individual turbine measuring purpose in reality due to the complex terrain in certain cases and the expensive cost involved in purchasing and installing the meteorological mast [96].

Therefore the wind farm operators tend to use the turbine nacelle anemometer reading as an alternative for wind speed measurement collection. The nacelle anemometer reading, however, cannot accurately represent the free-stream wind speed experienced by the turbine rotor since the incident wind is disturbed by the rotor disc itself. So a wind speed conversion from the anemometer measurement to the free-stream value is established based on the relationship between the anemometer and meteorological mast readings [96, 97, 98]. Reference [97] fits a 5<sup>th</sup> order polynomial curve between these two variables and states that the established relationship could only be transferred to other turbines of the same make and type if the rotor settings and the nacelle anemometer mounting remain unchanged plus the terrain is flat. But the authors in references [96, 98] claims that linear regression is adequate for the mast-nacelle anemometer relation.

The nacelle anemometer measurement can theoretically be approximately a third lower than the meteorological mast reading due to the fact that wind turbines are designed to operate at optimal  $C_p$  for below rated region, and the value of  $C_p$  is related to the axial flow induction factor, which indicates the proportion of wind speed that is slowed down at the rotor, by Equation (3-2), where the maximum  $C_p$  occurs when  $a = 1/3$  [99].

$$C_p = 4a(1 - a)^2 \quad (3-2)$$

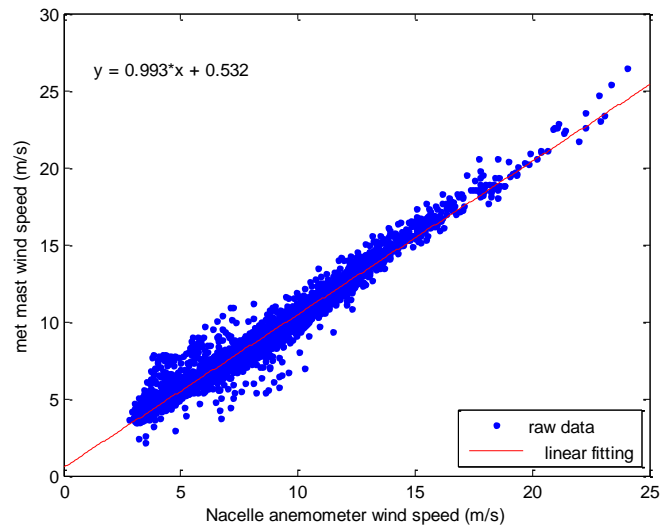


Figure 3-2: Relationship between Met mast and Nacelle anemometer wind speed for Turbine 1

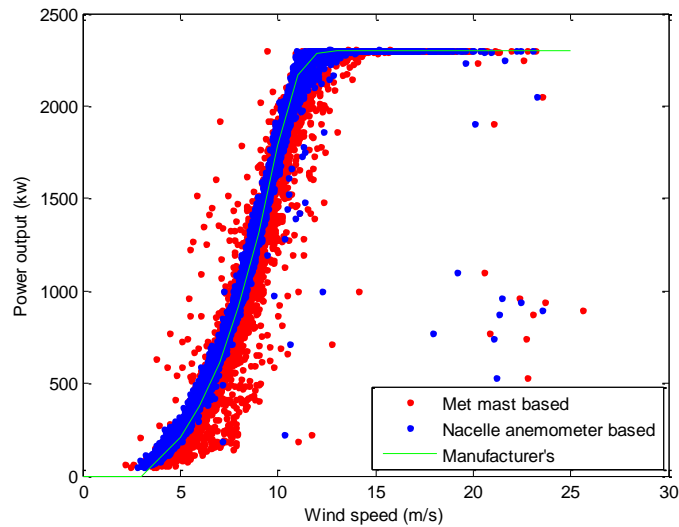


Figure 3-3: Comparison of power curves based on Met mast and Nacelle anemometer wind speed measurements for Turbine 1

An example of relationship between the meteorological mast reading and nacelle anemometer measurement (from the SCADA record) of wind speed from a healthy operational turbine (hereafter referred to as ‘Turbine 1’) is shown in Figure 3-2 in which

a linear regression fits the data remarkably well. It can be seen from this figure that the values for these two wind speed measurement are quite similar, which differs from the expectation of 1/3 difference as explained in the analysis above, implying that the nacelle anemometer measurement in the SCADA record may have already been corrected. This is also confirmed by the excellent matching between the nacelle anemometer based power curve with air density corrected (which will be introduced in the following section) and the manufacturer's curve as shown in Figure 3-3, which would otherwise show significant deviations from the reference curve. So, in the absence of any confirmation from the turbine operator, it is assumed that the nacelle anemometer measurement in the SCADA system has already been corrected to the free-stream value. And the same assumptions are made for the following analyses in this chapter, unless some systematic and significant deviations occur throughout the entire power curve even for healthy turbine operation.

Much less scatter can be observed in the power curve generated from the nacelle anemometer readings than from the met mast based power curve, as shown in Figure 3-3. This is because of the increased proximity of the nacelle anemometer to the rotor. The increased precision in the results indicates that the power curve based on the corrected nacelle anemometer wind speed could provide more accuracy.

### **3.1.2. Air density correction**

Air density correction has to be applied to the power curve measurements before any power curve based analyses can be undertaken since the power captured by the turbine rotor is proportional to the density of air passing through it as mentioned earlier. According to IEC standard 61400-12-1 [88], the air density correction for actively controlled wind turbine is conducted with regards to wind speed only using Equation (3-3)

$$V_C = V_M \left[ \frac{\rho}{1.225} \right]^{1/3} \quad (3-3)$$

where  $V_M$  and  $V_C$  are the measured and corrected wind speed, respectively. And the ambient air density,  $\rho$ , can be calculated by Equation (3-4)

$$\rho = 1.225 \left[ \frac{288.15}{T} \right] \left[ \frac{B}{1013.3} \right] \quad (3-4)$$

where  $T$  represents the ambient temperature in degrees absolute and  $B$  is the barometric pressure in mbar, both of which are 10-minute averaged values from the SCADA data. Usually the value of  $B$  is assumed to be the standard value of 1013.3 mbar, leaving  $T$  to be the only relevant parameter for air density calculation.

The corrected measurements are under standard air density conditions and could therefore be used for comparison purpose. It should be noted that the air density corrected wind speed is distinct from the corrected anemometer wind speed as introduced in previous section, and the anemometer wind speed correction, if needed, should be undertaken before the air density correction.

### 3.1.3. Sources of uncertainty

IEC standard [88] specifies the use of the ‘method of bins’ to form the power curve. SCADA data are grouped and averaged in 0.5 m/s wind speed bins, with uncertainties being illustrated by error bars for each bin. According to reference [100] the uncertainties associated with the power curve measurement can be classified as Category A, which takes account of the standard deviation of the scatter in each bin, and Category B, which is based on the knowledge of instrument. For the analyses in this chapter, only uncertainties associated with Category A are considered since the accuracy of power curve related sensors is unavailable in most SCADA systems. The uncertainties associated with Category B will be included in the power curve measurements and presented by the illustration. The main uncertainties,  $S_j$ , in Category A are for power variation and the appropriate expression is shown in Equation (3-5) for each wind speed bin  $j$ .

$$S_j = \frac{\sigma_j}{\sqrt{K_j}} \quad (3-5)$$

where  $\sigma_j$  represents the standard deviation of the power measurement in the  $j^{\text{th}}$  bin and  $K_j$  is the number of points in this bin. The term  $\frac{1}{\sqrt{K_j}}$  results from the Central Limit Theorem's measure of uncertainty, which gives an indication of the confidence in the expected value of the power curve at that wind speed point based on the number of observations in the bin [100].

Figure 3-4 shows power curve measurements for a two-month period (depicting 7257 pairs of data) of fault free operation from a pitch regulated variable speed wind turbine (hereafter referred to as 'Turbine 2') with a nominal rating of 2MW. The corresponding power curve, produced by binning as outlined above, is shown in Figure 3-5, where the error bars represent the uncertainties. The relatively large error bars at the high wind speed (values over 20 m/s) bins are not important here because it is known that the maximum power generated is well controlled and determined by the turbine control system, [101], as shown in Figure 3-4. These are due to the insufficient numbers of points in these particular bins reflecting the occasional nature of the very high wind speeds.

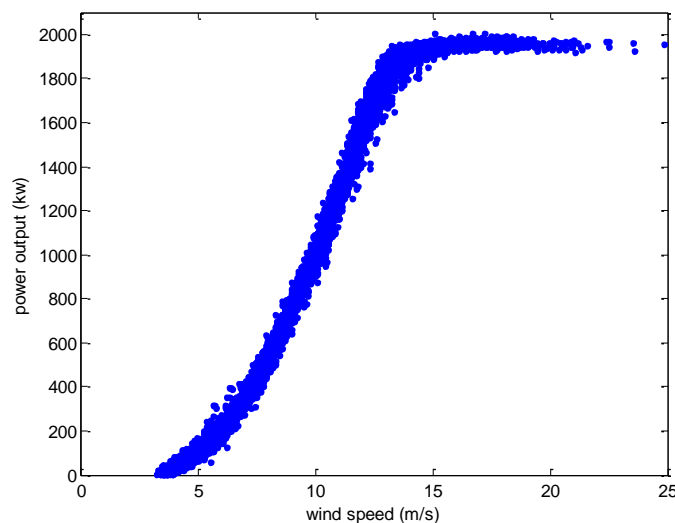


Figure 3-4: Scatter plot of power curve measurements for Turbine 2

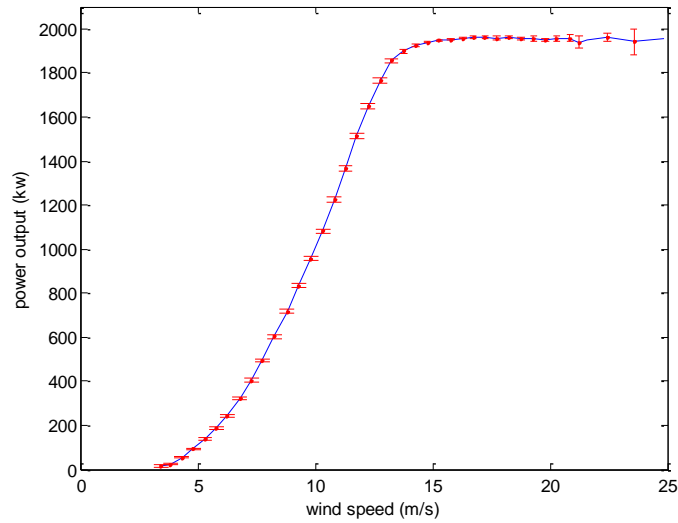


Figure 3-5: Power curve with error bars showing data uncertainty for Turbine 2

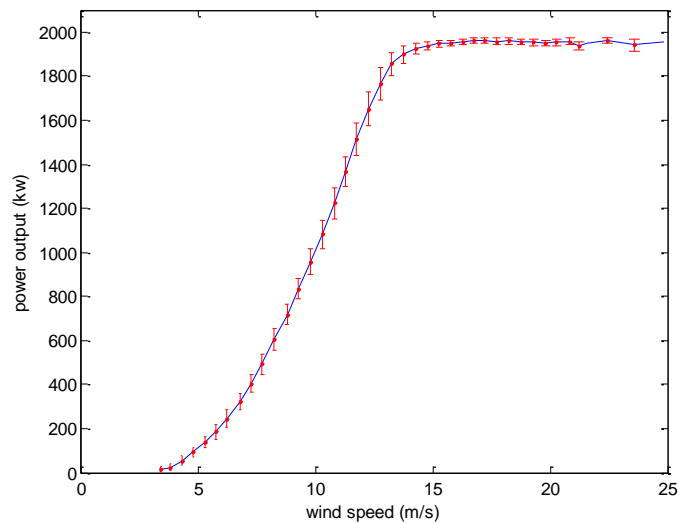


Figure 3-6: Power curve with error bars showing data dispersion for Turbine 2

The power curve has been re-plotted in Figure 3-6 with errors bars showing the value of the unmodified  $\sigma$ . In this case the size of error bars indicates the spread of data. It can be seen that the largest values of  $\sigma$  occur around and just below the rated wind speed of 13.5 m/s for reasons that will be discussed in Section 3.2.3.

### **3.2. Reference power curve construction using Copulas based model**

To be capable of early fault detection, small changes in power curve need to be detectable and an accurate power curve reference is required to guarantee the reliability of the subsequent fault detection. The reference power curve in this chapter is constructed based on the turbine operational data rather than using the manufacturer's data due to the consideration of both the environmental factors (such as wind shear, wind veer and turbulence) and the effect of bias errors associated with instruments as mentioned in the previous section.

Examination of most SCADA data reveals ten minute averaged power-wind speed pairs (as binned to create power curves) that lie well away from the bulk of points, and thus can be regarded as outliers. There are many reasons for such "erroneous" data. A common example is when a turbine changes status part way through the ten minute period, for example due to turbine cut out. The mean output will thus be much reduced, but the measured wind speed will be unaltered, such as those significant and isolated deviations illustrated in Figure 3-3 for Turbine 1. Not all SCADA data systems flag up such changes in status. This means that other approaches must be used to exclude such data, prior to final power curve determination. Here we make use of Copulas, which are capable of characterising multivariate nonlinear relationships in the form of multivariate probability distributions based on the individual univariate probability distributions [102].

The mathematical background of Copulas will be introduced first in this section, with particular attention being paid to the Frank Copula model and the Gaussian Mixture Copula Model (GMCM). The GMCM will be used to capture the two-dimensional power curve distribution using the operational data as illustrated in Figure 3-4 for Turbine 2 and the model's goodness of fit will be compared with that for the Frank Copula model and the Gaussian Mixture Model (GMM) using the Bayesian Information Criterion (BIC). The obtained bivariate probability distribution will then be used for

reference power curve construction by rejecting any statistically significant outliers present in the power curve measurements. An example of power curve cleaning using the Copulas for Turbine 1 will be presented at the end of this section.

### 3.2.1. Expressing Dependency through Copula Statistics

The term Copula was first employed by Sklar to mean bringing together the complex nonlinear dependency structure of a multivariate data set with its one-dimensional marginal distributions [103]. Sklar's theorem [102] forms the foundation for the development of Copula model development; according to this theorem, if a joint cumulative distribution function (CDF),  $F$ , exists for the random variables  $(x_1, x_2, \dots, x_n) \in R^n$ , then there must exist a Copula function  $C$  such that:

$$F(x_1, x_2, \dots, x_n) = C(F_1(x_1), F_2(x_2) \dots, F_n(x_n)) \quad (3-6)$$

where  $F_i(x_i)$  is the  $i^{\text{th}}$  marginal CDF for the  $i^{\text{th}}$  random variable. The Copula function  $C$  is uniquely determined if the  $F_i(x_i)$  are continuous, otherwise  $C$  is only unique within the value range of the marginal distribution [104]. Since the univariate marginal distributions lie within interval  $(0, 1)$ , the Copula function is defined on the unit hypercube, (i.e.  $(0, 1)^n \rightarrow (0, 1)$ ), [105]. If the joint CDF,  $F$ , the marginal CDF,  $F_i$ , and the Copula function,  $C$ , are all differentiable, then the joint probability density function (PDF) can be derived by differentiating both sides of Equation (3-6). The joint PDF,  $f$ , so obtained is given by:

$$f(x_1, x_2, \dots, x_n) = c(u_1, u_2, \dots, u_n) \times f_1(x_1) \times f_2(x_2) \times \dots \times f_n(x_n) \quad (3-7)$$

where  $f_i$  denotes the  $i^{\text{th}}$  marginal PDF and the original marginal CDF,  $F_i$ , is represented by  $u_i$  for simplicity. And  $c$  represents the Copula density function that unifies them.

#### 3.2.1.1. The Frank Copula

The choice of Copula is governed by the tail dependence implied by the data. In the bivariate case, tail dependence is expressed in terms of the relationship between the extreme values of the two marginal distributions. If one variable has exceeded a

particular threshold and the other has also exceeded this threshold with proportional likelihood, then the distribution is tail dependent [106]. Tail dependence can be visualised as a tightening of the scatter of observations around the extremes of the distribution, while low tail dependence will be exhibited as a greater degree of scatter. Reference [107] presents the multivariate joint distribution based on a variety of Archimedean Copulas which are introduced in depth in reference [108]. It shows that the Clayton Copula exhibits greater dependency in the lower tail; the Gumbel Copula has higher upper tail dependence; while the Frank Copula is symmetric in both tails. The distribution pattern and the characteristics of the tail dependency of the Frank Copula Model are consistent with those of the power curve variables as has been shown in reference [92], for which reason this particular Copula is selected here. The Frank Copula density function,  $c_{Frank}(u_1, u_2, \delta)$ , is given by,

$$c_{Frank}(u_1, u_2, \delta) = \frac{\delta \eta e^{-\delta(u_1+u_2)}}{[\eta - (1 - e^{-\delta u_1})(1 - e^{-\delta u_2})]^2} \quad (3-8)$$

where  $\eta = 1 - e^{-\delta}$  [108]. As shown in Figure 3-7, the larger the value of  $\delta$ , the stronger the dependence is between the variables related by the Frank Copula [108] throughout their bivariate distribution. The parameter  $\delta$  can be obtained by optimizing the model's fit for a given bivariate dataset based on some criteria such as maximum likelihood.

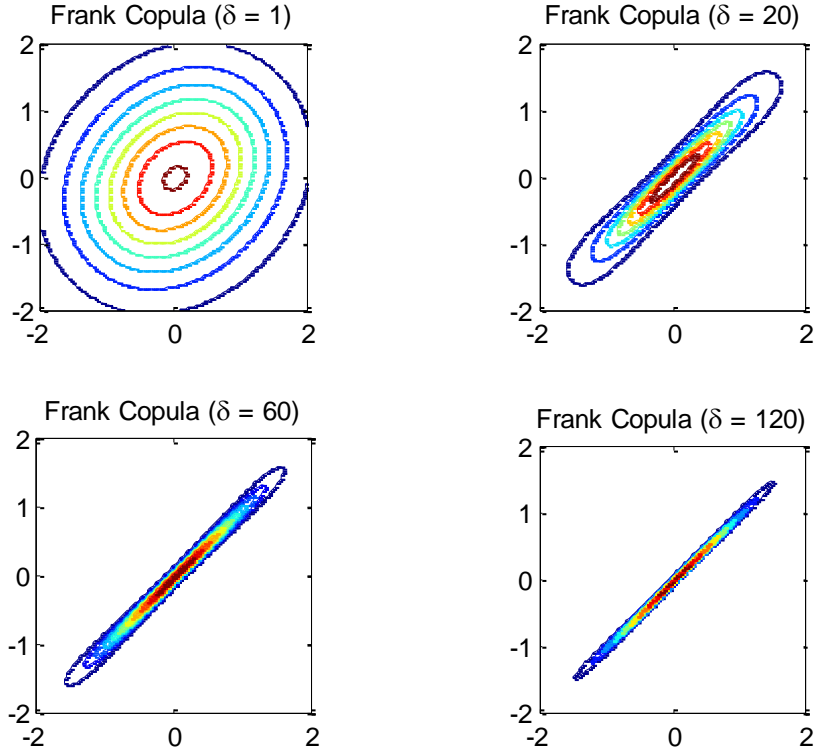


Figure 3-7: The impact of  $\delta$  value on variable dependency

### 3.2.1.2. The Gaussian Mixture Copula Model (GMCM)

Accommodating the complex shape of the power curve joint probability density is beyond the abilities of classical multivariate distributions and would necessitate a mixture model with a large number of parameters, running the risk of over-fitting and losing generalisation capabilities; where the Copula mixture adds benefit is in identifying the modes without requiring a large number of components to represent their dependency structure.

The GMM probability density function  $\varphi$ , comprises a weighted sum of  $M$  Gaussian density components, is given by

$$\varphi(x_1, x_2, \dots, x_n; \theta) = \sum_{k=1}^M \alpha_k N(x_1, x_2, \dots, x_n; \theta_k) \quad (3-9)$$

where  $\alpha_k$  are the weights for different components and all the elements of  $\alpha_k$  sum to unity. Parameter  $M$  indicates the modality number and will be determined in Section 3.2.2.1. Parameter  $\theta_k = \{\mu_k; \Sigma_k\}$ , with  $\mu_k$  representing the mean vector and  $\Sigma_k$  being the covariance matrix for the  $k^{\text{th}}$  component [109]. And the parameter set,  $\theta$ , combines the weight assignment and the statistics in  $\theta_k$  for each Gaussian component. Multivariate Gaussian distributions can only express linear dependency, and while the mixture model framework may afford a piecewise approximation of non-linearity, it is therefore clear that mixture components with a more complex dependency structure would allow a superior fit.

A Gaussian Mixture Copula Model (GMCM), [105], derived from a GMM with no implied covariance is capable of characterising multidimensional nonlinear statistics for multimodal data. The GMCM density function, derived from the GMM expression of Equation (3-9), is defined as:

$$c_{GMCM}(u_1, u_2, \dots, u_n; \theta) = \frac{\varphi(\Phi_1^{-1}(u_1), \Phi_2^{-1}(u_2), \dots, \Phi_n^{-1}(u_n); \theta)}{\prod_{i=1}^n \varphi_i(\Phi_i^{-1}(u_i))} \quad (3-10)$$

where  $\varphi_i$  and  $\Phi_i^{-1}$  denote the marginal density of GMM and the corresponding inverse distribution along each dimension. The parameter set  $\theta$  is optimised by maximising the log-likelihood function of the GMCM Copula function as shown in Equation (3-10).

Equation (3-7) is used to calculate the joint probability distribution based on the fitted Copula density function: Equation (3-8) for the Frank Copula model; and Equation (3-10) for GMCM, with the marginal PDF for each variable in Equation (3-7) is achieved through kernel density estimation.

### 3.2.2. Power curve density modelling with Copulas

In the specific application to wind turbine power curve analysis, the Copula model links the marginal distribution of wind speed and turbine power output to their two-dimensional joint probability density function.

The basic steps for Copula based outlier removal are as follows:

1) Pre-processing of power curve measurements

This includes the removal of null entries followed by air density correction of the raw data.

2) Model order determination

The modality number is derived using the self-organising map in Section 3.2.2.1 to facilitate the fitting of the GMCM.

3) GMCM fitting

In [105] a GMCM parameter optimisation process is proposed that is based on Expectation Maximization (EM) [110] followed by application of a gradient descent optimisation. The reason for this is the non-convex form of the log-likelihood function for the GMCM density function. The solution obtained from the Maximisation step of EM is not guaranteed to find the global optimum, thus necessitating the use of the Gradient Descent algorithm with initial conditions assigned by the EM solution within an iterative loop for global optimum investigation. This methodology for GMCM parameter estimation is retained in this work.

4) Outlier rejection

The outliers of power curve measurements are filtered using a probability contour based on the achieved density distribution.

The robustness of GMCM is shown by comparing goodness of fit between GMCM, the Frank Copula, and GMM, using the Bayesian Information Criterion (BIC).

### **3.2.2.1. Model order selection**

The optimal data modality is required when using mixture models such as GMCM. The self-organising map (SOM), originally conceived by Teuvo Kohonen, [111], is

employed here because of its ability to cluster the data in an unsupervised-learning manner. The main function of SOM is to construct a nonlinear projection of high-dimensional data onto a low-dimensional (usually 2D) space, in which the clustering of data and its topology are clearly shown and easily interpreted [111].

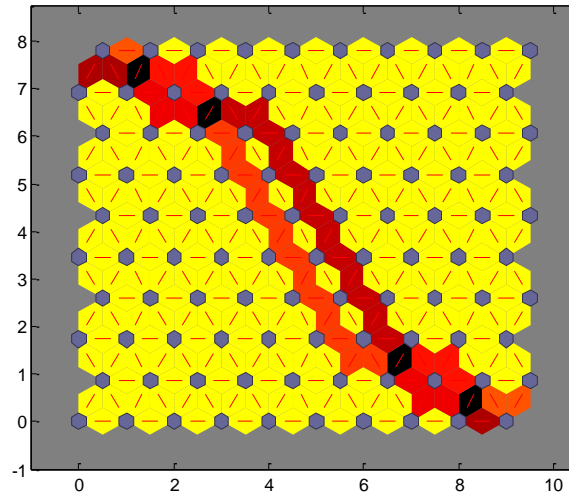


Figure 3-8: SOM neighbour weight distances for Turbine 2

The data set for Turbine 2 as shown in Figure 3-4 is used to determine the number of modes present in the data which will in turn inform the choice of modality for the optimal model. Three distinct data regions can be observed in this figure: near cut-in, below which the turbine does not operate (3.5 m/s in this example); above rated (13.5 m/s); and the region in between.

A 10×8 two-dimensional SOM is used to visualise the data clustering. The learning result is presented in the form of neighbour weight distances as illustrated in Figure 3-8, where the blue hexagons represent the neurons and neighbouring neurons are connected by red lines. The background colour indicates the distances between the neurons, with darker colours representing larger distances and lighter colours representing smaller distances. Three segments can be observed based on the colour coding scheme introduced: two distinct triangles at bottom left and top right; and a relatively weak

segment located approximately along the diagonal. They are separated from each other by dark colour bands.

The model order for this power curve data is three, corresponding to the number of distinct regions into which the space is divided, which matches the original assumption of three parts to the power curve, although of course the plot of weight distances does not directly reproduce the original data. This step of model order determination could be omitted in the future since almost all the commercial power curves share common characteristics, indicating a distinct model mode of three.

### 3.2.2.2. *Fitness analysis*

GMCM is capable of clustering data automatically once the data modality has been identified, as described in the previous section. The same SCADA data as used for Turbine 2 in Section 3.1.3 are used here to assess the model's fitness. The Bayesian Information Criterion (BIC), [112], is used here for model selection, with lower values of BIC indicating better models. It is based on the log-likelihood function,  $L(\Theta|x_1, x_2, \dots, x_n)$ , which sums the log of the probabilities of all data points and provides a convenient and easily calculated metric for goodness of fit, [113]. Overfitting is avoided by introducing a penalty term,  $p \log(N)$ , which takes account of the model complexity. BIC is defined as:

$$BIC = -2L(\Theta|x_1, x_2, \dots, x_n) + p \log(N) \quad (3-11)$$

where the log-likelihood function,

$$L(\Theta|x_1, x_2, \dots, x_n) = \sum_{i=1}^N \log f(x_1(i), x_2(i), \dots, x_n(i)|\Theta) \quad (3-12)$$

and  $N$  represents the sample size in both Equations (3-11) and (3-12), and has the value of 7257 in this case. And  $p$  is the number of parameters. For the Frank Copula  $p = 1$  whilst for the GMM and GMCM, it can be calculated using Equation (3-13), [114].

$$p = M(1 + n + \frac{n(n + 1)}{2}) \quad (3-13)$$

where  $M$  denotes the modality number, which is 3, as determined in the previous section and  $n$  indicates the data dimension, which is taken as 2 in this work. This results in a  $p$  value of 18.

	Bayesian Information Criterion value
GMCM	110597
Frank	112415
GMM	114993

Table 3-1: Goodness of fit for three models using BIC values

The different models (GMCM and Frank Copula) can be compared by calculating BIC for identical input data samples. Figure 3-9(a), Figure 3-9(b) and Figure 3-9(c) illustrate the probability density fitting for the GMCM models, Frank Copula and the GMM model respectively. The GMM is included here due to its capability of dealing with multimodal data, as introduced in Section 3.2.1.2. The BIC values of these three models are listed in Table 3-1, from which it can be seen that the GMCM model minimises BIC. The GMCM also has the advantage of dealing with multivariate distributions, which would readily accommodate more variables for further applications such as the inclusion of the environmental factors, whereas the Frank (or Archimedean) Copula could only be used for bivariate data characterisation. In conclusion, the Gaussian Mixture Copula Model is thus chosen for outlier rejection.

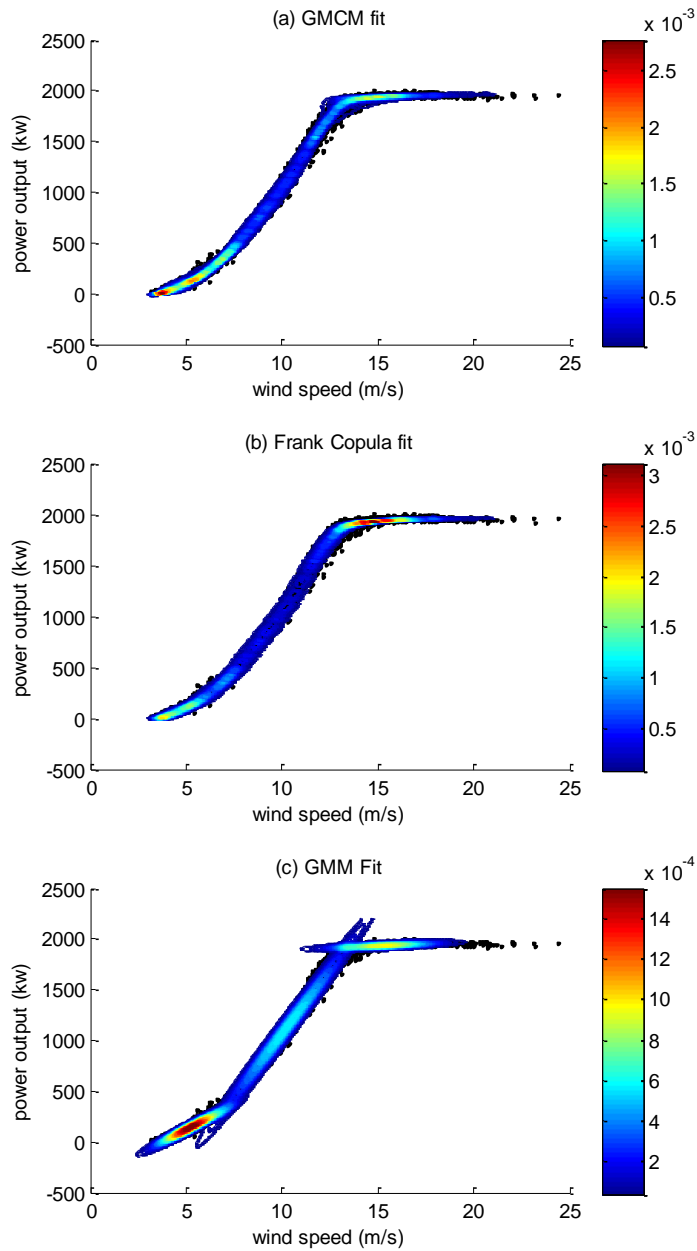


Figure 3-9: Fitness comparison of three presented models for Turbine 2

### 3.2.3. Power curve outlier rejection example using the GMCM

The previous section has demonstrated the goodness of fit of the GMCM for the power curve measurements. The obtained bivariate probability distribution can then be used for

reference power curve construction by rejecting any statistically significant outliers present in the power curve measurements. An outlier rejection example of the power curve illustrated in Figure 3-3 for Turbine 1 is presented in this section to verify the effectiveness of the proposed method.

For a modern pitch regulated variable speed wind turbine, good power control is available above the rated wind speed. It is shown in Figure 3-6 that the greatest scatter, as indicated by the error bars of size  $\sigma$ , occurs at around rated power where the turbine is continually changing between below rated operation where speed is varied to maximise aerodynamic efficiency, and above rated power where electronic control limits current and power from the generator [115]. The lower variance at the extremes means that the tail dependency is not likely to be a major source of error. A probability contour level at three standard deviations for data in the 0.5 m/s wind speed bin closest to rated wind speed is therefore judged to be appropriate. Points lying outside this contour are regarded as outliers and are eliminated accordingly.

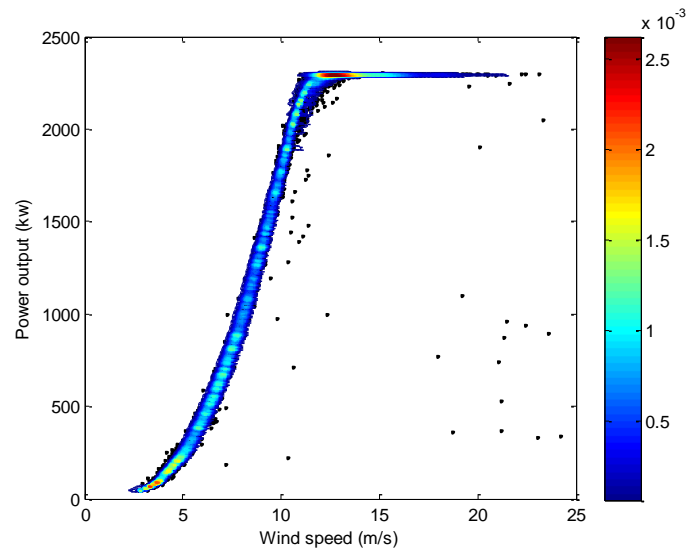


Figure 3-10: GMCMM fitting to the power curve example from Turbine 1

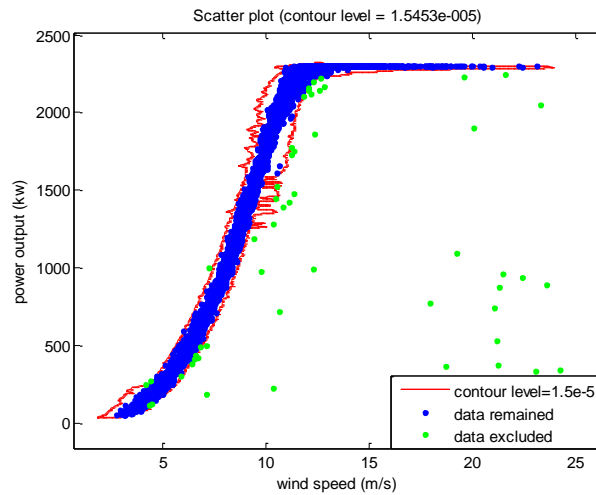


Figure 3-11: Data exclusion for Turbine 1 using GMCM based density contour

Figure 3-10 illustrates the GMCM fitting of power curve measurement for Turbine 1. Figure 3-11 shows the same power curves after outliers have been identified using the fitted Copulas and the density contour (defined as  $3\sigma$ ) illustrated by the red line, with green points indicating power curve measurements that are to be excluded. It can be seen from Figure 3-12 that the precision of the cleaned power curve has been significantly improved, which demonstrates the effectiveness of the proposed Copulas based outlier rejection method and the reliability of the subsequent anomaly detection is expected to be increased as well.

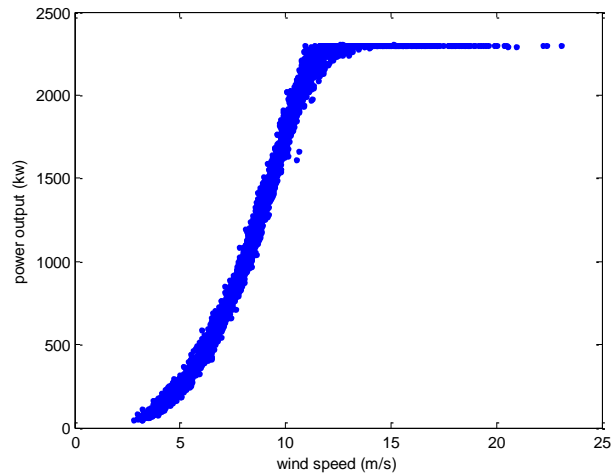


Figure 3-12: Power curve for Turbine 1 after cleaning

### **3.3. Bin-by-bin based online power curve condition monitoring**

Based on the reference power curve as constructed above, a power curve comparison/tracking method has been developed in this section to identify any statistically significant deviation from the reference power curve on a bin by bin basis. A crude filtration is first undertaken for each incoming 10-min SCADA data to remove the power curve pairs that contain invalid measurement such as negative or null values. The valid measurements with air density correction are then input to the proposed power curve comparison method which will be introduced in the following section. And the Welch's hypothesis test is employed here for the anomaly detection in each wind speed bin.

#### **3.3.1. Rolling power curve realization**

A rolling power curve idea has been developed for the online monitoring purpose motivated by consideration of both accuracy and efficiency. It is basically a real-time updating and detecting of turbine power output deviation on a bin-by-bin basis. Here the same wind speed bin interval of 0.5 m/s is utilized and the choice of 5 fixed points per bin is used as this provides the best compromise between accuracy and efficiency. A three-dimensional storage cell is employed to save the value of wind speed, power output and date&time information for each different wind speed bin. The data in the storage cell are continuously updated using the first-in-last-out rule for each incoming 10-min power curve data pair with air density corrected. Any significant deviations detected from the reference curve will be recorded with both the anomalous power curve values for the specific bins and the corresponding date&time information.

In this case, the detected results are recorded in the alarm log when two adjacent wind speed bins trigger the alarm simultaneously. The use of two adjacent detections is to reduce false alarms caused by isolated noise but clearly there is a trade-off here against the speed of detection. The Welch's hypothesis test, as will be introduced next, is employed here to determine whether the reference and rolling power values for any particular bin are inconsistent at a level of statistical significance.

### 3.3.2. Anomaly detection: the Welch's hypothesis test

According to [116], Welch's t test is an extension of Student's t test used when the variances of two testing samples are likely to be unequal. As such, it is used here to identify statistically significant deviations in each wind speed bin.

$$t = \frac{\overline{X}_{ref} - \overline{X}_{test}}{\sqrt{\frac{S_{ref}^2}{N_{ref}} + \frac{S_{test}^2}{N_{test}}}} \quad (3-14)$$

where  $\overline{X}$ ,  $S$  and  $N$  are the power average and standard deviation, and the sample size of the bin, with the subscripts ref and test indicating reference data and testing data, respectively. The probability of the test average falling below reference average is considered to be of significance when  $t > t_{\alpha}(v)$ , where  $t_{\alpha}(v)$  follows the student's t distribution with significance level,  $\alpha$ , and the number of degrees of freedom,  $v$ ,

$$v = \frac{\left(\frac{S_{ref}^2}{N_{ref}} + \frac{S_{test}^2}{N_{test}}\right)^2}{\frac{S_{ref}^4}{N_{ref}^2(N_{ref} - 1)} + \frac{S_{test}^4}{N_{test}^2(N_{test} - 1)}} \quad (3-15)$$

Note that the method could be easily extended to cover over-performance which is common and indicative of sensor error or poor calibration as will be discussed in the power curve fault logic in the next section. The corresponding modification is to add the criterion for the over-performance detection expressed as:  $t < -t_{\alpha}(v)$ .

The level of significance chosen will affect the balance between timely fault detection and reliability in terms of not producing false positives. It cannot thus be defined a priori; rather it should be selected based on operational experience and some sort of trial and error. Other requirements for anomaly detection can be added to help avoid false positives, for example putting minimum limits on the number of individual anomalous bin values.

### 3.4. General power curve fault logic

Statistically significant power curve deviations can be produced by technical problems in either the wind turbine itself or due to faults with the sensors, and they can also be the result of unusual environmental conditions such as extreme wind shear or veer and turbulence.

A trivial but instructive example is a power curve that exceeds the Betz limit below rated wind speed, but operates at rated power above rated wind speed. Since the power is as expected above rated, the power control and power measurement system would appear to be operating correctly and accurately. And there is no reason to believe this is not the case below rated, so the only obvious explanation is an under reading wind turbine anemometer (not uncommon with cup type anemometers).

A very provisional but general fault logic is presented below to indicate how analysis based on comparisons between a cleaned reference power curve and an updated, ideally real time, power curve for the same turbine might be interpreted for condition monitoring purposes. It is known that the environmental conditions have been taken into account to some extent by utilizing the operational data based reference, but these considerations are included in the fault logic below just in case of extreme cases.

- 1) Deviations above reference power curve could indicate:
  - a) Below rated wind speed: anemometer error, power transducer calibration error.
  - b) Above rated wind speed: controller setting error, power transducer calibration error.

Further confirmation can be achieved by investigation of the value of  $C_p$ . A  $C_p$  value exceeding the Betz limit ( $16/27$ ) is a clear indication of measurement sensor (anemometer or power transducer) error.

- 2) Consistent deviations below the reference/manufacture's power curve for below rated region could indicate: possible damage to the blade; inappropriate blade

pitch setting or control; yaw system issues; or possibly very large wind shear or wind veer [117].

- 3) Significant deviations above the reference power curve in the low wind speed region with the deviations falling to below the reference curve above rated power can be the result of high turbulence [117].

### **3.5. Yaw misalignment case study**

A case study of wind turbine exhibiting rotor yaw misalignment is presented in this section to verify the proposed method. The reference power curve is constructed using measurements for a three-month period of fault free operation from a pitch regulated variable speed wind turbine (referred to as ‘Turbine 3’) with a nominal rating of 2.5MW. All the power curve measurements used here have been air density corrected and it is assumed that the SCADA wind speed has been corrected to the free-stream value.

Figure 3-13 illustrates the identification of outliers for the selected data using the Copula method, with outliers to be excluded coloured green, in contrast to acceptable data coloured blue; the red line is the probability contour corresponding to  $3\sigma$  for outlier identification as explained in Section 3.2.3. The power performance data cleaned in this manner become more precise and they are then binned in the usual 0.5m/s wide wind speed intervals. The corresponding bin averages that make up the reference power curve together with the manufacturer’s curve are shown in Figure 3-14 with error bars indicating the Category A associated uncertainties for each bin. The constructed reference shows excellent agreement with the manufacturer’s curve, indicating the suitable selection of data, although some slight deviation can be observed. This disagreement is known to be due to the environmental conditions and potential bias errors associated with instruments as mentioned earlier, and it is the consideration of the effects from these factors that necessitates the usage of the operational data based reference. These results will be used for the power curve comparison later on in this section.

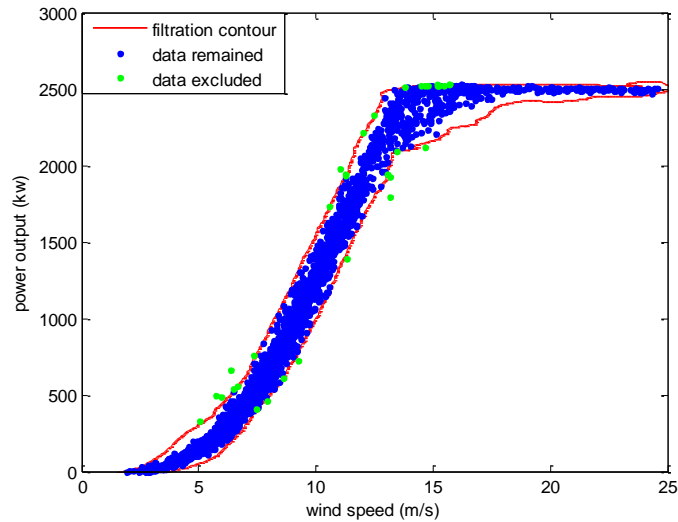


Figure 3-13: Filtration of raw reference power curve data for Turbine 3

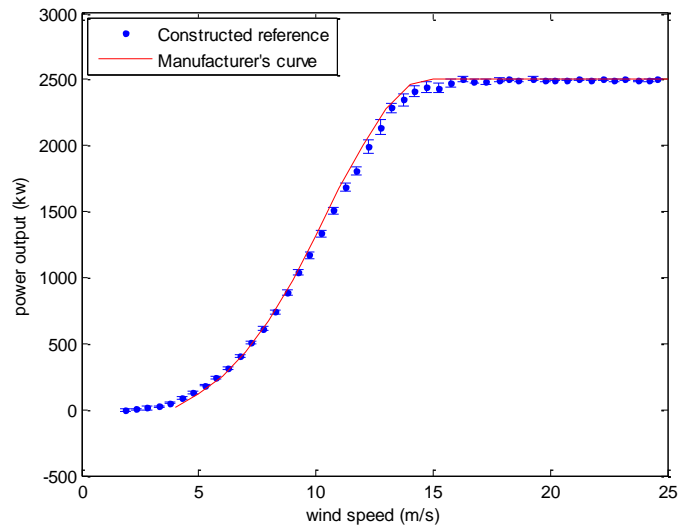


Figure 3-14: Constructed reference power curve vs. manufacturer's curve for Turbine 3

As indicated in the power curve fault logic in last section, yaw misalignment will result in deficit in power output. The magnitude of this power deficit is given remarkably well by the highly simplified cos cubed theory, [118], which states that the power output is scaled by the cube of cosine of yaw error (differences between wind direction experienced by the rotor and the nacelle direction). It should be noted that this parameter is sometimes, but by no means always recorded in the SCADA data since it is often

regarded as a control variable and thus not recorded. The SCADA data available for Turbine 3 in this study did include yaw error, and also nacelle position, on a ten minute averaged basis.

According to the cos cubed law a yaw error of 20 degree, which is highly unlikely under acceptable turbine yaw control, will lead to a significant power deficit of 17%. Since such a power deficit is unlikely to be acceptable to a wind farm operator, a yaw error threshold of 20 degree has been chosen. A time series of the absolute yaw error from an operational wind turbine is illustrated in Figure 3-15. It can be observed that the yaw error exceeds 20 degrees consistently for timestamps 200 to 240. This anomalous performance was confirmed to be yaw drive or yaw drive control issue. Figure 3-16 shows unambiguously that the nacelle position was stuck in a fixed position (approximately 200 degrees) for an extended time period, with no yaw activity, whereas the wind direction varied in a normal manner during this period.

A comparison between the real-time power curves for this period and the reference power curve constructed above is undertaken using the hypothesis test set at a 99.5% confidence level, i.e. a significance level of 0.005. This is a provisional figure selected on an intuitive basis and assuming that the calculated likelihood and statistical modelling are not unreasonable. Its provisional nature reflects the lack of field trial data. However, the final value would not be expected to be very different. The aggregate number of anomalous bin values across the entire power curve at each time point, determined according to this 99.5% criterion, are plotted as a time series, as shown by the red points in Figure 3-15, together with the corresponding value of the absolute yaw error. Using this approach an alarm would have been raised at 03:00 on 15/04/2009, 6 hours after the first anomalous yaw observation at 21:00 on 14/04/2009. Robust identification of a significant performance problem based on power curve tracking has thus been demonstrated.

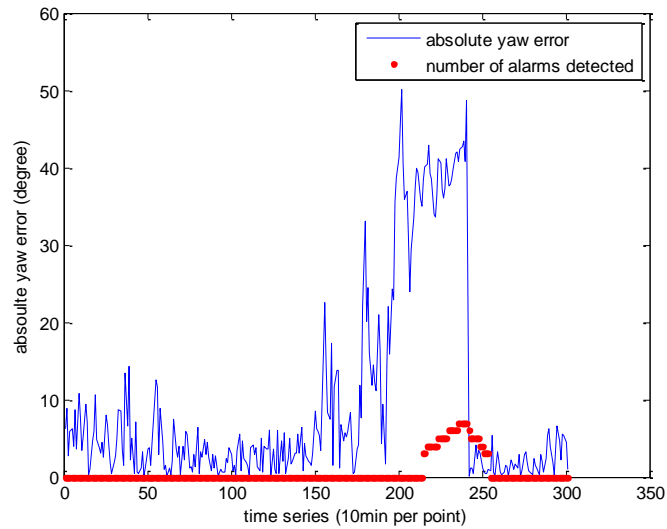


Figure 3-15: Absolute yaw error along with aggregate number of anomalous bins detected for Turbine 3

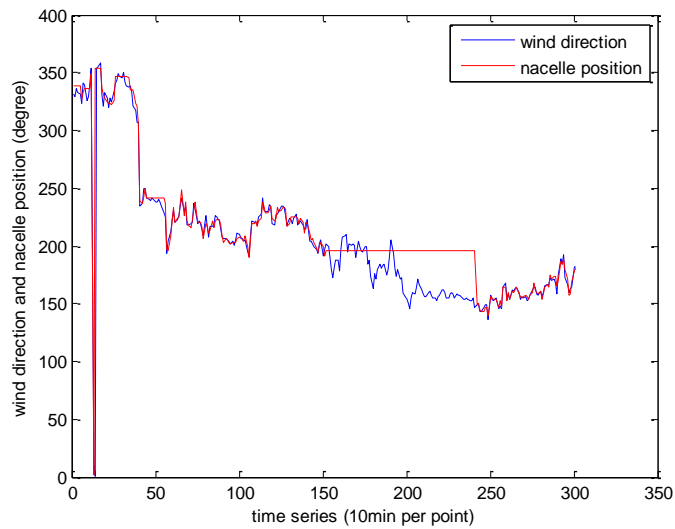


Figure 3-16: Time series of wind direction and nacelle position for Turbine 3

In this case the issue was faulty yaw control, and with the right SCADA data this could have been detected directly. However, as mentioned already, yaw error is often not included in SCADA data. It might be argued that 6 hours is too long. This could certainly be reduced by using less robust detection for example by reducing the confidence limits set for hypothesis test, but the result would inevitable be more false

alarms. Given that SCADA based condition monitoring is at an early stage of development and operators are highly concerned about excessive numbers of alarms, see for example reference [32], it seems better to err on side of robust with slightly less responsive algorithm design.

### **3.6. Application of the proposed method to pitching performance condition monitoring**

Based on the successful identification of a significant power curve deviation as demonstrated in the previous section, the proposed online power curve condition monitoring method is applied to monitor the pitching performance, which can be characterised by the pitch angle – wind speed operating curve. The main purpose is to check if the pitching system is controlled and operating accurately. Any performance deviation in each wind speed bin will result in a statistically significant number in the Welch’s t test and hence trigger the alarm.

The deviations from the reference pitch angle – wind speed curve could result from anemometer errors, pitching related issue such as controller error (e.g. setting error) or hydraulic system error (e.g. hydraulic oil leak). All these categories could be confirmed by double checking the power curve performance with the reference. For example, if the pitch deviation is caused by the anemometer error then the corresponding power curve plot should present a shifted version of the reference data. And other reasons will lead to power deficit which would be presented in the power curve plot.

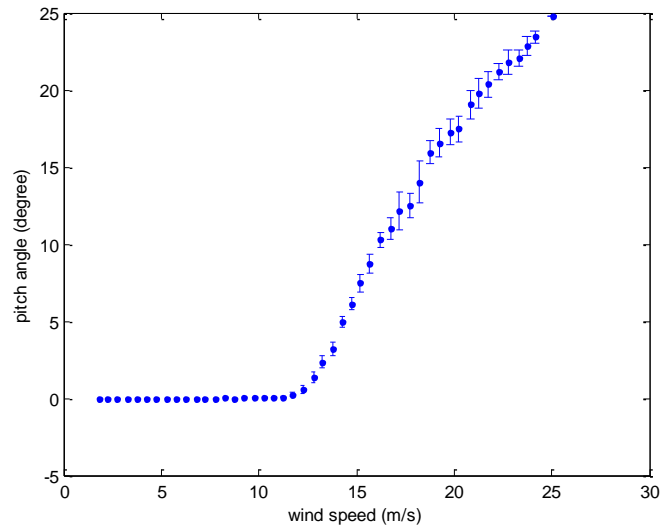


Figure 3-17: Pitch angle – wind speed reference with error bars for Turbine 3

A pitch performance monitoring example for Turbine 3 is used in this section to validate the proposed method. Since the pitching operation depends on the generated power which is proportional to the associated air density, the wind speed measurement should undergo the air density correction as depicted in Section 3.1.2 before any analyses. A pitch angle – wind speed reference constructed from three months healthy data with outliers excluded by the GMCM is shown in Figure 3-17.

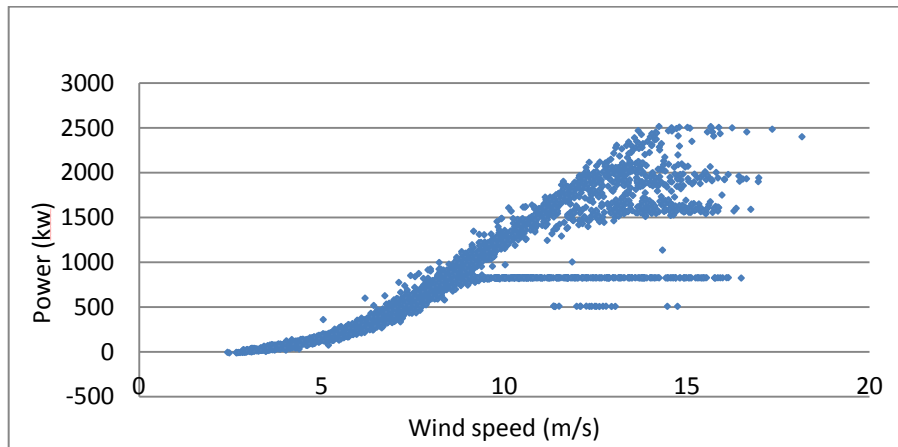


Figure 3-18: Power curve scatter for testing data from Turbine 3

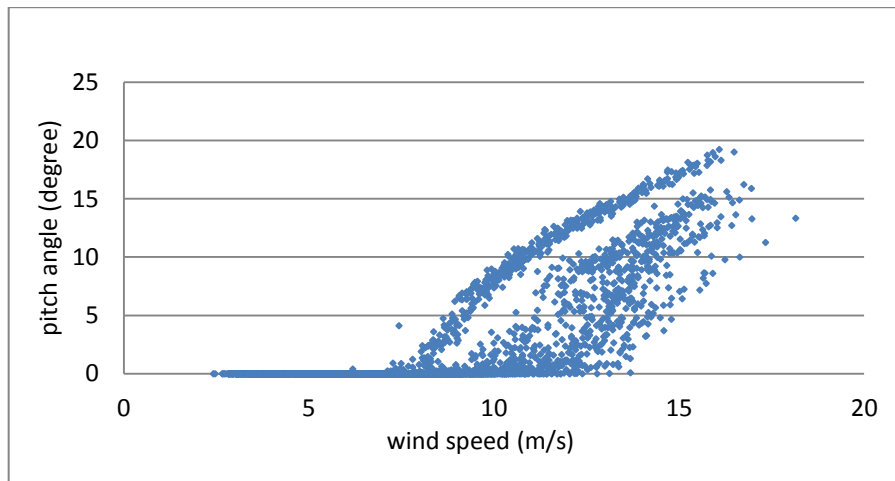


Figure 3-19: Scatter of pitch angle vs. wind speed for testing data from Turbine 3

In this case the only available one-month testing data included periods of curtailment, which will result in early pitching. The power curve scatter of these data and the corresponding pitch angle – wind speed are illustrated in Figure 3-18 and Figure 3-19, respectively, which clearly show the power curtailment and the associated pitching performance. It should be noted that as part of the active network management, the power generation from wind turbines is sometimes instructed to be curtailed due to capacity constraints on the local transmission network, particularly during periods of high wind production and low local demand, [119]. A number of Scottish wind farms were curtailed during the high winds of early January of 2012, [120]. This data is used to validate the effectiveness of the developed method, but surely does not indicate pitch system anomaly.

The associated detection result of the testing data for Turbine 3 is shown in Figure 3-20, where the curtailment flag (with high level indicating non-curtailment and vice versa) time series is plotted with the aggregate alarm number detected. It can be seen that the curtailment, which result from early pitching, is picked up efficiently as the derating flags move to low levels. This demonstrates the effectiveness of the developed technique.

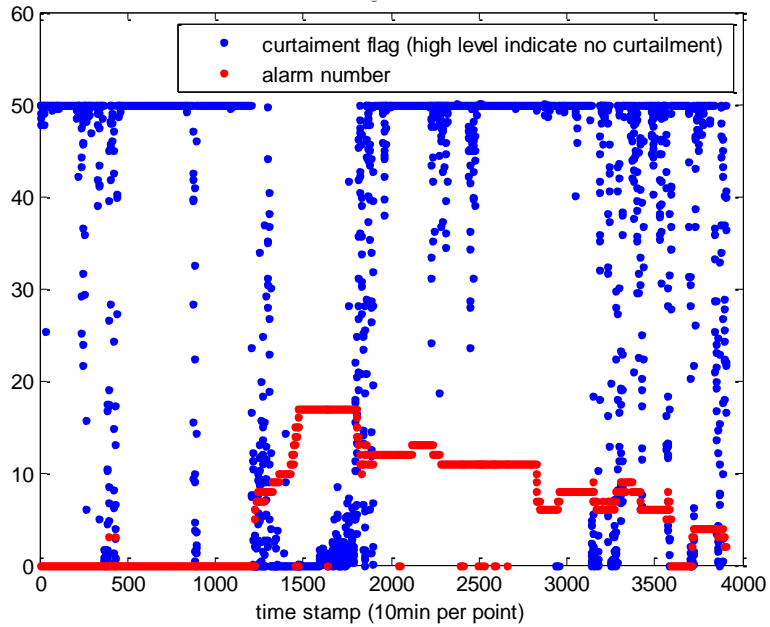


Figure 3-20: Pitching performance detection results for testing data with derated operation for Turbine 3

The early pitching is very difficult to distinguish from real pitch anomalies without a curtailment flag in the SCADA. Power curves can be used to detect curtailment but this takes time and is not straightforward. The clear message is that a curtailment flag is required for confident processing of pitch angle data and associated power characteristics.

### 3.7. Chapter summary

The Gaussian Mixture Copula Model outperforms the Frank Copula and the Gaussian Mixture Model in fitting the nonlinear relationship between the two power curve variables. The outlier rejection using the probability contour effectively removes the statistically significant deviations in the potential power curve reference measurements, thus improving the precision of the selected reference and increasing the reliability of the subsequent anomaly detection.

Based on the constructed reference using the Copula model, the proposed power curve based real-time wind turbine condition monitoring method allows a case by case based

approach to interpretation which can be encapsulated by the so called power curve fault logic. With a properly constructed reference power curve, the real-time power curve comparison based method can provide a simple and effective tool for wind turbine condition monitoring using the Welch's hypothesis test. The accurate and efficient detection of wind turbine yaw misalignment based on power performance data has proved the effectiveness of the approach outlined in this chapter. A similar approach applied to pitching performance monitoring has shown promising results although the presented example with power curtailment does not indicate an actual pitch system anomaly. However, it is accepted that far more examples of successful detection are required before the method can be regarded as ready for real world application. And it should be recalled that tuning of key parameters, such as the significance level in the Welch's t test, based on extensive operational data from field trials is still required.

### 3.8. Chapter references

95. Leithead, W. E., Dominguez, S., *Active regulation of multi-MW wind turbines: an overview*, UK EPSRC Grant No. EP/D034566/01, *Power Systems Technology*, 31 (20), pp. 24-34, 2007.
96. Smith, B., Link, H., Randall, G., McCoy, T., *Applicability of Nacelle Anemometer Measurements for Use in Turbine Power Performance Tests*, Portland, AWEA 2002.
97. Antoniou, I., Pedersen, T.F., *Nacelle Anemometry on a 1MW Wind Turbine: Comparing the power performance results by use of the nacelle or mast anemometer*, Risø-R-941(EN), August 1997.
98. Hinsch, C., Westermann, D., *Power Performance Measurement by means of an anemometer located on the nacelle*, DEWI Technical Note, 19.08.96.
99. Burton, T., Sharpe, D., Jenkins, N., Bossanyi E., *Wind Energy Handbook, Ch3: Aerodynamics of Horizontal-Axis Wind Turbines*, John Wiley & Sons, Ltd, 2002.
100. Burton, T., Sharpe, D., Jenkins, N., Bossanyi E., *Wind Energy Handbook, Ch4: Wind-turbine Performance*, John Wiley & Sons, Ltd, 2002.
101. Manwell, J. F., McGowan, J. G., Rogers, A. L., *Wind Energy Explained: Theory, Design and Application*, 2nd edition, John Wiley & Sons, pp.397-399, 2010.
102. Sklar, A., *Fonctions de repartition a n dimensions et leurs marges*, vol. 8, pp. 229-231, Publ. Inst. Statist. Univ. Paris, 1959.
103. Nelsen, R. B., *An Introduction to Copulas*, ser. Springer Series in Statistics, 2nd ed., New York: Springer, 2006.
104. Dorey, M., Joubert, Ph., *Modelling Copulas: An Overview*, The Staple Inn Actuarial Society report, pp. 1-27, July, 2007.
105. Tewari, A., Giering, M.J., Raghunathan, A., *Parametric Characterization of Multimodal Distributions with Non-gaussian Modes*, 2011 IEEE 11th International Conference on Data Mining Workshops (ICDMW), vol. 11, no. 11, pp. 286-292,

Dec. 2011.

106. Schmidt, R., *Tail Dependence*, In Statistical tools in finance and insurance (eds P.Čížek, W.Härdle & R.Weron), 65–91. Springer Verlag, Heidelberg, 2005.
107. Berks, P., Wood, F., Pillow, J., *Characterizing Neural Dependencies with Coupled Models*, Advances in Neural Information Processing Systems, Vol. 21, pp.129 -136, 2009.
108. Joe, H., *Multivariate Models and Dependence Concepts*, 1st ed., New York: Chapman & Hall, pp. 139-166, 1997.
109. McLachlan, G. J., Peel, D., *Finite Mixture Models*, Wiley Series in Probability and Statistics, pp. 80-85, Nov. 2000.
110. McLachlan, G. J., Krishnan, T., *The EM Algorithm and Extensions*, Wiley, New York, 1997.
111. Kohonen, T., *Self-Organizing Maps*, Springer Series in Information Sciences, 3rd edition, Springer, Berlin, 2001.
112. Konishi, S., Kitagawa, G., *Information Criteria and Statistical Modeling*, Springer New York, 2008.
113. Hosmer, D. W., Lemeshow, S., *Applied Logistic Regression*, Wiley, New York, pp. 7-10, 1989.
114. Penny, W.D., *Variational Bayes for d-dimensional Gaussian Mixture Models*, University College London, July 2001.
115. Hansen, A. D., Jauch, C., Sorensen, P., *Dynamic Wind Turbine Models in Power System Simulation Tool DIGSILENT*, Risø-R-1400(EN), National Laboratory, 2003.
116. Sawilowsky, S.S., Fermat, Schubert, Einstein, Behrens-Fisher, *The probable difference between two means when  $\sigma_1 \neq \sigma_2$* , Journal of Modern Applied Statistical Methods, Vol. 1, (2), pp. 461–472, 2002.
117. Wagner, R., Antoniou, I., Pedersen, S. M., Courtney, M. S., Jørgensen, H. E., *The*

*Influence of the Wind Speed Profile on Wind Turbine Performance Measurements*,  
Wind Energy, Vol. 12, Issue 4, pp. 348-362, 2009.

118. Mamidipudi, P., Dakin, E., Hopkins, A. F., Belen, C., Leishman, J. G., *Yaw Control: The Forgotten Controls Problem*, EWEA Brussels, 2011.
119. Fink, S., Mudd, C., Porter, K., Morgenstern, B., *Wind Energy Curtailment Case Studies: May 2008 – May 2009*, NREL Subcontract Report, Oct. 2009.
120. National Grid, *How we balance the country's electricity transmission system*, [Online]. Available: <http://www2.nationalgrid.com/UK/Our-company/Electricity/Balancing-the-network/> (Accessed 20<sup>th</sup> December 2013), 2013.

## **4. NSET model applications to fault detection of subassemblies for individual turbine**

The Nonlinear State Estimation Technique (NSET) provides a state based vector recognition technique that can be applied to wind turbine condition monitoring. The algorithm of the NSET model and the associated memory matrix construction for models will be specified in this chapter first, followed by the introduction of anomaly detection based on the NSET estimation. The effectiveness of the proposed method will then be demonstrated in detail with applications to anomaly detection of wind turbine gearbox malfunction and generator failure.

### **4.1. Anomaly detection based on NSET model: Methodologies**

For a specific model to be implemented, the main analysis procedures undertaken are:

- 1) Identify all the variables that are closely related to the model output parameter of interest based on a combination of domain knowledge [121] and correlation analysis.
- 2) Construct a state memory matrix from the training data following the framework provided in Section 4.1.2.
- 3) Validate the constructed model by using a validating data set according to Equations (4-2) and (4-7) below, and then set thresholds for the fault detection algorithm based on the results.
- 4) Assess designated testing data according to Equations (4-2) and (4-7), and then record any alarms that are reported by the fault detection algorithm described in Section 4.1.3.

Each step is explained in more detail below and illustrated by case studies in later sections of this chapter, both to make these procedures clearer and to demonstrate the potential of the technique for wind turbine fault detection.

#### 4.1.1. NSET algorithm

A state memory matrix  $\mathbf{D}$ , expressed by Equation (4-1), is utilized to store state vectors for selected data records [84]. Each column (vector) represents a system operational state measured at a particular time and each row records the readings from a specific sensor. It is important to note that the sensor readings for model output are also included in the matrix for computing the similarity between current input and historical states, as is the convention.

$$\mathbf{D} = [\mathbf{X}(1) \ \mathbf{X}(2) \ \cdots \ \mathbf{X}(m)]$$

$$= \begin{bmatrix} x_1(1) & x_1(2) & \cdots & x_1(m) \\ x_2(1) & x_2(2) & \cdots & x_2(m) \\ \vdots & \vdots & \ddots & \vdots \\ x_n(1) & x_n(2) & \cdots & x_n(m) \end{bmatrix} \quad (4-1)$$

There are  $m$  observation vectors for the  $n$  sensor variables in the memory matrix. After construction, the matrix can be utilized to model a turbine component performance, and the NSET is capable of producing reliable estimation as long as the matrix consists of valid and proper data that encompasses the range of normal operation of the item being modelled, in our case, a wind turbine [81]. More details regarding matrix construction will be discussed in the next section. For each new input vector  $\mathbf{X}_{obs}$ , the output  $\mathbf{X}_{est}$  is obtained from the product of the memory matrix  $\mathbf{D}$  and a weighting vector  $\mathbf{W} = [w_1 \ w_2 \ \cdots \ w_m]^T$  as shown in Equation (4-2). All the vectors here are by default column vectors and the superscript  $^T$  denotes the transposition of matrices.

$$\mathbf{X}_{est} = \mathbf{D} \cdot \mathbf{W} = w_1\mathbf{X}(1) + w_2\mathbf{X}(2) \cdots + w_m\mathbf{X}(m) \quad (4-2)$$

The weighting vector captures the degree of similarity between the input and each of the states within the matrix. The residual, which is the difference between the observed output and the model estimate  $\mathbf{X}_{est}$ , is presented in Equation (4-3).

$$\boldsymbol{\varepsilon} = [\varepsilon_1 \ \varepsilon_2 \ \cdots \ \varepsilon_n]^T = \mathbf{X}_{obs} - \mathbf{X}_{est} = \mathbf{X}_{obs} - \mathbf{D} \cdot \mathbf{W} \quad (4-3)$$

And by minimizing the sum of square of the residuals, which is shown in Equation (4-4), the estimation of the weighting vector,  $\mathbf{W}$ , can be obtained using a conventional least squares approach.

$$\begin{aligned} \sum_{i=1}^n \boldsymbol{\varepsilon}_i^2 &= \boldsymbol{\varepsilon}^T \cdot \boldsymbol{\varepsilon} = (\mathbf{X}_{obs} - \mathbf{D} \cdot \mathbf{W})^T \cdot (\mathbf{X}_{obs} - \mathbf{D} \cdot \mathbf{W}) \\ &= \mathbf{X}_{obs}^T \cdot \mathbf{X}_{obs} - \mathbf{X}_{obs}^T \cdot \mathbf{D} \cdot \mathbf{W} - \mathbf{W}^T \cdot \mathbf{D}^T \cdot \mathbf{X}_{obs} + \mathbf{W}^T \cdot \mathbf{D}^T \cdot \mathbf{D} \cdot \mathbf{W} \end{aligned} \quad (4-4)$$

To minimise the value of  $\sum_{i=1}^n \boldsymbol{\varepsilon}_i^2$  (i.e. to ensure maximal model accuracy), its first order derivative is set to zero as shown in Equation (4-5), the associated derivation can be found in reference [122].

$$\frac{d \sum_{i=1}^n \boldsymbol{\varepsilon}_i^2}{d\mathbf{W}} = -2\mathbf{D}^T \cdot \mathbf{X}_{obs} + 2\mathbf{D}^T \cdot \mathbf{D} \cdot \mathbf{W} = 0 \quad (4-5)$$

which results in:

$$\mathbf{W} = (\mathbf{D}^T \cdot \mathbf{D})^{-1} \cdot (\mathbf{D}^T \cdot \mathbf{X}_{obs}) \quad (4-6)$$

Equation (4-6) gives the general least squares solution for the weight vector. However, a problem arises in the difficulty of inverting the so-called recognition matrix  $(\mathbf{D}^T \cdot \mathbf{D})$  that results from a potential linear interrelationship between state vectors in the memory matrix [85]. This issue can be resolved by replacing the dot product within the bracket in Equation (4-6) with a nonlinear operator. The NSET weight vector  $\mathbf{W}$  so modified is expressed as:

$$\mathbf{W} = (\mathbf{D}^T \otimes \mathbf{D})^{-1} \cdot (\mathbf{D}^T \otimes \mathbf{X}_{obs}) \quad (4-7)$$

where the nonlinear operator  $\otimes$  calculates the Euclidean distance of the operands, as shown in Equation (4-8), since the Euclidean distance outperforms the other nonlinear operators in reference [85] in terms of prediction accuracy. The same distance metric is also applied in reference [84].

$$\mathbf{x} \otimes \mathbf{y} = \sqrt{\sum_{i=1}^n (x_i - y_i)^2} \quad (4-8)$$

The mathematics described above can be viewed as process to calculate the nearest possible vector to the observation vector that can be formed from a linear combination of the vectors in the memory matrix. Distances in this n-dimensional space are calculated using the Euclidean norm. It is difficult to see how such a linear combination of memory matrix vectors can extrapolate to a region of the space outside the domain of the memory matrix.

#### **4.1.2. State memory matrix construction**

Selection of the model variables and construction of the memory matrix are both critically important since these will directly affect the accuracy and efficiency of the NSET model. Domain knowledge together with correlation analysis is employed to select relevant variables for a specific model.

Once the relevant variables to be included in the model have been chosen, the state memory matrix must be built up through selection of measured state vectors from the available operational data. This process is analogous to training in other models like neural nets. Three factors need to be taken into account. First, in order to achieve a good model representation and hence performance, the selected data should encompass enough states to cover the complete range of normal operation, including expected behaviour under extreme conditions. Second, the potentially large number of states involved can make the matrix operations used in the algorithm numerically time consuming, and moreover, the increase in state numbers beyond a certain limit is known not to contribute to increased model accuracy. Consequently, a data selection algorithm should be used, such as that presented in [84], to choose state vectors evenly and economically from the training data set. With this approach the number of states can be reduced dramatically, making the model much more effective yet still representative. Similar to the idea of cluster number decision in reference [94], the matrix size is

determined based on a plot of validation accuracy against matrix size in this study. This provides a straightforward means of avoiding unnecessarily large memory matrices. An example memory matrix sizing will be shown in Section 4.3.1. Last but not least, no repeated states are allowed in the memory matrix since this will result in a singularity associated with the matrix inversion used to solve for the weighting matrix (Equation (4-7)).

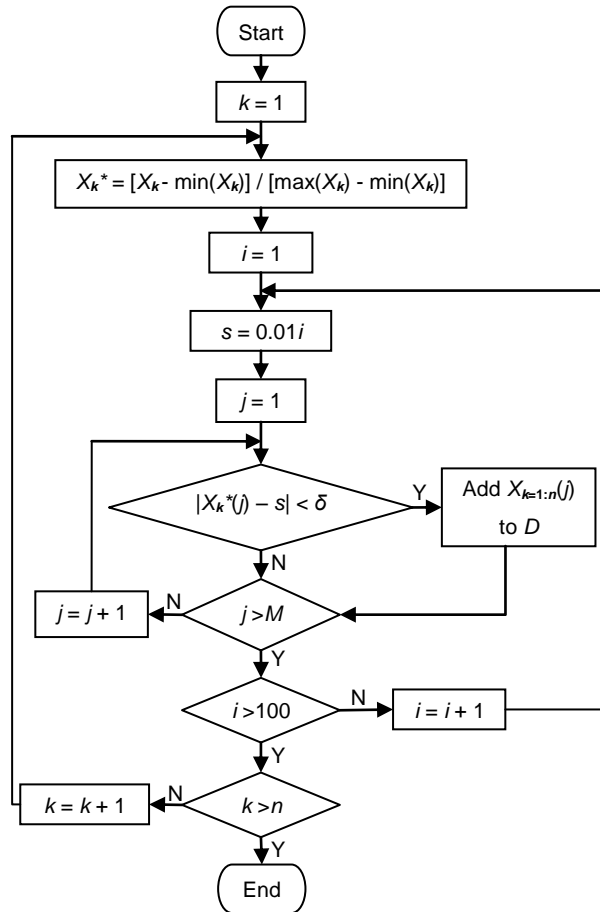


Figure 4-1: Data selection flow chart for memory matrix construction

The flow diagram in Figure 4-1 outlines a matrix construction algorithm in which the data are selected evenly for each normalised variable varying from 0 to 1 [84]. Parameter  $\delta$  is a predefined small positive value close to zero, and  $X_k$  represent a row vector that records  $M$  readings for each of the  $n$  different sensors, where parameters  $M$  represents the number of state vectors in the training data and  $n$  have the same meaning

as in equation (4-1). In this work the increment is set to 0.01, which implies that the value range of each variable of interest is divided evenly into 100 pieces, and those values closer than  $\delta$  to the dividing line are selected. The corresponding historical state vector containing the records for all variables is then imported into the memory matrix. Preliminary matrix construction is undertaken by applying the algorithm outlined above to each of the relevant training variables in turn. The memory matrix is then refined to remove any repeated state vectors. This completes the memory matrix construction.

#### 4.1.3. Fault detection algorithm

The constructed model is then applied to the validation data set, which must not have been used for the training process, and the residuals obtained are then passed through an infinite impulse response (IIR) low pass filter to remove noise in the form of spikes in the residuals stemming from transitions in the turbine's operational state rather than from turbine faults.

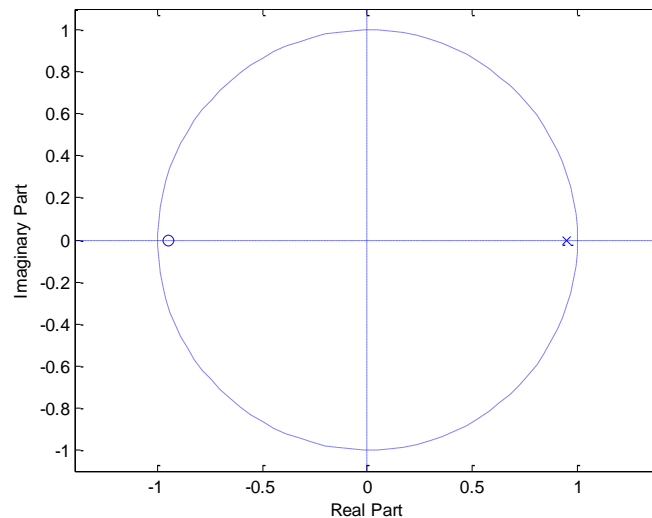


Figure 4-2: Pole and zero illustration of the selected low pass filtered in Z-plane

The pole-zero diagram for this low pass filter is illustrated in Figure 4-2 where the pole, indicated by a small circle, and zero, indicated by a cross, are located at (0.95, 0) and (-0.95, 0) within the unit circle. The pole on the positive side of horizontal axis will allow low frequency signals to pass and the zero on the negative side of horizontal axis will

cut the high frequency signals off, which makes the low pass filter work. The equivalent Z-domain expression given the pole and zero of this filter is shown in Equation (4-9).

$$H(z) = \frac{Y(z)}{X(z)} = C \times \frac{z + 0.95}{z - 0.95} \quad (4-9)$$

where parameter  $C$  decides the magnitude of the frequency response of this filter, and  $z = e^{j\Omega}$  which in effect goes along the unit circle in the complex Z-plane, as shown in Figure 4-2, as the signal frequency,  $\Omega$ , varies from  $-\pi$  to  $\pi$ . The parameter  $C$  is calculated by assuming unit response to DC signals, in which case  $H(z) = 1$  and  $z = 1$  since  $\Omega = 0$ , and this results in  $C = 1/39$ .

So we have,

$$\frac{Y(z)}{X(z)} = \frac{1}{39} \times \frac{z + 0.95}{z - 0.95} = \frac{1}{39} \times \frac{1 + 0.95z^{-1}}{1 - 0.95z^{-1}} \quad (4-10)$$

Rearranging Equation (4-10) will lead to,

$$Y(z) = 0.95z^{-1}Y(z) + \frac{1}{39}X(z) + \frac{0.95}{39}z^{-1}X(z) \quad (4-11)$$

According to the inverse Z transform provided in reference [123], the time domain expression for this low pass filter is achieved based on Equation (4-11) and expressed in Equation (4-12). And the corresponding frequency response for the designed filter is shown in Figure 4-3.

$$y[n] = 0.95y[n - 1] + \frac{1}{39}x[n] + \frac{0.95}{39}x[n - 1] \quad (4-12)$$

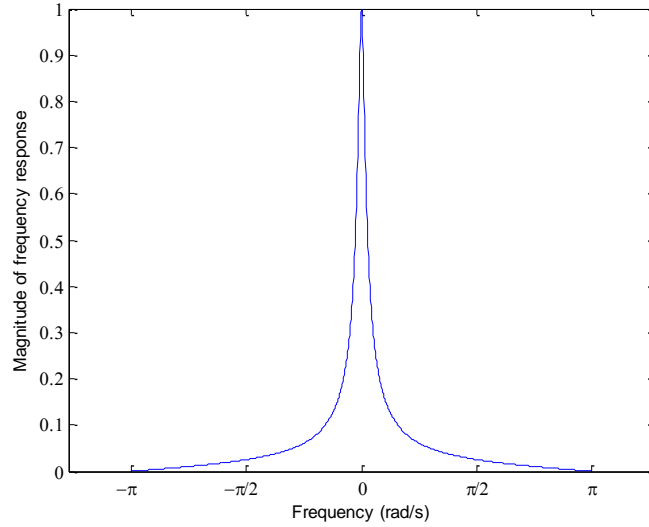


Figure 4-3: Magnitude of frequency response for the low pass filter within one period

Although NSET can be used to represent many components and parameters a common application is to component temperatures, where elevated temperatures that can result in overheating are indicative of a problem [36]. In such cases, only the positive residuals are of importance. The maximum of the filtered residual and the corresponding standard deviation are analysed using Welch's t test to identify statistically significant anomalies.

As has been introduced in the last chapter, Welch's t test is an extension of Student's t test that can be used when the variances of two testing samples are likely to be unequal. For the turbine gearbox model, a one-sided hypothesis test is used as only overheating of the gearbox is of concern, i.e. unexpected low gearbox temperatures are ignored. If the residual average rises above the reference average, the rise is considered significant if the statistic  $t > t_{\alpha}(v)$ , where  $t_{\alpha}(v)$  follows the Student's  $t$  distribution as introduced in the previous chapter and the t statistic is given by:

$$t = \frac{\overline{X}_{test} - \overline{X}_{ref}}{\sqrt{\frac{S_{test}^2}{N_{test}} + \frac{S_{ref}^2}{N_{ref}}}} \quad (4-13)$$

where  $\bar{X}$ ,  $S$  and  $N$  are the residual average, residual standard deviation and the window length, with the subscript ‘ref’ and ‘test’ indicating validation data and testing data, respectively.

#### 4.1.4. Discussion of the modified NSET algorithm

In addition to the NSET algorithm as introduced in Section 4.1.1, which will be referred to as the standard NSET model hereafter in the thesis, a modified version of NSET is also proposed in reference [81], and this will be referred to as the modified NSET model. The algorithm of the modified model is presented below and its differences from the standard one will be pointed out.

Since the variable that is used as the condition indicator for the system under investigation is expected to take on anomalous values following system degradation, it has been suggested that this indicative variable should be removed from the state memory matrix that is used for the weighting vector calculation. The modified weighting vector,  $\widehat{W}$ , is now:

$$\widehat{W} = (\widehat{D}^T \otimes \widehat{D})^{-1} \cdot (\widehat{D}^T \otimes \widehat{X}_{obs}) \quad (4-14)$$

where  $\widehat{D}$  denotes the modified memory matrix as shown in Equation (4-15), in which  $[x_1(1) \ x_1(2) \ \dots \ x_1(m)]$  is the vector for the indicative variable and has been taken out. The same action is applied to the observation vector, leading to its modified version,  $\widehat{X}_{obs}$ .

$$\begin{aligned} \widehat{D} &= [\widehat{X}(1) \ \widehat{X}(2) \ \dots \ \widehat{X}(m)] \\ &= \begin{bmatrix} x_2(1) & x_2(2) & \dots & x_2(m) \\ x_3(1) & x_3(2) & \dots & x_3(m) \\ \vdots & \vdots & \ddots & \vdots \\ x_n(1) & x_n(2) & \dots & x_n(m) \end{bmatrix} \end{aligned} \quad (4-15)$$

The model estimation,  $X_{est}$ , in this case is the product of the standard memory matrix as shown in Equation (4-1) and the modified weighting vector, as expressed in Equation (4-16).

$$\mathbf{X}_{est} = \mathbf{D} \cdot \widehat{\mathbf{W}} \quad (4-16)$$

The modified NSET model is believed to produce more reliable results than the standard model since the indicative variable, which is directly affected by the physical state of the monitored component, is masked out in the estimation process and the results are based on the measurements from valid sensors only, [81].

Different possibilities for NSET model implementation will be explored throughout the following sections: a comparison between the standard NSET model and the modified model will be presented; the NSET results will also be compared with those from the Neural Network model; the necessity of additional null and maximal state vector will be justified; the impact of reduced parameter and time lagged variable on model performance, the contributions of manipulative factors, such as memory matrix normalisation and parameter weighting, to the model improvement will also be investigated.

## **4.2. Background information of wind farm SCADA data for NSET applications**

The turbine gearbox and generator are analysed in this chapter based on NSET models and the associated anomaly detection that has been specified in the previous section. These two key components are investigated here since they have been identified earlier to be responsible for much of the turbine downtime and because their temperatures are commonly included in SCADA data. The SCADA data used here come from a wind farm in the UK with 26 identical fixed-speed stall regulated wind turbines rated at 600kW. Figure 4-4 illustrates the layout of this wind farm with the 26 turbines marked by blue points and two meteorological masts indicated by red crosses.

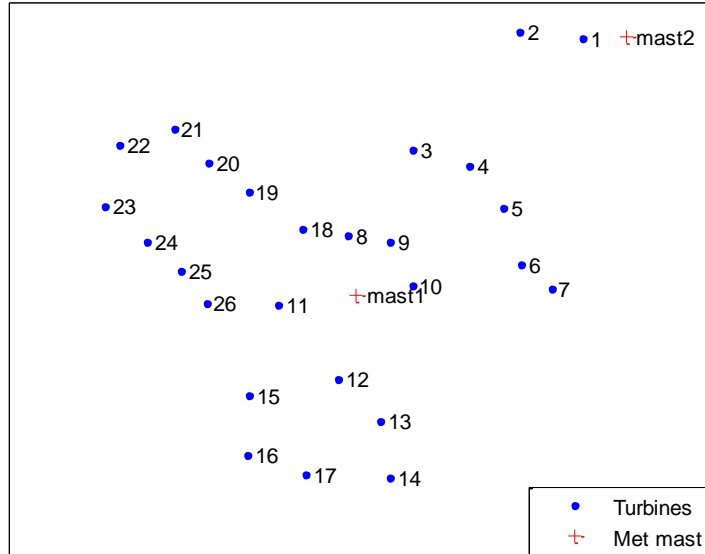


Figure 4-4: Wind farm layout

Turbine No.	Anomalous component	Failure time
T8	Generator	Nov. 2006
T16	Gearbox	Jan. 2006
T17	Gearbox	Apr. 2005

Table 4-1: List of events for analysis

Table 4-1 lists the gearbox and generator events that are used for the analyses. An intuitive input selection for both the gearbox and generator model is made based on domain knowledge. The wind turbine rotor captures partial kinetic energy out of the incident wind and converts it into mechanical energy which is then transmitted to the turbine drive train, where the rotational speed is stepped up by the gearbox to an appropriate level to drive the generator which converts the energy in its final electrical form. It can be seen from this process that the mechanical load of gearbox, indicated by its temperature, is closely related to the turbine power output. A similar situation applies

to the generator where the electrical load is indicated by the voltage and current (or equivalently power output), hence will also be relate to its temperature. The temperature from either the gearbox or generator is affected by its immediate ambient environment so the nacelle temperature is also considered in both cases. Table 4-2 lists the available 10-min SCADA data where the relevant parameters are ticked for both models.

SCADA tag	Gearbox model	Generator model
Wind speed (m/s)		
Active power (kW)	✓	✓
Reactive power (kVar)		
Gearbox bearing temperature (°C)	✓	
Gearbox cooling oil temperature (°C)	✓	
Generator winding temperature (°C)		✓
Nacelle temperature (°C)	✓	✓

Table 4-2: List of available SCADA data in 10-min format and intuitive input selection for the gearbox and generator model

### 4.3. NSET application to wind turbine gearbox case study

Operational data from five healthy turbines within the wind farm, namely T3, T4, T5, T7 and T10, are averaged to provide a representative model training dataset that defines a healthy turbine across its complete operational range. Both references [58] and [124] utilize three month's worth of training data. Similarly a period of 3 months, from the beginning of April to the end of June of 2005, is chosen for this training process, including 11246 valid states. One month of operational data from the problem free turbine T1 is employed for validation purpose, from which the statistics can be obtained for further fault detection using the Welch's hypotheses test. The testing data come from two turbines with confirmed gearbox failures, i.e. T16 and T17 as listed in Table 4-1. Operational data up to half a year prior to the final failure of T16 is used in testing case

II whereas only one month of testing data from T17 is available for analysis in testing case I.

Output parameters	Gearbox cooling oil temperature
Input parameters	
Gearbox cooling oil temperature (°C)	1
Gearbox bearing temperature (°C)	0.9491
Power output (kW)	0.8282
Nacelle temperature (°C)	0.6891

Table 4-3: Pearson’s correlation coefficients between gearbox model input and output parameters

Any wear and damage developed in the gearbox will tend to result in extra heat being generated which will then be conducted to the cooling oil. It should thus be able to monitor the wind turbine gearbox with the gearbox cooling oil temperature being the condition indicator, and therefore the model output. The selected inputs of model should be closely related to the model output in order to construct an accurate representation for the turbine component. Table 4-3 adds confidence to the variable selection of model inputs by exhibiting high correlation coefficients between the proposed input parameters and the model output, with the exception of nacelle temperature which shows slightly worse correlation. This parameter is not so strongly linked with the gearbox oil temperature but represents the effect of ambient temperature on the model output as mentioned, so it has been retained.

As mentioned before, errors in the SCADA system or measurement sensors can result in null and invalid readings in SCADA records. A crude filtration depicted in Table 4-4 is applied here to remove these entries and make the analysis meaningful. The percentage of values being removed in this process for the training, validation and testing data is listed in this table. The range of values of the four proposed variables after the filtration is also provided.

It should be noted that low values (below 0°C) of nacelle temperature could exist during winter season since it is affected by ambient temperature, and the crude filtration to remove such data is inappropriate. In this presented case study, however, the minimum nacelle temperature reading is 1°C, i.e. above the threshold setting, and hence no negative temperatures have been removed.

The significant amount of data being removed in this filtrating process indicates poor data quality, the potential effect of which on the model performance will be discussed in Section 4.3.10. However, since the comparison of different model options always makes use of the same filtered data sets, there should be no adverse impact. It also can be seen in Table 4-4 that the maximal gearbox cooling oil temperature in both of the testing cases exhibits higher levels than those in the training/validation set. Since the extrapolation capability of the model is uncertain, including a maximal vector that covers wider data range could be expected to improve the model's capability to extrapolate to higher temperatures. In this case, the maximal vector,  $[582.2, 69.0, 62.0, 24.4]^T$  (the variable values are presented in the same order as in Table 4-4), has been selected from data for a single healthy turbine outwith the 3-months of training data. An additional null vector,  $[0\ 0\ 0\ 0]^T$ , has also been added into the matrix to enhance the model performance when the oil temperature drops gradually during periods of non-generation that are caused by either low wind speed or turbine shut down. The effects of these additional vectors within the memory matrix will be investigated in Section 4.3.5.

Data usage	Variables	Filtration criteria	Value range after filtration		Percentage of values being removed (%)
			min	max	
Training set (T3, T4, T5, T7 and T10; April – June 2005)	Active power (kW)	> 25	25.01	596.30	33
	Gearbox bearing temperature (°C)	> 0	38.80	61.80	
	Gearbox cooling oil temperature (°C)	> 0	32.98	54.43	
	Nacelle temperature (°C)	> 0	3.95	28.40	
Validation set (T1; January 2006)	Active power (kW)	> 25	25.00	633.50	35
	Gearbox bearing temperature (°C)	> 0	26.00	60.00	
	Gearbox cooling oil temperature (°C)	> 0	22.08	55.00	
	Nacelle temperature (°C)	> 0	3.40	21.00	
Testing set in case I (T17; April 2005)	Active power (kW)	> 25	25.65	586.25	42
	Gearbox bearing temperature (°C)	> 0	41.00	66.00	
	Gearbox cooling oil temperature (°C)	> 0	32.17	61.00	
	Nacelle temperature (°C)	> 0	4.91	19.51	
Testing set in case II (T16; August 2005 – January 2006)	Active power (kW)	> 25	25.02	659.47	36
	Gearbox bearing temperature (°C)	> 0	11.00	69.00	
	Gearbox cooling oil temperature (°C)	> 0	10.48	67.00	
	Nacelle temperature (°C)	> 0	1.00	29.17	

Table 4-4: Filtration criteria of the selected variables for gearbox case study and the corresponding results

### 4.3.1. Memory matrix size decision

Since the NSET works in effect as a state based vector recognition technique, the corresponding model accuracy should depend on the matrix size in a proportional way. According to the state memory matrix construction algorithm outlined in Section 4.1.2, the total number of states in the matrix increases as the vicinity criterion,  $\delta$ , increases. The Root Mean Square (RMS) value of the validation residuals is employed here as an accuracy metric for model estimation and it is plotted against the corresponding matrix size in Figure 4-5 by varying the parameter  $\delta$ .

It can be seen from this figure that increasing the matrix size beyond 1000 state vectors makes little additional contribution to model accuracy, making this size a reasonable choice; in fact the matrix in this study has 989 states, giving a matrix  $D$  of size  $4 \times 989$ .

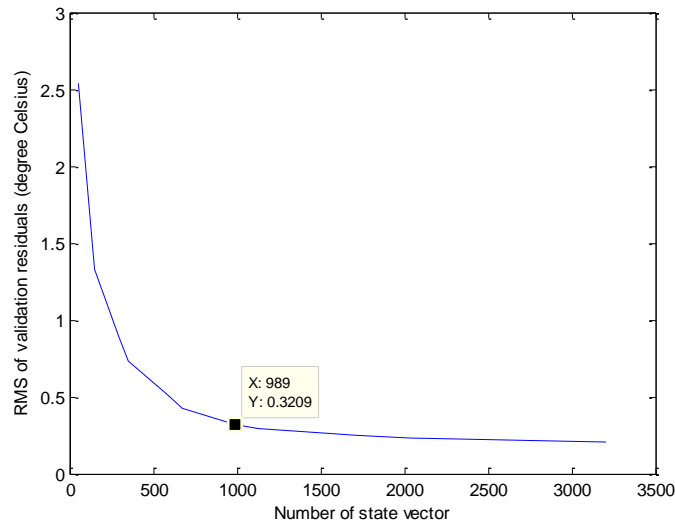


Figure 4-5: Memory matrix size decision

### 4.3.2. Model validation

The standard NSET model is validated using one month of data for the normal, fault free operation of turbine T1, as presented in Figure 4-6. The excellent agreement between model estimations, illustrated by the blue line, and the observations, indicated by the red curve, in Figure 4-6(a) shows the accuracy of NSET model. The corresponding residuals are plotted by the blue curve in Figure 4-6(b), where the majority of the residuals vary

within an acceptable range except for some isolated large spikes. The associated deviations in model estimation are caused by wind turbine operational transitions, such as those from the end of a non-production period during which the oil temperature drops gradually to ambient temperature. Most of the non-production associated data can be removed by the crude filtration expect when the turbine starts to operate, in which case the 10 minute averaged power output could easily exceed the filtration threshold whereas the oil temperature takes time to recover to the normal range due to the thermal mass.

Since these isolated residual spikes do not indicate actual system faults, a suitably designed IIR low pass filter as introduced in Section 4.1.3, taking the form expressed by Equation (4-12), is employed to remove this unwanted noise. And the filtered validation residual is shown by the green curve in Figure 4-6(b) along with the raw value. The maximum of the filtered residual together with its corresponding standard deviation will be used for fault detection.

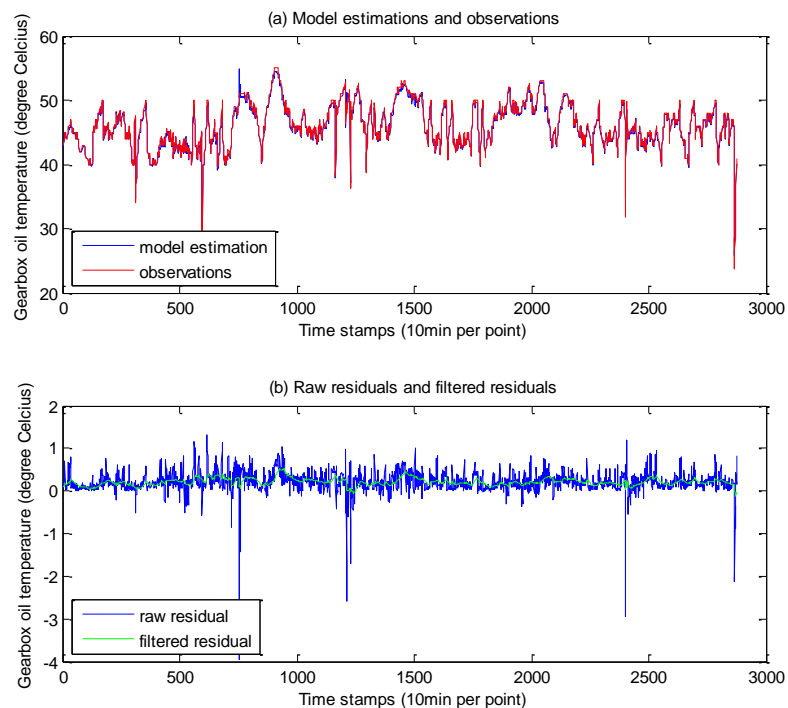


Figure 4-6: Validation results of T1 for standard NSET

### 4.3.3. Model testing and anomaly detection

Testing cases I and II with confirmed gearbox failures in T17 and T16 are utilized in this section to demonstrate the detection capability of the standard NSET model. Figure 4-7(a) shows the testing results for T17 with one month worth of data covering the whole April prior to the final failure at the end of this month. This figure shows a gearbox cooling oil temperature peak of  $61.0^{\circ}\text{C}$ , which lies below the upper limit of  $62.0^{\circ}\text{C}$ , set by the maximal vector in the state memory matrix. As has been stated in Section 4.3, and will be demonstrated in Section 4.3.5, the model accuracy and overall performance is improved by the presence of this maximal vector. Significant deviations between model estimations and the observations can be seen in this figure, and these also correspond to the large and prolonged residual as shown in Figure 4-7(b). This provides an initial indication of the gearbox overheating caused by the impending gearbox failure, and the Welch's hypothesis test as introduced in Section 4.1.3 is employed for rigorous fault detection.

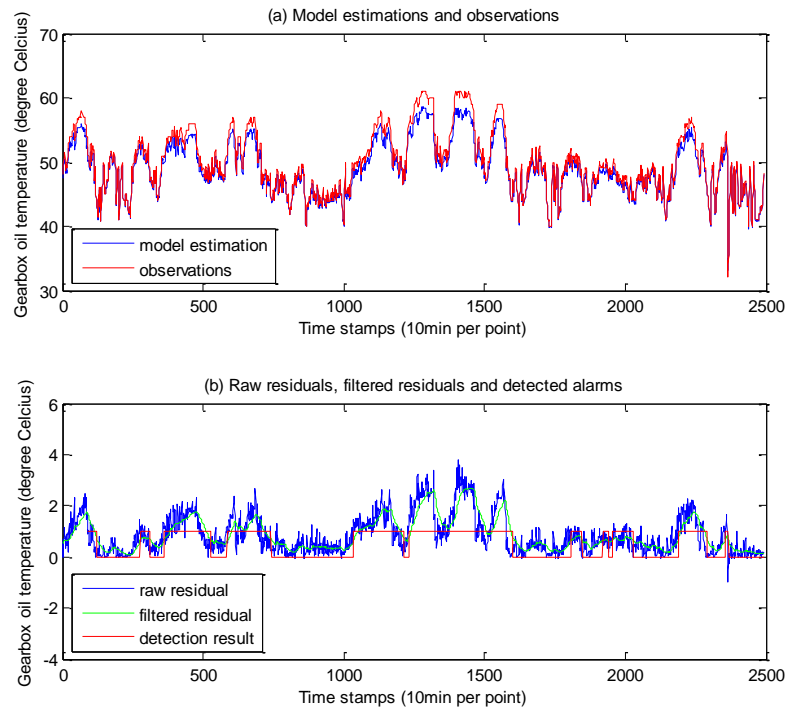


Figure 4-7: Testing results and anomaly detection of T17 for standard NSET

Recall the low pass filter shown in Equation (4-12), where the recursive term in this filter reflects contributions from previous outputs, which effectively applies a time-weighted averaging process to the data. 90 time steps, which is equivalent to 15 hours, are required to achieve the attenuation of contribution from previous outputs to less than 1%, leading to an effective window length of 90.

This low pass filter is applied to both the validation and test residuals to achieve much smoother residual time series as shown by the green curve in Figure 4-6(b) and Figure 4-7(b) respectively. The filtered results of the test residuals ( $X_{test}$ ) and the corresponding standard deviation ( $S_{test}$ ) are then tested against the maximum of the filtered validation residuals ( $X_{ref}$ ) and the corresponding standard deviation ( $S_{ref}$ ) using the Welch's t test. The effective window length of 90 is used for the test, and a significance level of 0.005 is chosen in this case to achieve robust detection and to minimise false alarms. A binary recorder is used to log the results, where the high level implies anomalous turbine gearbox behaviour and the low level indicates normal or acceptable operation. These records would be made available to wind turbine operators and anomalies would be flagged up if alarms appeared either for too long or too frequently.

In Figure 4-7(b), the red line shows a series of alarms from the beginning of the assessment period, revealing anomalous behaviour, and demonstrating consistency between the algorithm developed here and the observations of residuals. It can also be seen in the same figure that the alarms are reported immediately following each steep increment in the testing residuals. This shows the capability of the NSET model accurately to detect incipient anomalies within a wind turbine gearbox before they develop into catastrophic faults.

Ideally the detection method should have been compared with simple threshold based fault detection. However, there were very few occasions when high temperatures arose when turbines were operating normally and these data points had to be used as part of the training set and could not, therefore be used for testing. These data points did include

temperatures of 62 °C which, realistically, would be above any simple threshold. It is thus clear that with such a threshold, false alarms would have arisen. It is also clear that setting thresholds any higher, to avoid these false alarms, would have resulted in a failure to detect real faults.

Testing case II makes use of data from turbine T16. Operational data of half a year prior to the failure of this turbine, from August of 2005 to January of 2006, are used to confirm the anomaly detection capability of the model. The gearbox failure occurred immediately after the end of this testing period.

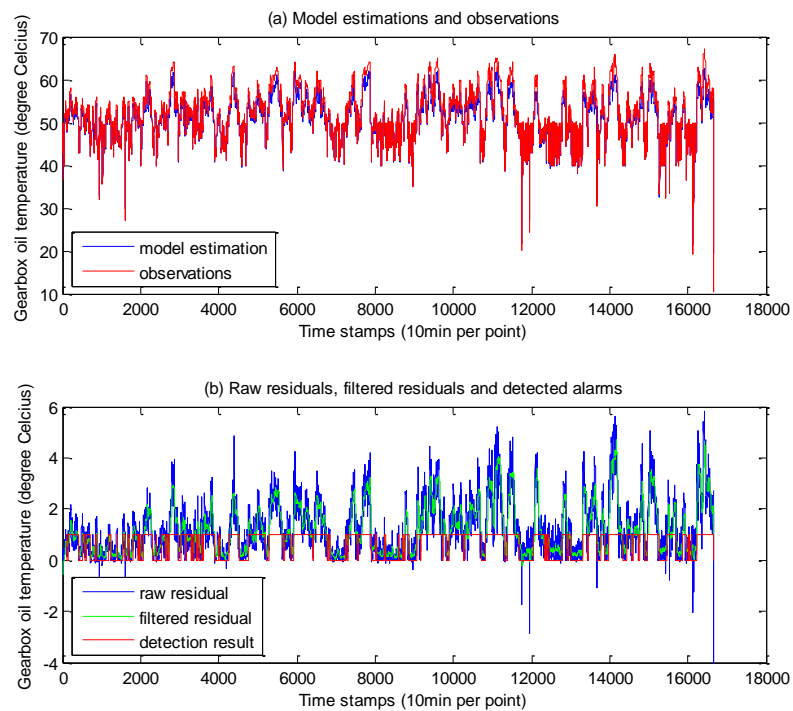


Figure 4-8: Testing results and anomaly detection of T16 for standard NSET

Anomaly detection in this case follows exactly the same procedures as for turbine T17, and the same validation result from turbine T1 is used as the reference for the hypothesis testing. Successful anomaly detection results are illustrated in Figure 4-8(a) and Figure 4-8(b), which leaves up to half a year for the turbine operator to make decisions regarding shut down and maintenance scheduling and demonstrates the robustness of

model. It can also be seen in Figure 4-8(b) that the test residuals exhibit an increasing trend throughout this six-month period, which is indicative of the progressive degradation of the turbine gearbox.

As can be seen in both Table 4-4 and Figure 4-8(a), the maximum oil temperature measurement is 67.0°C which is above the upper limit of 62.0°C as introduced by the maximal vector. The maximum modelled temperature corresponding to this peak is 62.6 °C demonstrating that the NSET can extrapolate beyond the memory matrix maximum values, albeit to a very limited degree, and with uncertain accuracy. Nevertheless, the model accuracy and overall performance is definitely improved by the addition of the maximal vector, as will be shown in Section 4.3.5.

#### **4.3.4. Comparison with a Neural Network model**

In order to prove the effectiveness of the NSET model, a performance comparison is carried out in this section with a Neural Network (NN) model similar to that successfully applied to wind turbine gearbox condition monitoring in references [58, 59]. Unlike the NSET model which calculates the weights based on the similarity between the state vectors including the entire set of input parameters, NN models are designed to capture data interrelationships between input parameters and outputs using weight and bias parameters for individual neurons. These weights are established through a training process, often using the back propagation algorithm [125]. The Levenberg-Marquardt algorithm is employed here since it is claimed to be the fastest algorithm for training small and medium-sized networks [126].

The NSET model utilized in the case study, being an auto-associative model as introduced in Chapter 2, effectively has 4 inputs and 4 outputs, so a 4-input 4-output NN model is used for fair comparison with identical validation data from turbine T1 and testing data from T16 and T17. The ‘tansig’ transfer function as shown in Table 2-1 is selected for the neurons in both of the hidden layer and output layer. And a hidden layer consisting of 3 neurons as used in reference [46] is employed here due to its best performance in model accuracy compared with other layouts such as that with 2 hidden

neurons. The state vectors that construct the memory matrix, with size of 989 in this case, are normalised before being used for NN model training and the same procedures for fault detection as introduced in Section 4.1.3 are adopted based on NN model estimation.

Validation and testing results are shown in Figure 4-9, Figure 4-10 and Figure 4-11. It can be seen by comparing these figures with those from the NSET model (Figure 4-6 for validation results; Figure 4-7 and Figure 4-8 for testing results and the associated fault detection) that the NSET model is more accurate than the NN model by producing smaller validation residuals, and also more capable of timely fault detection for the testing cases, particularly in case I for turbine T17 as shown in Figure 4-10 which fails to pick up any signatures for the anomaly. This demonstration of NSET model performance over the NN model confirms its robustness.

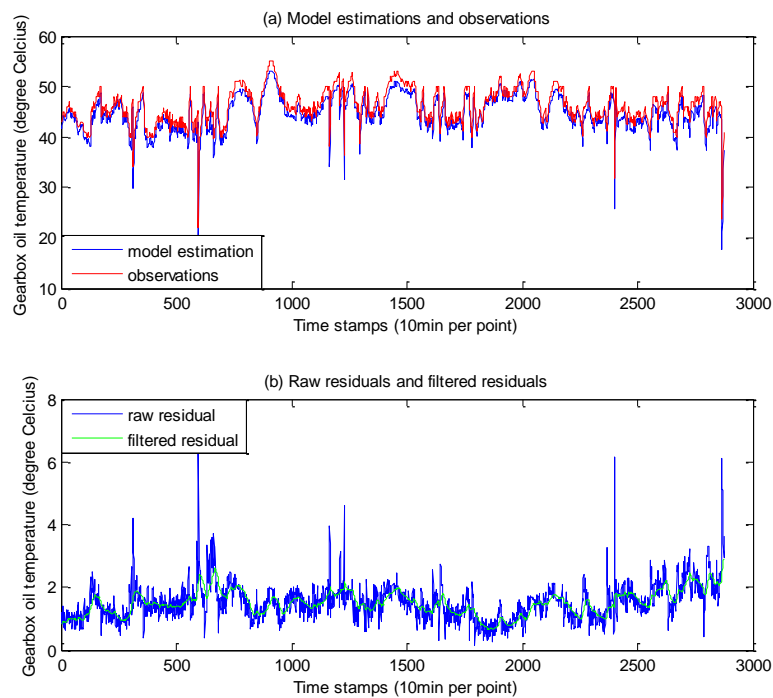


Figure 4-9: Validation results of T1 for NN model

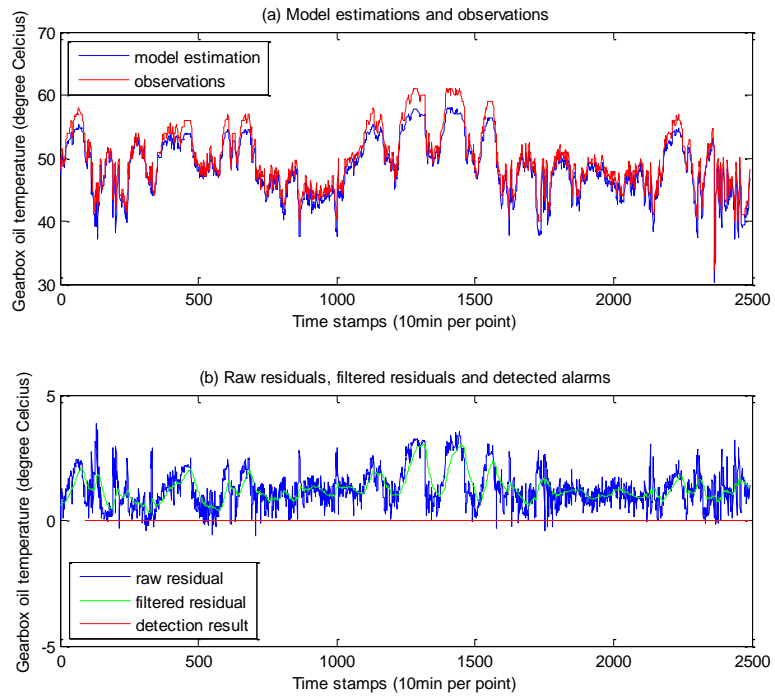


Figure 4-10: Testing results and anomaly detection of T17 for NN model

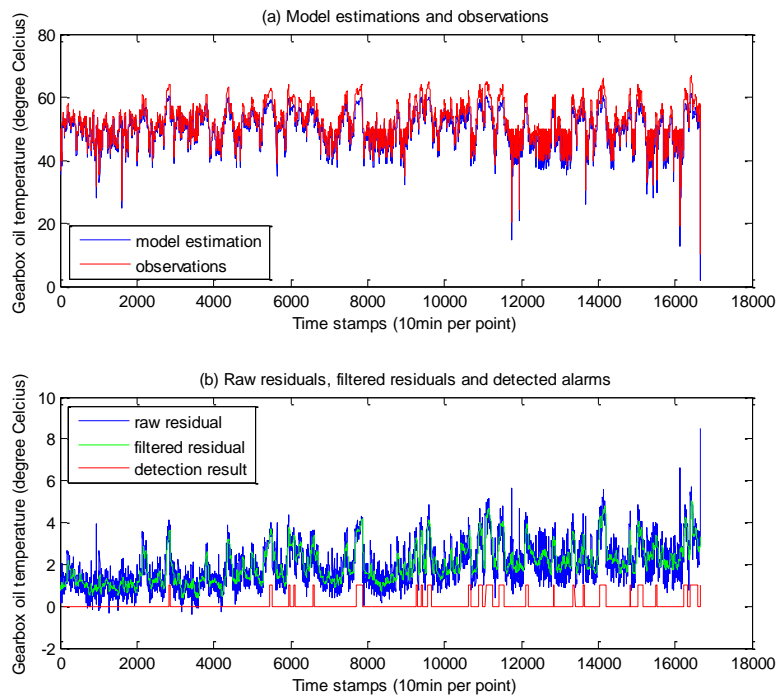


Figure 4-11: Testing results and anomaly detection of T16 for NN model

#### **4.3.5. Justification for use of the augmented state memory matrix**

The improvements to model performance achieved by inclusion of the null and maximal vectors are investigated in this section by using the validating data and testing data in both testing cases.

The main reason for adding the null vector is to improve the model accuracy especially in the context of missing/null data values. It also helps to improve modelling of the gearbox oil temperature following a turbine shutdown that will result in a gradual decay in temperature. It should be noted however that the missing/invalid data and the entries associated with the periods of shut down have been removed by the crude filtration, make the null vector slightly redundant.

The observation state vector with the maximal oil temperature to be included in the augmented memory matrix is [582.2, 69.0, 62.0, 24.4]. This vector is selected as it includes the highest oil temperature reached by any healthy turbine from the wind farm during the period in which data was available. This vector is added to the memory matrix to improve model accuracy in the case of high temperatures. Of course, if the temperature exceeds this value, as in testing case II for T16, some deterioration in model performance can be expected. One concern that remains is that improving model performance might make anomaly detection more difficult since the detection is based on the magnitude of residuals. However, the case studies in the previous section demonstrate successful fault identification. It is believed that improved models will result in fewer false alarms.

Table 4-5 demonstrates the impact of additional vectors on the model validation and testing performance, including four possibilities of memory matrix format: no augmentation, with only null vector, with only maximal vector and with both vectors. The average and RMS values of the validation and testing residuals for gearbox cooling oil temperature are used to measure model performance in each case, with smaller RMS values for validation residuals indicating better model accuracy. And a Residual Ratio (RR) that calculates the RMS ratio of testing residuals over the validation residuals is

used to indicate the degree of deviation for the testing data and also to some extent the potential for fault detection. A concept of Detection Ratio (DR) is also employed here for the testing data to present the proportion of testing instances being detected out of the complete testing set. For example, 8164 alarms are raised out of 16559 testing instances for turbine T16 in the augmented NSET model, leading to a DR value of  $8164/16559=49.3\%$  as shown in Table 4-5. According to this, larger values of DR for anomalous data indicate higher sensitivity of anomaly detection.

	Validation: T1		Testing I: T17				Testing II: T16			
	Mean (°C)	RMS (°C)	Mean (°C)	RMS (°C)	RR	DR (%)	Mean (°C)	RMS (°C)	RR	DR (%)
No augmentation	0.199	0.418	0.922	1.246	2.98	37.3	1.313	1.877	4.49	50.7
With null vector only	0.216	0.327	0.906	1.226	3.75	35.0	1.316	1.882	5.76	46.0
With maximal vector only	0.195	0.419	0.880	1.161	2.77	50.2	1.181	1.604	3.83	62.0
With both vectors	0.212	0.321	0.862	1.139	3.55	49.3	1.181	1.591	4.96	61.2

Table 4-5: Model effectiveness comparison to justify the additional null and maximal vectors

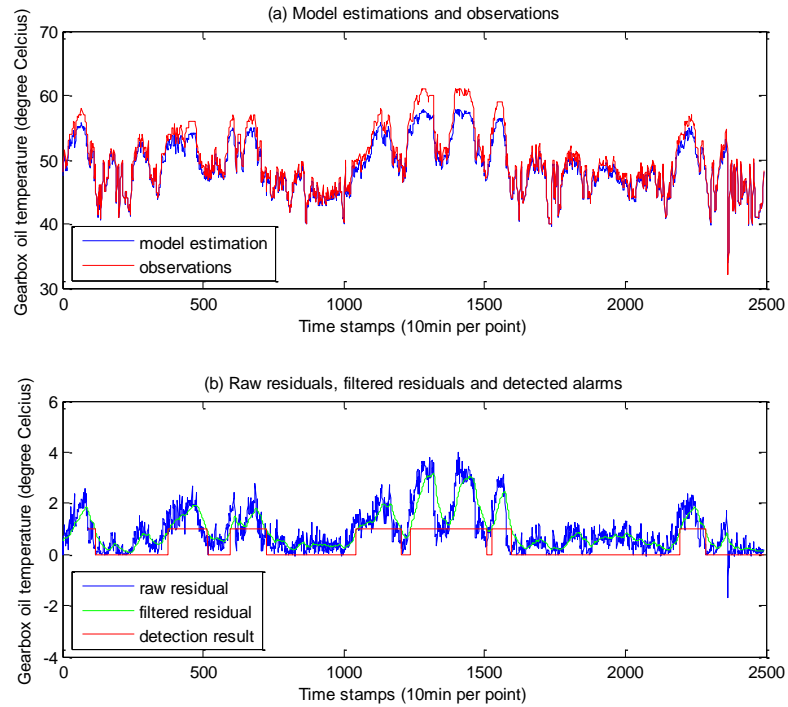


Figure 4-12: Testing results and anomaly detection of T17 for standard NSET with non-augmented state memory matrix

By comparing the non-augmented model and the one with the presence of the maximal vector in Table 4-5, it can be seen that the addition of the maximal vector improves the model accuracy in both testing cases by reducing the RMS value of the corresponding residual as expected. And surprisingly the largest DR values show up in the maximal vector present model in both testing cases even though the associated RR values are the lowest, demonstrating the improved model detectability introduced by the maximal vector. The validation accuracy is hardly affected by the maximal vector though since the value of variable in this case stays in the normal range. The null vector plays an insignificant role here due to the data filtration as mentioned earlier. The comparison between the non-augmented model and the null vector present model in Table 4-5 also gives such indication. All in all, the best performed model belongs to the one with both vectors in since it shows the lowest residuals RMS in all validation and testing cases albeit the DR values are slightly worse than the model only with the presence of the

maximal vector. More clear illustrations are shown in Figure 4-12 and Figure 4-13 for the testing results of T17 and T16 respectively with non-augmented model, which could be compared with Figure 4-7 and Figure 4-8 that result from fully augmented model.

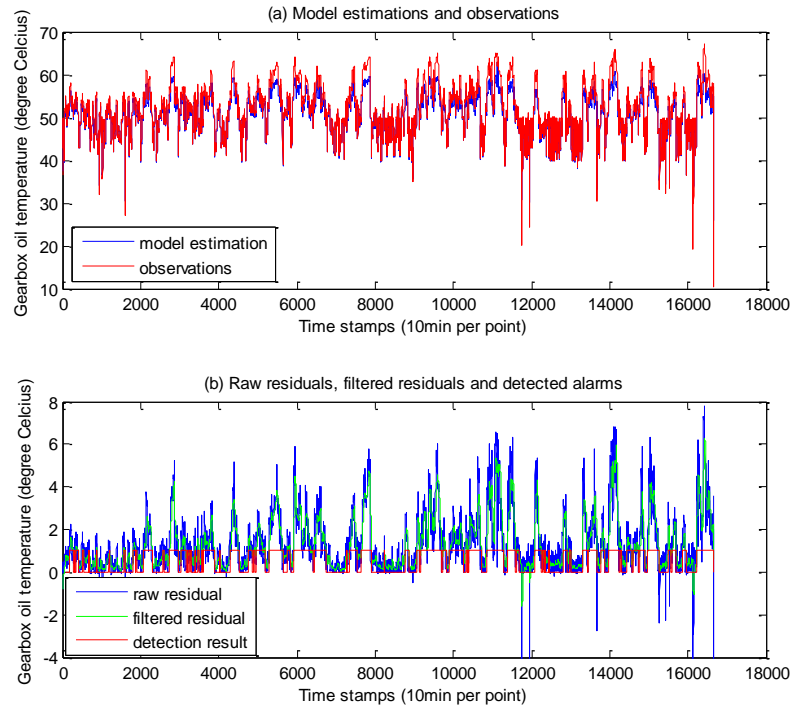


Figure 4-13: Testing results and anomaly detection of T16 for standard NSET with non-augmented state memory matrix

#### 4.3.6. Comparison with the modified NSET model

Recall the modified NSET model that has been proposed in Section 4.1.4, where the indicative variable in the state memory matrix and the observation vector is omitted for the weight vector calculation. This version of model is believed to produce more reliable results than the standard model since the results are based on the measurements from valid sensors only. The effectiveness of the modified model is investigated in this section and the results are compared to those from the standard model using the same gearbox case studies as presented in previous sections.

The gearbox cooling oil temperature is excluded from the memory matrix for weight vector calculation in the modified NSET model, leaving the involved variables to be the gearbox bearing temperature, nacelle temperature and the turbine power output. The size of memory matrix for the standard model was chosen to be  $4 \times 989$ . The same number of state vectors including those two additional vectors is retained in the modified model for a fair comparison. And all the validation and testing data here are also kept exactly the same as used in the standard model.

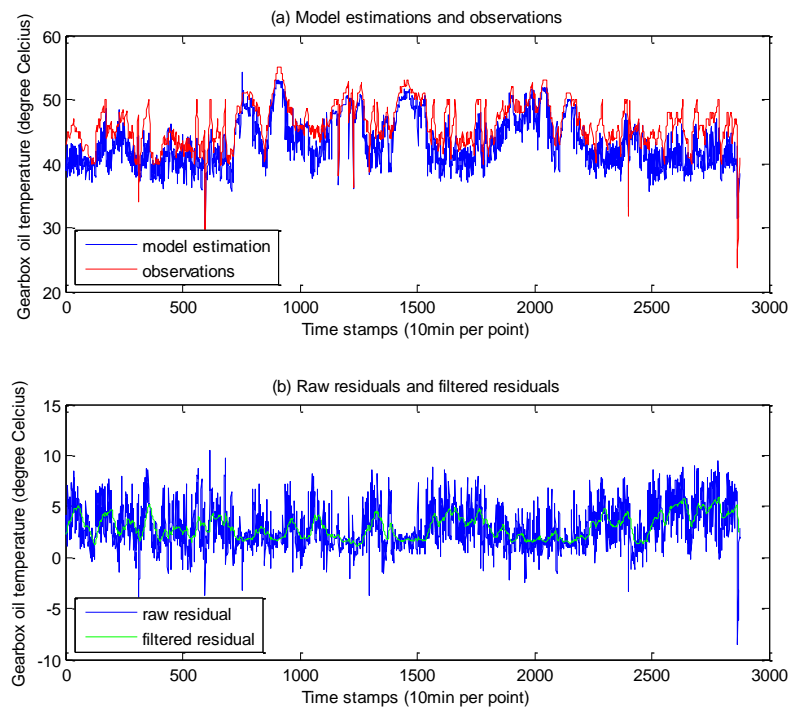


Figure 4-14: Validation results of T1 for modified NSET

The model validation results as illustrated in Figure 4-14 exhibit significant degradation from those for the standard model as shown in Figure 4-6. The summarised statistics for validation residuals in Table 4-6 also provides indication of deteriorated accuracy for the modified model. Similar observations can be found for the testing cases from both the testing statistics in Table 4-6 and the comparison between Figure 4-15 and Figure 4-7 for turbine T17 and Figure 4-16 and Figure 4-8 for turbine T16. An additional observation is the dramatic reduction in detected alarms compared with the standard

model, in particular for the testing case of T17 as shown in Figure 4-15(b), where only few isolated and inconsistent alarms are recorded. The value of both the residual ratio and the detection ratio in Table 4-6 also imply a reduced effectiveness of the modified model.

The poor model performance in terms of accuracy and detection sensitivity is very likely due to the lack of model input variables. Unlike the reference [81], in which the successful implementation of modified NSET model is based on more than 20 highly model-relevant parameters, only 3 variables are available in this case. Further inclusion of gearbox oil related variables is expected to improve the modified version of model. For example, the rotor/generator rotational speed (but in this case it is a fixed speed stall regulated turbine) is directly associated with the gearbox loading and hence being believed to improve the model accuracy. This variable is included in the input sets in the gearbox related model developed in reference [121], but it is not available in the SCADA data for the presented case studies.

For the reasons mentioned above, the modified NSET model will not be used in the following analyses in this chapter and instead the standard NSET model is chosen.

	Validation: T1		Testing I: T17				Testing II: T16			
	Mean (°C)	RMS (°C)	Mean (°C)	RMS (°C)	RR	DR (%)	Mean (°C)	RMS (°C)	RR	DR (%)
Standard NSET	0.212	0.321	0.862	1.139	3.55	49.3	1.181	1.591	4.96	61.2
Modified NSET	2.968	3.644	4.577	5.145	1.41	0.12	5.172	5.747	1.58	20.7

Table 4-6: Model effectiveness comparison between standard model and modified model

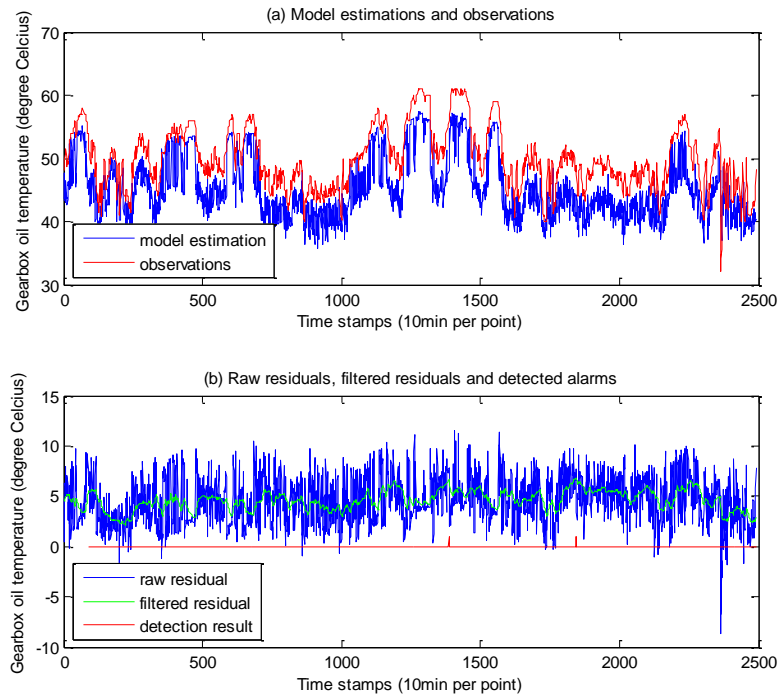


Figure 4-15: Testing results and anomaly detection of T17 for modified NSET

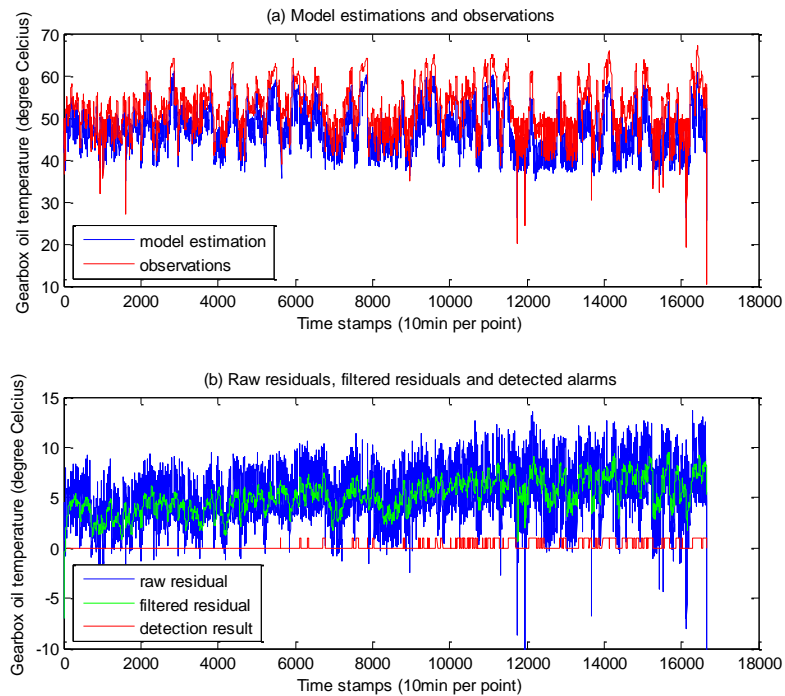


Figure 4-16: Testing results and anomaly detection of T16 for modified NSET

### 4.3.7. Impact of memory matrix normalisation on model performance

The standard NSET model keeps the original value of variables in the state memory matrix in order to calculate the weight vector applied to the different states when calculating the estimate of the variable of interest. In Section 4.1.1 it was explained that a Euclidean distance operator was used for the weight vector estimation. However, it is clear that a Euclidean distance calculated from the raw values of the various variables would be dominated by the variable with the largest range of values. In this case the value of turbine power output is of the order of  $10^2$  kW and the rest of the temperature related variables in the standard model are of the order of  $10^1$  °C, so the power output obviously make the most contribution, which may not be desirable. In order to eliminate this bias, it is preferable to normalise all the variables individually with respect to their respective ranges, as implemented in reference [84]. The effect of normalising variables on the model performance is explored as follows.

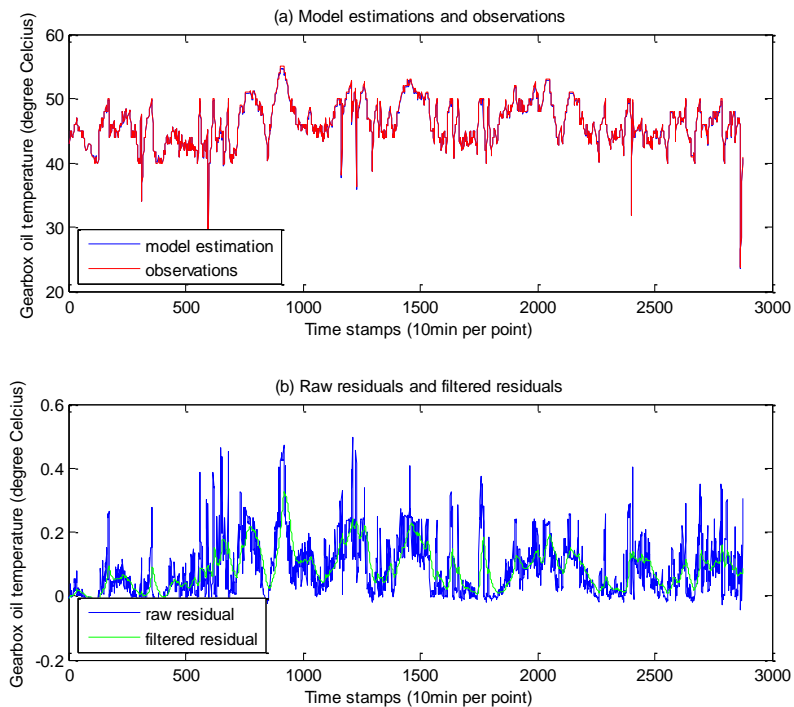


Figure 4-17: Validation results of T1 for normalised NSET

The same validation and testing data are retained for the analyses here and the corresponding results are presented in Figure 4-17, Figure 4-18 and Figure 4-19 with their residual statistics summarised in Table 4-7.

It can be found that the general model accuracy in all the validation and testing cases has been significantly enhanced by normalising the variables. However, the downside of the normalised NSET model is the reduction of the detection sensitivity, which is expressed by both the DR value in Table 4-7 and the anomaly detection results in Figure 4-18(b) and Figure 4-17(b) for testing cases I and II. In particular, Figure 4-18(b) shows a slower and much less frequent detection for T17 compared to the results in Figure 4-7(b).

An additional period of testing data is chosen with one month of healthy operational data from July of 2006 for turbine T16 after its gearbox was replaced following the known failure. This extra case, referred to as testing case III, is employed to investigate the model's resistance to false alarms and the corresponding results are presented in both Figure 4-20 and Figure 4-21 and Table 4-7. Ideally the model's resistance to false alarms should be explored based on data from healthy turbines operating with high gearbox oil temperatures, but these occasions are very rare and the only available data points had to be used as part of the training set and could not, therefore be used for testing.

Figure 4-20 and Figure 4-21 illustrate the results of the standard and normalised NSET model for testing case III. The figures show relatively low level of cooling oil temperature even though it was in July, confirming a healthy gearbox as mentioned earlier, in which case the detection ratio should be zero as shown in Figure 4-21. However, false alarms could be observed in Figure 4-20, making the standard NSET model less effective than the normalised model.

The normalised NSET model generally performs better than the standard one in terms of model accuracy and resistance to false alarms although it shows less detection sensitivity. As might be expected greater detection sensitivity results in more false alarms. Choosing the best model must reflect this trade-off. The next section will further investigate the impact of weighted variables on the performance of normalised model.

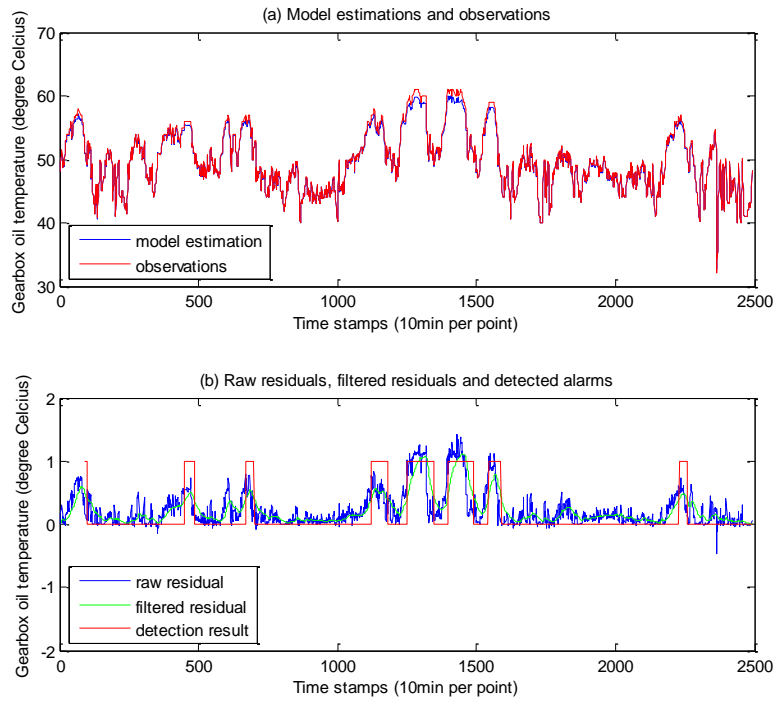


Figure 4-18: Testing results and anomaly detection of T17 for normalised NSET

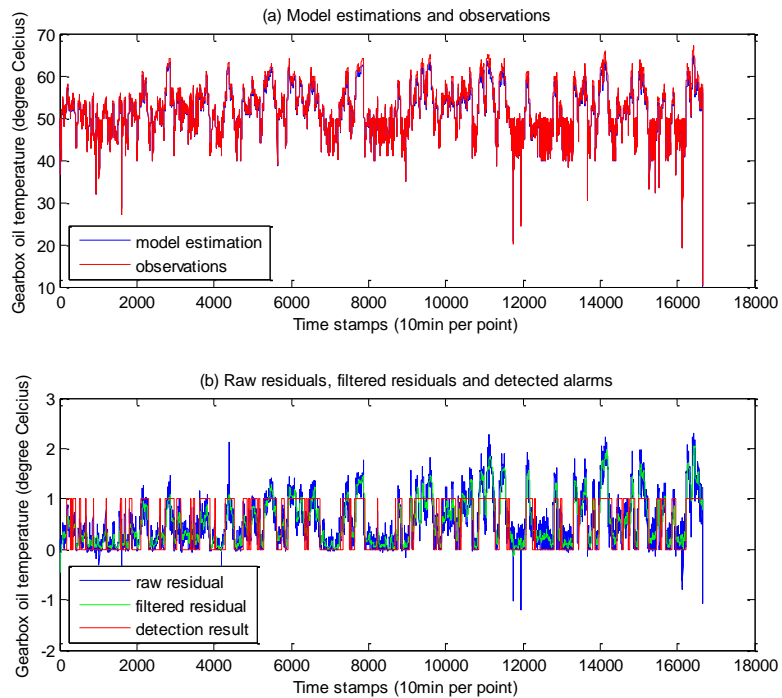


Figure 4-19: Testing results and anomaly detection of T16 for normalised NSET

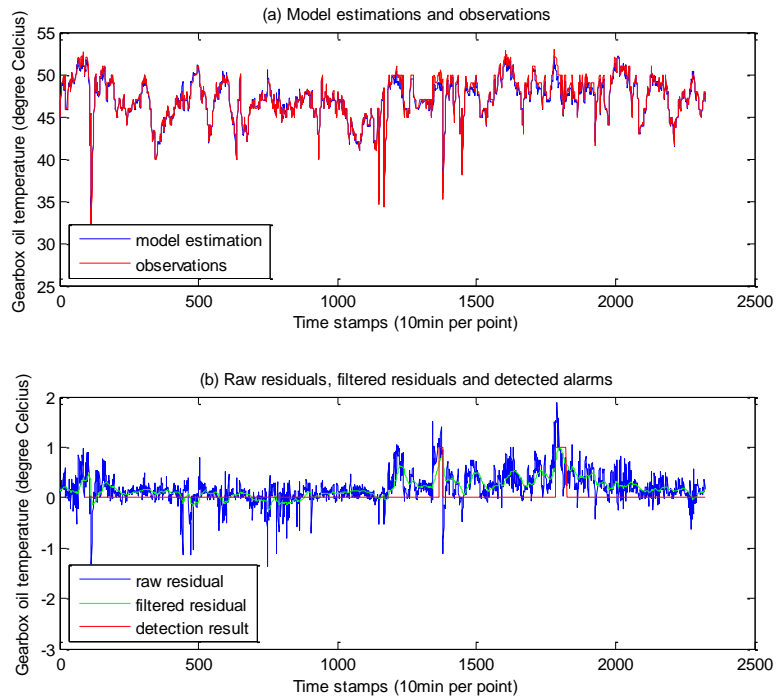


Figure 4-20: Testing results of healthy T16 in testing case III for standard NSET

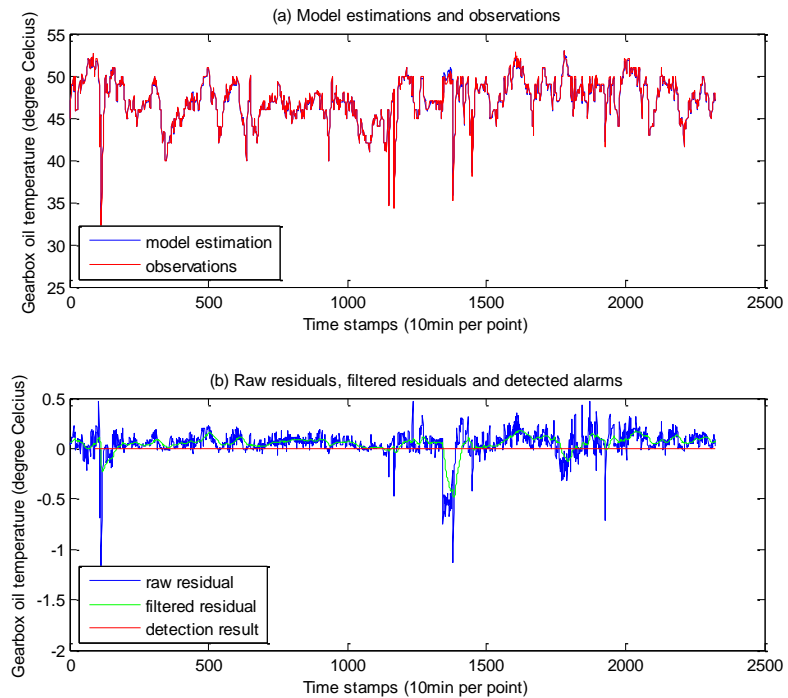


Figure 4-21: Testing results of healthy T16 in testing case III for normalised NSET

	Validation: T1		Testing I: T17				Testing II: T16				Testing III: T16			
	Mean (°C)	RMS (°C)	Mean (°C)	RMS (°C)	RR	DR (%)	Mean (°C)	RMS (°C)	RR	DR (%)	Mean (°C)	RMS (°C)	RR	DR (%)
Standard NSET	0.212	0.321	0.862	1.139	3.55	49.3	1.181	1.591	4.96	61.2	0.189	0.366	1.14	2.55
Normalised NSET	0.086	0.125	0.229	0.367	2.94	16.5	0.526	0.720	5.76	48.5	0.049	0.146	1.17	0
Normalised NSET with weighted variables	0.059	0.091	0.142	0.254	2.79	12.1	0.396	0.547	6.01	47.2	0.031	0.100	1.10	0
Reduced parameter NSET	0.002	0.025	0.110	0.176	7.04	39.9	0.153	0.220	8.80	56.5	-0.055	0.155	6.2	0
Time lagged NSET	0.003	0.027	0.127	0.196	7.26	40.1	0.166	0.240	8.89	54.1	-0.096	0.227	8.41	0

Table 4-7: Further model effectiveness comparison under different situations for gearbox case study

#### **4.3.8. Impact of weighted variables in the distance norm on model performance**

The contribution of different variables to the calculation of the Euclidean distance has been discussed in the last section and this leads to the idea of refining the distance calculation using weighted variables. In this case, the nonlinear operator  $\otimes$  used for weighting vector calculation as shown in Equation (4-7) is updated with Equation (4-17) where the weighting parameter,  $k_i$ , are assigned with the associated correlation coefficients for the variables with the cooling oil temperature as shown in Table 4-3.

$$\mathbf{x} \otimes \mathbf{y} = \sqrt{\sum_{i=1}^n k_i (x_i - y_i)^2} \quad (4-17)$$

This is believed to enhance the model accuracy since the more relevant, i.e. more highly correlated, variables such as the gearbox bearing temperature, can then make a greater contribution through weighting of the distance metric than the less relevant variables, such as the nacelle temperature.

The statistics of the corresponding residuals for the validation and testing cases are listed in Table 4-7 to form a contrast with the results from the normalised NSET model which is at this point the preferred model. It can be seen through the RMS values for validation residuals that the model accuracy is improved by assigning weighting to different variables in the distance norm calculation. The resistance to false alarms is also retained in this case and the detection sensitivity is very slightly worse. Although the ability to detect anomalies is slightly reduced, the overall model performance is excellent. The impact of reduced parameter on the model performance is explored in the next section based on the normalised NSET model with weighted variables.

#### **4.3.9. Discussions of the model performance by removing the parameter of Gearbox bearing temperature**

It can be seen from Table 4-4 that both the maximal gearbox cooling oil temperature and the bearing temperature in the testing cases exhibit higher levels than those in the

training/validation set. More clear relationships are illustrated in Figure 4-22 and Figure 4-23 where the cooling oil and bearing temperatures are plotted against the turbine power output for T16 in testing case I and T17 in testing case II, respectively. The pattern formed between the cooling oil temperature of anomalous turbines and their power output in both figures shows significant deviations from that of the healthy turbines. This demonstrates the sensitivity of the gearbox cooling oil temperature to the impending failure and hence demonstrating the importance of this variable as an effective condition indicator. The relationship between anomalous gearbox bearing temperature and the corresponding power production also exhibits differences (increasing trend similar to the cooling oil temperature case) from the normal conditions in these two figures, though with less degree of discrepancy than the cooling oil temperature case. This is understandable since the bearing temperature is affected by the progressive degradation within the gearbox and the associated increase in temperature through heat conduction between the two. It should also be noted that it has been confirmed that neither test case involved a main bearing failure. However the inclusion of such variable could potentially degrade the model's effectiveness in fault identification since the elevated bearing temperature would lead to higher model estimations of oil temperature than with the bearing temperature absent from the model, and hence resulting in smaller testing residuals and potential failure in anomaly detection.

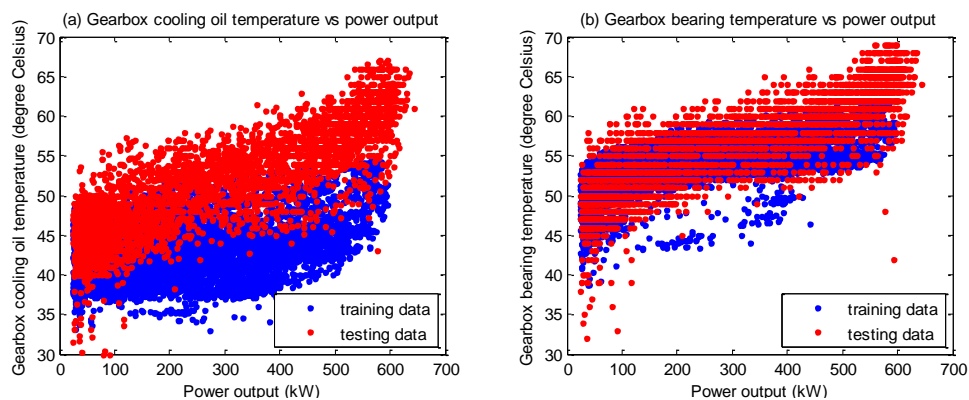


Figure 4-22: Gearbox temperature vs. power output for T16 in testing case I

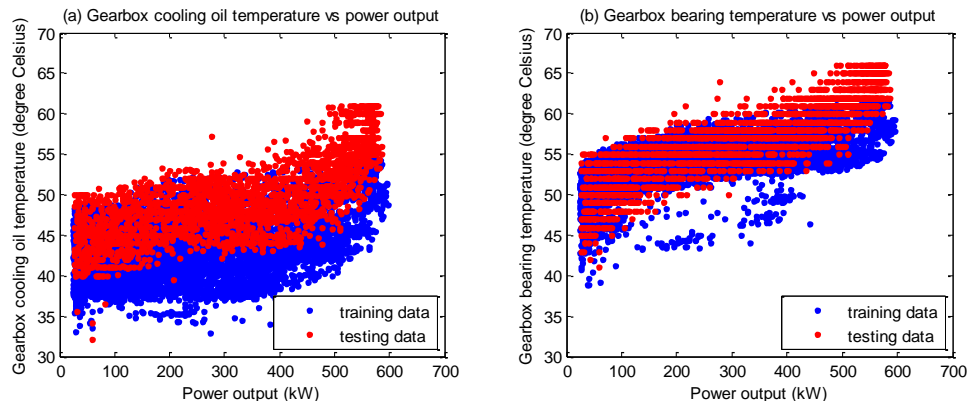


Figure 4-23: Gearbox temperature vs. power output for T17 in testing case II

The effect of removing the gearbox bearing temperature on the model performance is explored in this section based on the normalised NSET model with weighted variables since this model has been proved to be more effective than the standard model and the basic normalised model, particularly in terms of model accuracy. The explored model here is referred to as the reduced parameter model. The same validation and testing data as used in the previous section are retained and the results are presented in Figure 4-24, Figure 4-25, Figure 4-26, Figure 4-27 and Table 4-7, which could be compared with results under other conditions in Table 4-7 and figures as shown in previous sections to observe the differences induced by the reduced parameter model.

It is noticed that the RR value is consistent with the DR value for most of the analyses with some exceptions such as testing case III in Table 4-7, where the relatively large RR value for the reduced parameter model does not contribute to the alarm detection. This is due to the large negative residuals, as shown in Figure 4-27, which increase the associated residual RMS and RR value but are not relevant to anomaly detection. Moreover, it can be seen that both the model accuracy and detection sensitivity are further improved by employing the reduced parameter NSET model. The residuals for both testing cases I and II are smaller in the reduced parameter model than in the normalised model with weighted parameters, which is contrary to expectation. Also the resistance to false alarms is retained here.

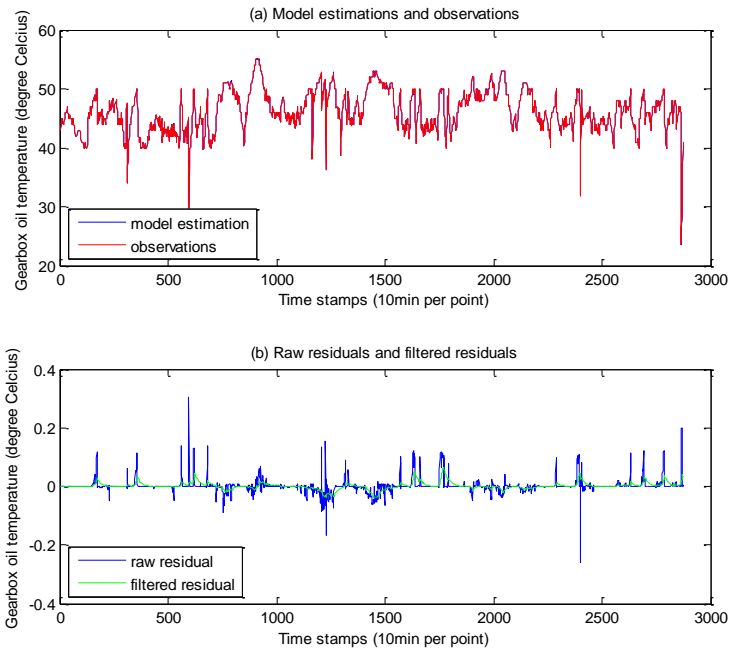


Figure 4-24: Validation results of T1 for normalised NSET with reduced parameter and weighted variables

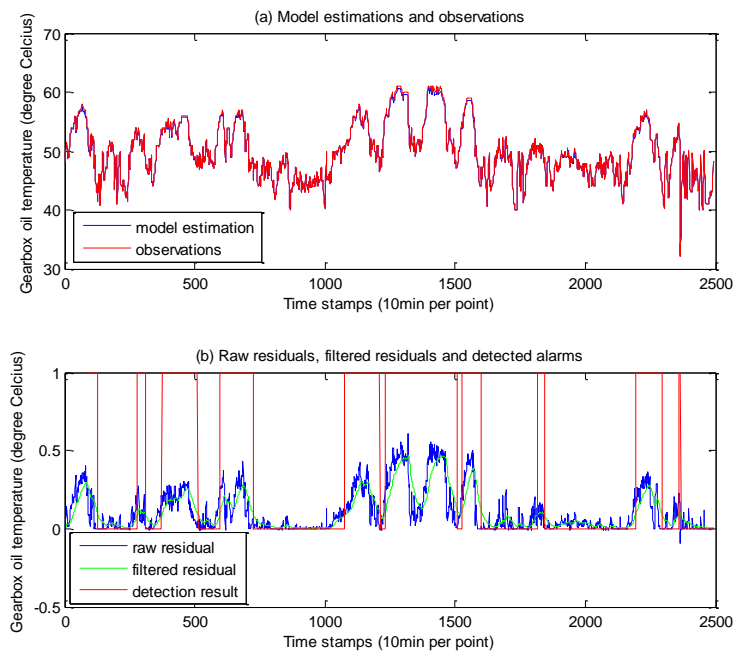


Figure 4-25: Testing results and anomaly detection of T17 for normalised NSET with reduced parameter and weighted variables

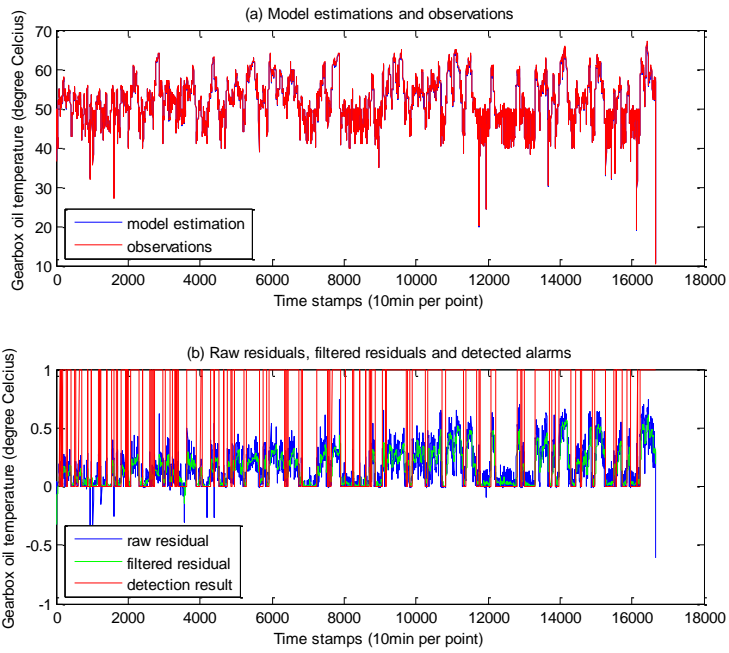


Figure 4-26: Testing results and anomaly detection of T16 for normalised NSET with reduced parameter and weighted variables

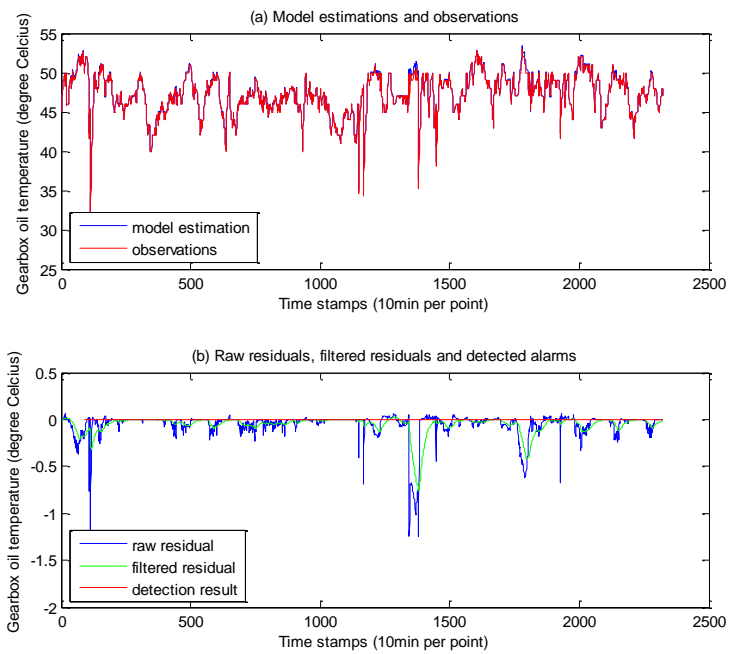


Figure 4-27: Testing results of healthy T16 in testing case III for normalised NSET with reduced parameter and weighted variables

#### 4.3.10. Discussions of the effect of time-lagged variable on model performance

Heat generation within the gearbox that is associated with power production will result in a rise in gearbox cooling oil temperature but there will be some time delay due to the inherent thermal mass of the gearbox. Consequently time-lagged power is anticipated to be more highly correlated with the gearbox oil temperature than concurrent values. It is therefore interesting to explore whether using suitably time-lagged power values in the memory matrix can improve the NSET models and make fault detection more effective. This idea is supported by earlier work reported in references [58] and [59], in which the generated power in the cooling oil temperature model is delayed by 3 and 2 time steps respectively, with each step being 10 minutes, as in this case. In this section the influence of time delay in power output on the model performance is examined based on the best performing model so far, i.e. the normalised model with weighted distance norm and with reduced parameters, as presented in the previous section.

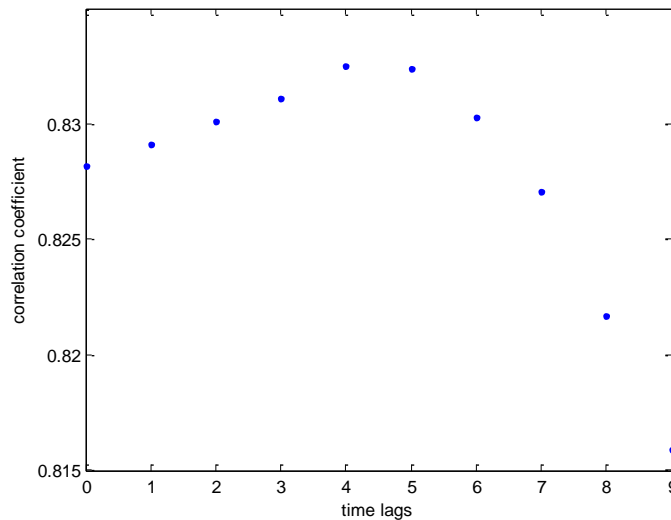


Figure 4-28: Correlation coefficients between cooling oil temperature and turbine power output with different time delays

The correlation coefficients between the cooling oil temperature and the power production for different time delays are shown in Figure 4-28, from which it can be observed that the highest correlation, 0.8325, occurs at power output with 4 steps delay,

i.e. a 40 minutes lag, and the coefficient without delay is slightly less at 0.8282 as shown in Table 4-3 (and Figure 4-28). So the reduced variable model with 3 inputs as shown in last section is updated by replacing the concurrent power output with its value at (t-4), which is referred to as the time lagged model. The corresponding results are summarised in Table 4-7.

Contrary to expectation, the time lagged model shows slightly worse model accuracy than the reduced parameter model and the detection sensitivity also shows no sign of improvement. One reason for this could be the quality of the data and subsequent data filtering to remove invalid measurements resulting in an incomplete time series. So the time lagged power output could at times actually be further back in time, leading to deteriorated model effectiveness. In this case, the percentage of values that are removed by the filtration is 36% and 42% for the testing cases from turbines T16 and T17 respectively as shown in Table 4-4, indicating relatively poor data quality and thus confirming the proposed interpretation. It is possible that with high quality data, the use of lagged power values could be advantageous, but it is left to further research to establish this. The time lagged model is not further considered here and the reduced parameter NSET model is retained for its best performance.

#### **4.3.11. Discussions of other model performance metrics**

The model accuracy and detection ratio have been employed to indicate the ability of a model to correctly estimate the variable value and effectively detect the performance deviation that is caused by the approaching system failure, respectively. Based on these criteria the reduced parameter model shows the best performance so far. Two other metrics, auto-sensitivity and cross-sensitivity, are introduced in this section and used to further assess the performance of the preferred NSET model as an auto-associative model as has been introduced in Chapter 2.

Auto-sensitivity measures the ability of an auto-associative model to make correct estimations of the variables when they are distorted due to either a faulty sensor or degradations in the monitored system. The auto-sensitivity,  $S_{A i}$ , is defined as the change

in the estimation of a particular variable caused by the drift in its corresponding sensor measurement [127], which is expressed by Equation (4-18) below.

$$S_{A i} = \frac{1}{N} \sum_{k=1}^N \left| \frac{\hat{x}_{ki}^{drift} - \hat{x}_{ki}}{x_{ki}^{drift} - x_{ki}} \right| \quad (4-18)$$

where the denominator shows the drifted values of a specific variable and the numerator is the corresponding change in the variable estimation; and N is the number of samples used in the prediction. A robust auto-associative model would produce small or ideally no changes in the variable prediction for small drifts in the fault-free variable values. An ideal auto-sensitivity value is 0, which indicates that the model is capable of producing reliable predictions in spite of drifted sensor measurements. An extreme case with auto-sensitivity value of 1 implies the inability of a model to detect anomaly since the model prediction would follow the input drift and result in residuals of zero in this case. In the common cases the model's auto-sensitivity value is between 0 and 1, which means that the resultant residuals will underestimate the drifts in sensor reading, i.e. the signature of the fault [82].

Cross-sensitivity for each individual variable in the model,  $S_{C i}$ , is defined by Equation (4-19) below.

$$S_{C i} = \frac{1}{N} \sum_{k=1}^N \left| \frac{\hat{x}_{ki}^{drift} - \hat{x}_{ki}}{x_{kj}^{drift} - x_{kj}} \right| \quad (4-19)$$

where the numerator and denominator retain the same meaning as in the auto-sensitivity expression with the exception of  $i \neq j$ , indicating the consideration of the effect from a problematic sensor on the prediction of other variables [127].

The auto- and cross-sensitivity are calculated for the best performing model so far, i.e. the reduced parameter model, using the validation data with artificial modification of the time series data for the parameters of interest. The performance metrics are calculated

using Equation (4-18) and Equation (4-19) with regards to the gearbox oil temperature since it is the condition indicator used for the gearbox case study.

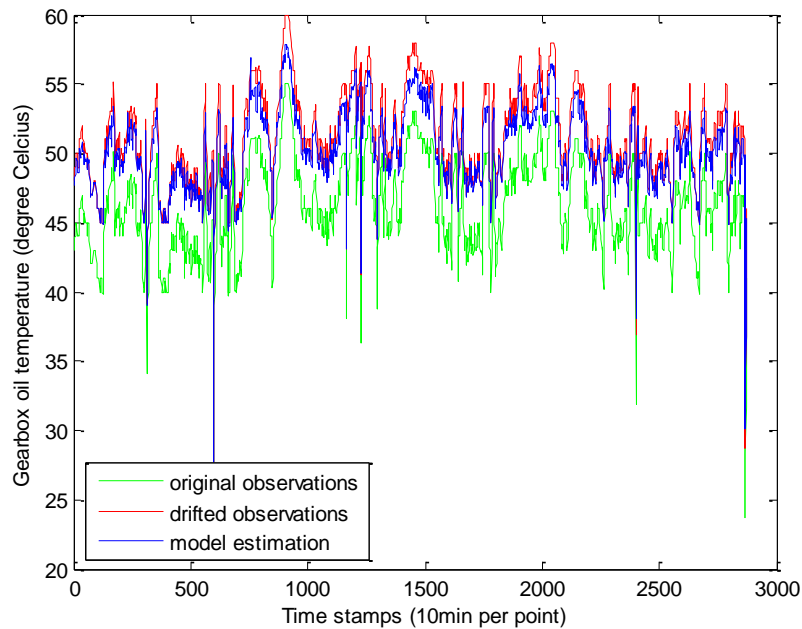


Figure 4-29: Illustration of auto-sensitivity performance using the validation data

Figure 4-29 shows the auto-sensitivity results where a consistent drift of  $+5^{\circ}\text{C}$  is added to the original oil temperature observation of the validation data, which is illustrated by the green line. The modified observation and the corresponding prediction are illustrated in the same figure by the red and blue curve respectively. It can be seen that the model prediction is affected by the faulty inputs and the associated auto-sensitivity value is 0.82. The corresponding residual would also underestimate the actual sensor drift, which would theoretically reduce the model's detectability to some extent. This inherent nature of the auto-associative NSET model is reflected by the conflict between NSET model accuracy and detection sensitivity. However the successful anomaly detection in the previous section has demonstrated the robustness of model and suggests that even a high value of the auto-sensitivity need not be a problem. Similarly the cross-sensitivity values due to artificial drift in power output and nacelle temperature are 0.02 and 0.07, respectively. This results in an average cross-sensitivity value of approximately 0.05,

which is reasonably low and indicates that the model prediction of oil temperature is impervious to faulty inputs from other variables.

#### 4.4. NSET application to wind turbine generator case study

Successful NSET application to gearbox condition monitoring has been presented in previous sections. The effectiveness of the NSET model is further demonstrated here using a generator case study. Three available variables including turbine power output, generator winding temperature and nacelle temperature are chosen for the condition monitoring purpose for generator based on the domain knowledge in Section 4.2, with the generator winding temperature being the condition indicator for the generator.

Output parameters	Generator winding temperature
Input parameters	
Generator winding temperature (°C)	1
Power output (kW)	0.9066
Nacelle temperature (°C)	0.3008

Table 4-8: Pearson’s correlation coefficients between generator model input and output parameters

The correlation between the generator winding temperature and the other variables is listed in Table 4-8. The power output is required due to the high correlation to the winding temperature and the nacelle temperature is also needed for the same reason as mentioned in the gearbox analysis.

The generator failure for turbine T8 occurred on November of 2006 as introduced earlier. Two months of data prior to the final failure are used as the testing data. The gearbox case study employed a generic model that takes the training data from the averaged values from a group of healthy turbines and then the model could also be validated and tested on different turbines. The analysis of generator here uses a specific model, the training, validation and testing data of which come from the same turbine, T8 in this case. The reason is that the upper limit of generator winding temperature from other

healthy turbines does not approach that of turbine T8 during the testing period, and the data from T8 itself exhibits a much wider winding temperature range throughout the available period.

Data from turbine T8 are used as training data in order to get rid of the concern of model's inability to extrapolate and the very beginning three months (April to June of 2005) out of the available period are chosen to avoid involving deteriorating performance in the training set and hence eliminating false negatives in the detection results. The operational data of the following month (July of 2005) are used for validation purpose. An additional testing data from August of 2005, which are assumed to represent a healthy generator, are employed to investigate the model's resistance to false alarms. Table 4-9 lists the value ranges for different data sets and the crude data filtration that was applied in the same manner as for the gearbox case study. It can be noticed in this table that the maximal training generator winding temperature is 154°C, which is the highest available even though it is still 2°C less than the testing maximum.

A memory matrix size of  $3 \times 818$  is chosen based on the same method as used in Section 4.3.1 for the gearbox analyses. Three different NSET models, including the standard model, the normalised model and the normalised one with weighted parameters, are then validated and tested, and the results are summarised in Table 4-10. The results are not presented here due to the consideration of space occupation and also because they are similar in nature to those already presented. They can be found instead in Appendix I.

All these three models show successful detections to actual fault and a lack of false positives. It can be seen from Table 4-10 that the model accuracy is improved significantly by normalising the memory matrix and the addition of the weighting the parameters. However, the detection sensitivity exhibits opposite trend with the model accuracy, which shows consistency with the results of the gearbox application in Table 4-7 for the three models mentioned. The NSET model performance was further improved by removing a redundant variable in the gearbox case study, but all variables here are considered highly relevant for the generator analyses. So it can be concluded

that no simple rules can be applied regarding the model selection and compromises between model accuracy and detection sensitivity are required.

Data usage	Variables	Filtration criteria	Value range after filtration		Percentage of values being removed (%)
			min	max	
Training set (April – June 2005)	Active power (kW)	> 25	30.09	634.59	70
	Generator winding temperature (°C)	> 0	13.00	154.00	
	Nacelle temperature (°C)	> 0	5.00	28.62	
Validation set (July 2005)	Active power (kW)	> 25	50.29	611.04	28
	Generator winding temperature (°C)	> 0	23.00	131.00	
	Nacelle temperature (°C)	> 0	9.00	29.09	
Testing set I (anomalous; October – November 2006)	Active power (kW)	> 25	30.02	626.10	49
	Generator winding temperature (°C)	> 0	11.00	156.00	
	Nacelle temperature (°C)	> 0	5.82	22.92	
Testing set II (healthy; August 2005)	Active power (kW)	> 25	30.10	586.22	46
	Generator winding temperature (°C)	> 0	23.00	116.00	
	Nacelle temperature (°C)	> 0	10.00	25.29	

Table 4-9: Filtration criteria of the selected variables for generator case study and the corresponding results

	Validation		Testing I (anomalous)				Testing II (healthy)			
	Mean (°C)	RMS (°C)	Mean (°C)	RMS (°C)	RR	DR (%)	Mean (°C)	RMS (°C)	RR	DR (%)
Standard NSET	-0.011	0.757	3.530	5.928	7.83	66.3	-0.012	0.263	0.35	0
Normalised NSET	0.052	0.460	1.653	2.844	6.18	38.6	0.026	0.167	0.36	0
Normalised NSET with weighted variables	0.035	0.390	1.350	2.375	6.09	31.8	0.024	0.149	0.38	0

Table 4-10: Model effectiveness comparison under different situations for generator case study

## **4.5. Chapter summary**

Turbine gearbox and generator anomalies in all testing cases (i.e. turbines T16 and T17 for gearbox applications and T8 for generator application) are successfully detected based on the NSET estimation and leave sufficient time for the turbine operator to make decisions for maintenance schedules before the final gearbox failure. In the gearbox case study the normalised 3-inputs model with weighted parameters outperforms the rest of models in terms of model effectiveness and resistance to false alarms. Nevertheless, no definite model could be chosen in the generator analyses and compromises between model accuracy and detection sensitivity are needed.

Another key feature revealed by the two gearbox examples is that the NSET model as fitted here, based on operational data from five turbines collected over three months of spring 2005, works well when dealing with other turbines of the same type and for operation at different times of year when metrological conditions are different. Thus NSET models constructed in the manner proposed here are applicable to turbines regardless of seasons and location within the wind farm. This simplifies the development and application of such models for condition monitoring as generic models so developed can be widely applied.

However, the generic model becomes unfeasible sometimes, such as in the generator example where the value range of variables in the training data poses a problem for the generic multi-turbine model and a specific model has to be used instead. The next chapter will explore the NSET model in spatial applications where the estimation of the indicative variable from the turbine of interest is based on the simultaneous measurements from the turbines nearby. This is believed to overcome the issues of training data insufficiency that are confronted by the generic model such as in the generator example since the training data would be extracted from a turbine subgroup and the spatial model would regard the value range difference in the training set as an embedded relationship in the model.

## 4.6. Chapter references

121. Schlechtingen, M., Santos, I.F., Achiche, S., *Wind Turbine Condition Monitoring Based on SCADA Data using Normal Behavior Models, Part 1: System description*, Applied Soft Computing, Volume 13, Issue 1, Pages 259-270, Jan.2013.
122. Heij, C., de Boer, P., Franses, P.H., Kloek, T., van Dijk, H.K., *Econometric methods with applications in business and economics, Chapter 3: Multiple Regression*, Oxford University Press, 2004.
123. *Z-Transform Digital Signal Processing*, e-TECHNote from IRDC India, 2009.
124. Schlechtingen, M., Santos, I.F., *Comparative Analysis of Neural Network and Regression Based Condition Monitoring Approaches for Wind Turbine Fault Detection*, Mechanical Systems and Signal Processing, Volume 25, Issue 5, Pages 1849-1875, Jul. 2011.
125. Rojas, R., *Neural Networks: A Systematic Introduction*, Springer-Verlag, Berlin, 1996.
126. Yu, H., Wilamowski, B.M., *Levenberg-Marquardt Training*, The Industrial Electronics Handbook, Vol. 5 - Intelligent Systems, 2nd ed., CRC Press, Boca Raton, 2011.
127. Hines, J.W., Garvey, D., *Development and Application of Fault Detectability Performance Metrics for Instrument Calibration Verification and Anomaly Detection*, Journal of Pattern Recognition Research, Vol. 1, 2006.

## **5. Spatial application of NSET model for wind turbine gearbox fault detection**

Individual turbine based anomaly detection across the wind farm will involve lots of data analyses and therefore cannot be done by hand. The development of spatial data-mining techniques that can analyse the SCADA data from part of or complete wind farms with large numbers of identical make of turbines would significantly reduce the efforts of repeated model construction for each individual turbine.

Following the successful application to individual turbine gearbox condition monitoring in Section 4.3, the NSET method is applied to multiple turbines in a spatial context using the same gearbox examples from turbines T16 and T17; it is used to capture relationships among wind turbines across the wind farm. In this case the state vectors in memory matrix include records of the gearbox oil temperature and other associated variables from a group of turbines that are closely located within the wind farm, and thus experience similar wind conditions and operational status. The model outputs are estimations of the indicative variables for all the turbine members within the group, which saves considerable effort compared to the development of individual turbine models. Apart from the difference in the state vector composition of the memory matrix, all the algorithms, including weighting vector calculation, memory matrix construction and hypothesis test based fault detection, are implemented in the same manner as introduced in Section 4.1 from last chapter. The selection of the turbine group for model construction here relies on the correlation coefficients of wind speed between the turbine of interest and its surrounding turbines.

The implementation will be specified in detail in the following sections. The input parameter combination that results in the best model performance will be explored and the impact of normalising the memory matrix and weighting the parameters on model performance will also be examined. The effectiveness of the modified model, which showed unsatisfactory results in the case of the individual turbine model, will be

explored in this chapter. The model's capability of extension and generalisation will be investigated and the limitations of the spatial application of NSET model will be discussed as well. A brief comparison between the spatial and individual NSET model will also be made at the end of this chapter.

### **5.1. Data usage for model training, validation and testing**

The data selection for training, validation and testing purposes of the spatial NSET model requires overall consideration of data availability across the entire wind farm or the selected group rather than simply the turbine of interest as in the individual turbine analyses. The operational status of the sub-group members should be guaranteed to be normal for the training and validation sets, and the testing data from turbines T16 and T17 are used to demonstrate the model's effectiveness.

The wind farm layout and the gearbox failure information for T16 and T17 have been introduced in Section 4.2 from last chapter. It can be seen from Figure 4-2 that T16 and T17 are located next to each other, indicating a high correlation between these two turbines. Therefore, these two turbines would very likely to be included together in a sub-group used for spatial NSET modelling. Since the confirmed failure for turbine T17 was on April of 2005, which is within the training period (April to June of the same year) for the individual turbine gearbox example, the training data will need to be reselected.

The fact that the available data only starts from April of 2005 removes the possibility of selecting the training set at an earlier time. Taking training data from between the failures of T17 and T16 would also be unsuitable since the downtime of T17 ended on August of 2005 by which signs of degradation for T16 have already appeared as shown in the testing results from last chapter. Turbine T16 was taken offline for gearbox replacement immediately after the reported failure at the end of January of 2006 and was back to production at end of March of 2006. Due to all the considerations above, the training period is chosen to be from April to June of 2006 where both T16 and T17 were normally operating and there were no reported issues for the remainder of turbines being

considered for inclusion in the sub-group. The following month is used to validate the model and the testing period for these two turbines remains the same as for the individual turbine analyses, i.e. April 2005 for testing case I for T17 and from August 2005 to January 2006 for testing case II for T16. In this case, the model's resistance to false alarms is investigated based on the healthy turbines in the selected sub-group during the validation period.

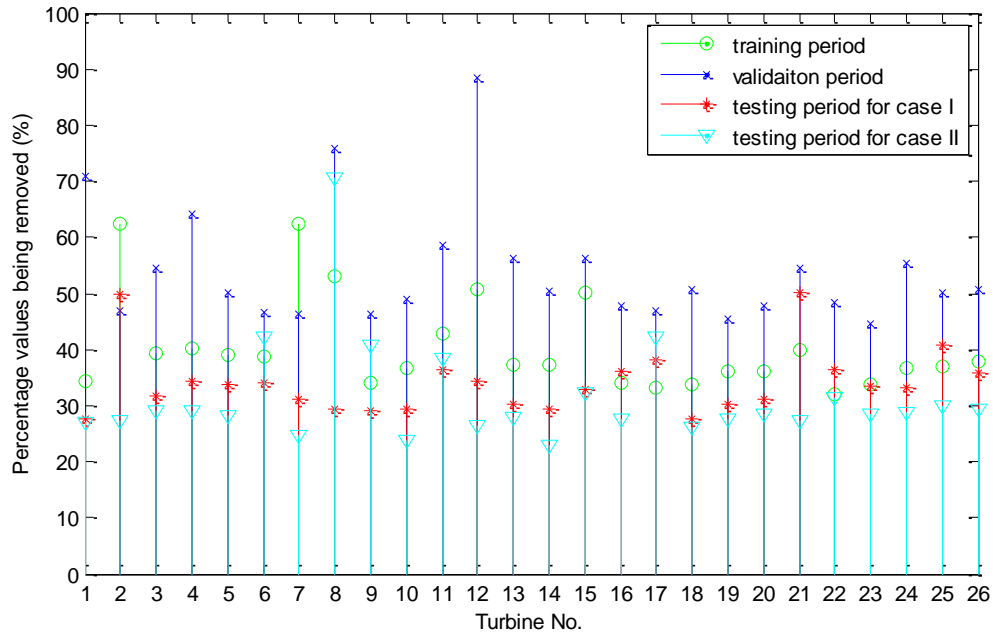


Figure 5-1: Proportion of invalid data entries in different data usage for each turbine

Unlike in the individual NSET model where the data is filtered only based on the turbine of interest, the data filtration in this case needs to take the complete wind farm or sub-group into consideration, i.e. the simultaneous measurements for the group of turbines would become disqualified in case any one of them shows an invalid entry. Figure 5-1 illustrates the proportion of invalid data entries in each turbine for different data usage, including the training period, validation period, and the testing periods for turbines T16 and T17. The filtration here is based on three variables, namely the gearbox cooling oil temperature, the power output and nacelle temperature. The gearbox bearing temperature is excluded from the filtration basis since it is known from the previous

chapter to be better avoided due to concern about false negatives. The validation data in this figure generally shows a large percentage of invalid entries being removed, with its peak of nearly 90% for turbine T12 followed by T1 and T8. The over filtration in such cases will not only lead to much less valid data, it is also possible that the anomalous data from the testing sets are partially or completely removed due to the invalid data from other turbines during the same period. For this reason turbines with an excessive elimination rate such as T1, T8 and T12 are removed for the sake of validation data. Similarly T2, T4, T6, T7, T9 and T22 are also eliminated from the group for the following analyses due to the consideration of training and testing cases.

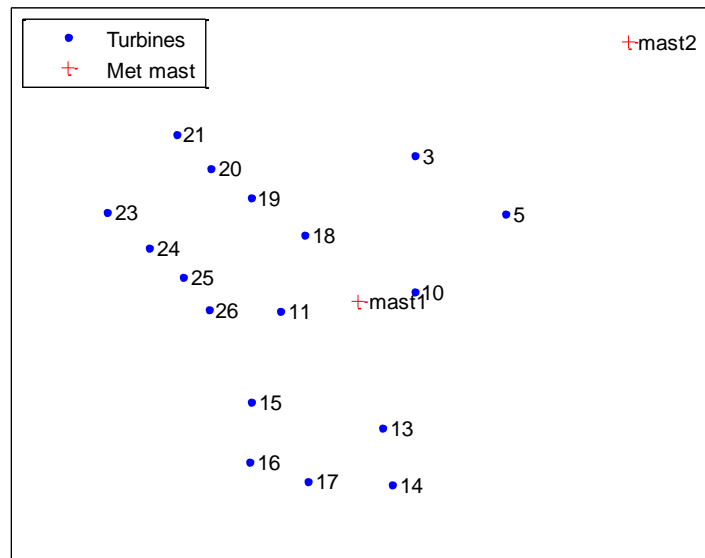


Figure 5-2: New wind farm layout with disqualified turbines removed

This eliminates 9 turbines from the original group and leaves 17 available turbines for analysis in this chapter. The new layout of wind farm that contains only the valid turbines is illustrated in Figure 5-2. Operational data of this selected group is filtered with regards to each candidate using the same criteria as for the individual model and the results are listed in Table 5-1. The percentage of values being removed in this case is generally much higher than that for the individual turbine analyses since each turbine

within the sub-group contributes to the filtration. The generally high elimination rate in this table indicate the relatively poor data quality but fortunately the extreme values of gearbox cooling oil temperature are retained for the training and testing sets. The maximum cooling oil temperature of 57.36°C in the validation set comes from turbine T14 and the associated data are used for the false alarm investigation, referred to as testing case III. The potential issues due to the over filtration across the turbine group will be presented in Section 5.5.

Data usage	Variables	Filtration criteria	Value range after filtration		Percentage of values being removed (%)
			min	max	
Training set (April – June 2006)	Active power (kW)	> 25	25.01	657.66	67
	Gearbox cooling oil temperature (°C)	> 0	6.61	62.00	
	Nacelle temperature (°C)	> 0	2.24	28.43	
Validation set/false alarm testing (July 2006)	Active power (kW)	> 25	25.02	596.16	80
	Gearbox cooling oil temperature (°C)	> 0	15.03	57.36	
	Nacelle temperature (°C)	> 0	11.00	31.62	
Testing set in case I (April 2005)	Active power (kW)	> 25	25.28	640.71	61
	Gearbox cooling oil temperature (°C)	> 0	13.49	61.00	
	Nacelle temperature (°C)	> 0	2.65	21.28	
Testing set in case II (August 2005 – January 2006)	Active power (kW)	> 25	25.03	658.61	78
	Gearbox cooling oil temperature (°C)	> 0	6.62	67.00	
	Nacelle temperature (°C)	> 0	0.58	28.05	

Table 5-1: Wind farm based data filtration (for 17 qualified turbines) and the corresponding results

## 5.2. Model implementation within a sub-group

The anomalous turbine T16 is used as the sub-group selection basis for the following analyses in this chapter so that the two turbines of interest, T16 and T17, will always be included in the sub-group due to their high correlation with each other. The spatial model that involves sub-groups with different sizes or even the complete wind farm will be presented in Section 5.3. As a start here, the model candidates are selected based on the correlation of wind speed. Turbines T10, T11, T13, T14 and T17 all have nacelle anemometer correlation with T16 in excess of 0.96, so they are selected to be in the sub-group, leading to a sub-group size of 6. It can be seen from Figure 5-2 that the selected turbines are geographically close to each other since the correlation of wind speed, used as the selection basis, is in general inversely related to the distance between measurement locations.

It has been shown in the last chapter that the 3-inputs model including oil temperature, power output and nacelle temperature gave the best performance. Considering also the fact that trade-offs between model accuracy and detection sensitivity are always required among the standard, normalised and weighted-variable NSET models, the spatial NSET model with three mentioned inputs is investigated first in this section based on the standard model within the selected sub-group, followed by the discussions of the necessity of nacelle temperature and the role played by gearbox bearing temperature.

For spatial application of the NSET model the state vectors in memory matrix, symbolised by  $\mathbf{X}(m)$  in Equation (4-1) from last chapter, represent records of the gearbox cooling oil temperature and other associated variables from the sub-group of turbines. For example, for the three inputs model with the determined sub-group here, each state vector comprises 18 variables comprising oil temperature, generated power and nacelle temperature for each of the 6 sub-group members.

The differences in memory matrix composition for the various models to be explored will lead to a different optimal matrix size where the model with more variables requires more historical state vectors to cover the complete operational range. The matrix size

decision with all three variables present is illustrated in Figure 5-3. It can be seen from this figure that a good state number is around 1000 based on the compromise between model accuracy and computational complexity as discussed in Section 4.3.1, resulting in a matrix  $D$  of size  $18 \times 1000$ . A memory matrix size with 1017 state vectors is used for all the following analyses within the selected sub-group in order to make fair comparisons whilst retaining the model accuracy.

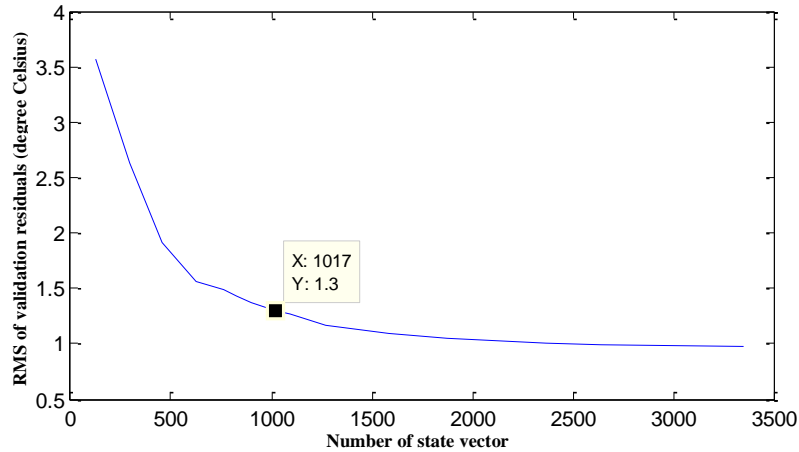


Figure 5-3: Memory matrix size decision

The implementation of the algorithms for the spatial NSET model and the associated hypothesis test based fault detection is identical with that for the individual turbine model in last chapter. The matrix is constructed with 1017 historical states and the model is then validated on turbine T16 with the results being illustrated in Figure 5-4 which shows acceptable model accuracy. The maximum of the smoothed validating residual is used as reference for further fault detection. The anomalies of turbine T17 and T16 are successfully detected from the beginning of the testing period, as shown in Figure 5-5 and Figure 5-6, demonstrating the model's effectiveness of anomaly detection. Figure 5-7 further shows the model's resistance to false alarms using the healthy operational data from turbine T14 which contribute to the maximum of gearbox cooling oil temperature during the selected period as mentioned before. This illustrates that high temperatures can be reached by a perfectly healthy turbine.

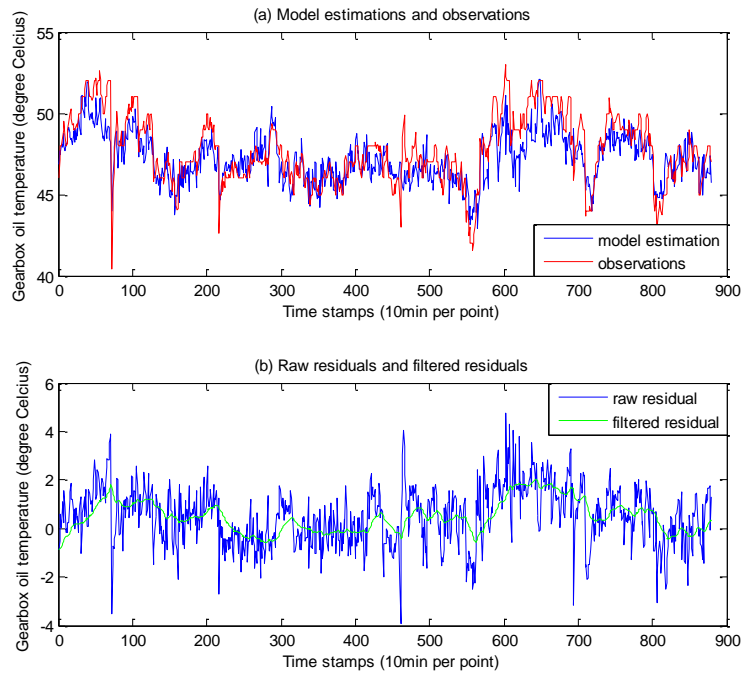


Figure 5-4: Validation results of T16 for standard spatial NSET

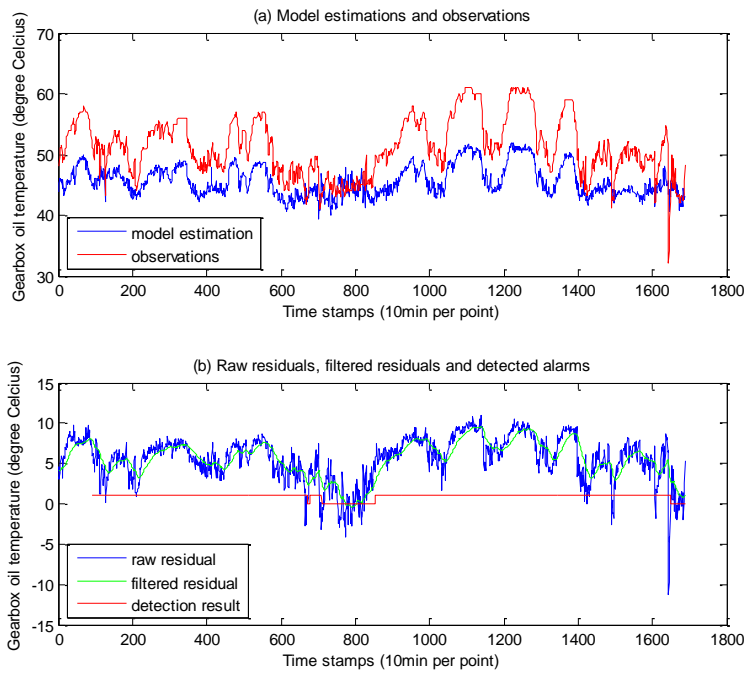


Figure 5-5: Testing results and anomaly detection of T17 for standard spatial NSET

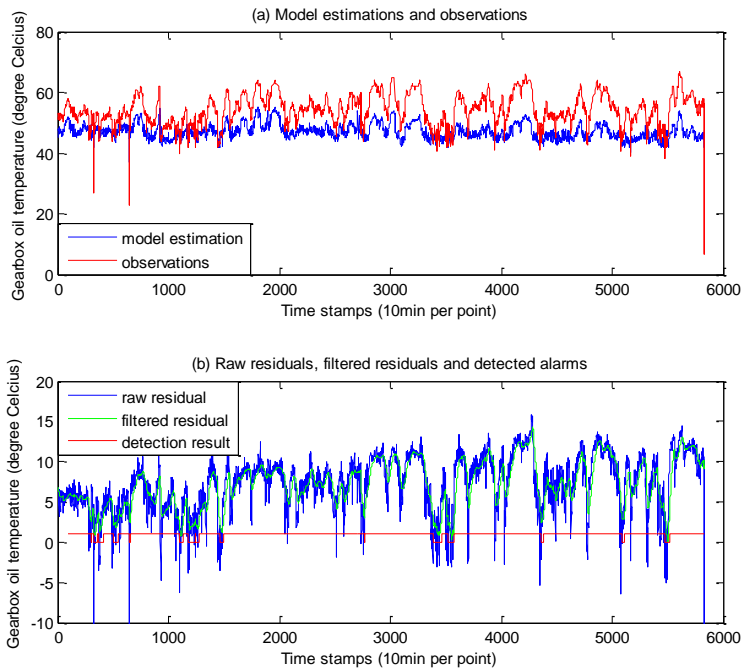


Figure 5-6: Testing results and anomaly detection of T16 for standard spatial NSET

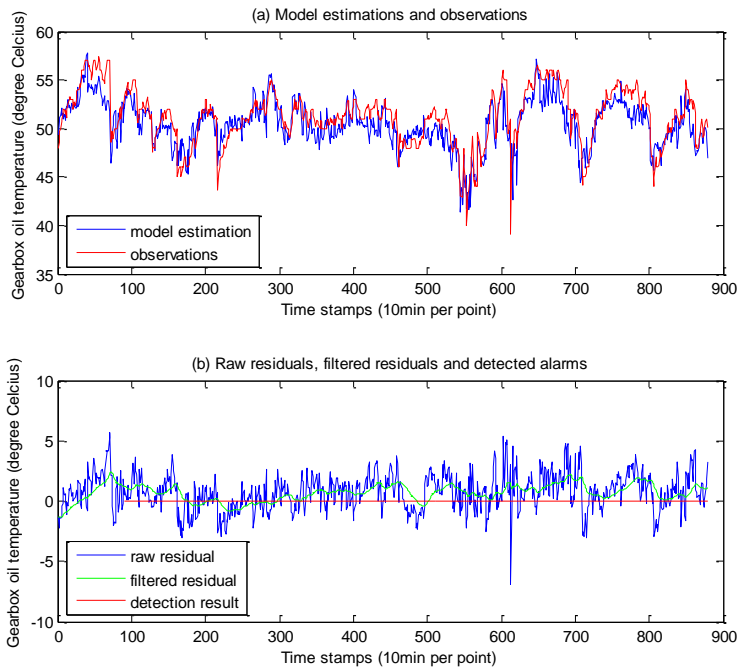


Figure 5-7: Testing results of healthy T14 for false alarm testing with standard spatial NSET

### 5.2.1. Discussions of the necessity of nacelle temperature

The turbine nacelle temperature is physically affected by both the ambient temperature and the gearbox temperature. Because the selected turbine can be assumed to share a common ambient temperature with the other turbines, this might reduce the importance of nacelle temperature in the modelling. The effectiveness of an NSET model without nacelle temperature in the modelling. The effectiveness of an NSET model without nacelle temperature, i.e. only containing power output and cooling oil temperature, is investigated here using identical data as introduced earlier.

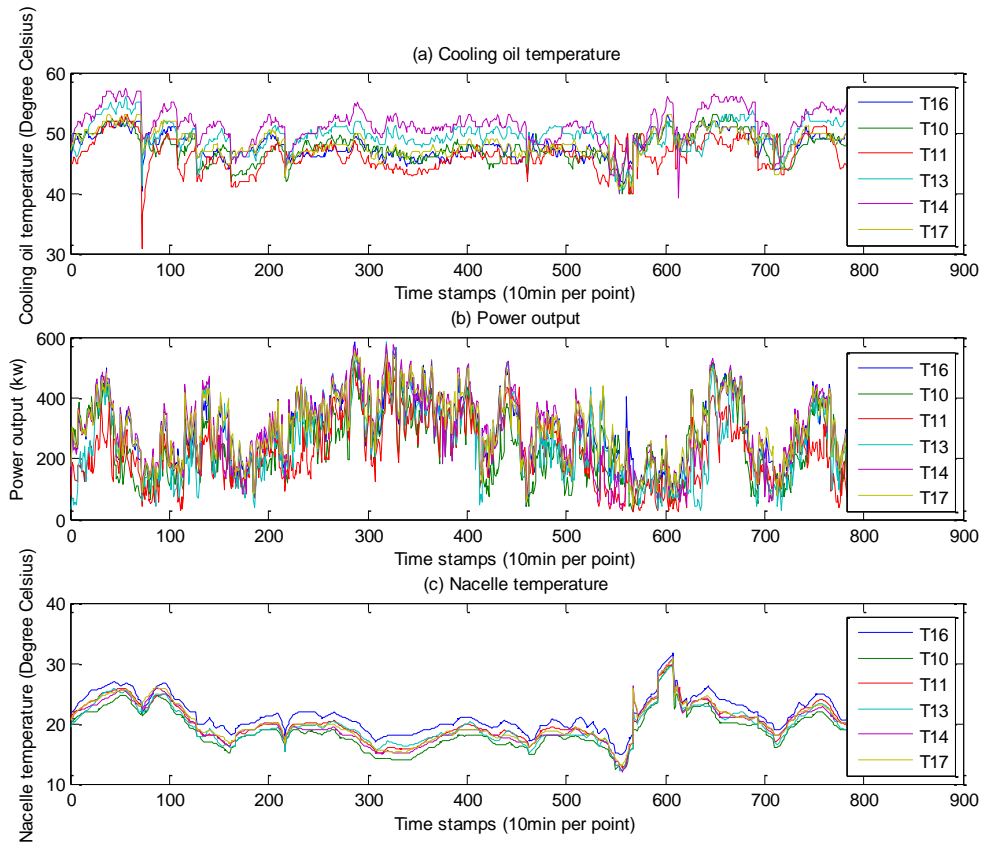


Figure 5-8: Time series of the validation data for all of the sub-group candidates

The validation time series of oil temperature, power output and nacelle temperature for the six selected turbines within the sub-group is shown in Figure 5-8, from which it can be seen that the oil temperature peaks at time instance of around 600 corresponding to the peaks in the nacelle temperature. These are known to be primarily due to the high ambient temperature, and in this instance the associated power production is rather low.

It is therefore clear that in this case the oil temperature peaks are driven mainly by the high ambient temperature, indicating the importance of the ambient temperature (not available in this SCADA data set) and hence nacelle temperature on the model output.

The validation results for the 2-inputs NSET model are illustrated in Figure 5-9, where the exact oil temperature measurement peak of 53°C for the validated turbine T16 can be observed at time instance of 602. The associated estimations from the 2-inputs and the 3-inputs model, as shown in Figure 5-4, are 49.81°C and 51.07°C respectively, showing a higher degree of accuracy of the 3-inputs model and hence further confirming the necessity of the inclusion of nacelle temperature in the spatial NSET model.

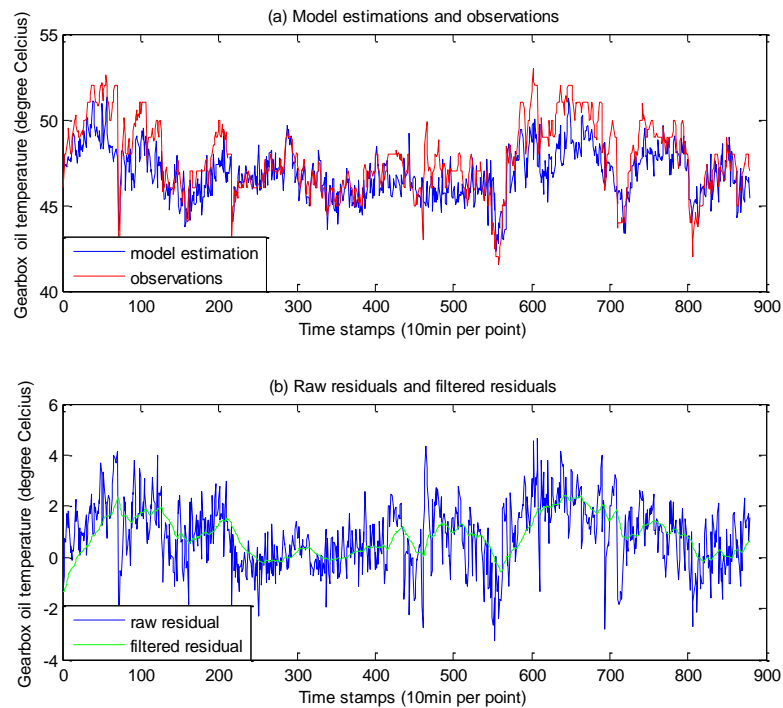


Figure 5-9: Validation results of T16 for 2-inputs standard spatial NSET

Table 5-2 (on Page 153) further summarises the validation and testing statistics for the 2-inputs model and also compares these with those for the 3-inputs model as presented in the previous section. It can be seen from the table that the 3-inputs model performs

better than the 2-inputs model by showing higher validation accuracy and a larger detection ratio for the testing data.

### **5.2.2. Impact of gearbox bearing temperature on model performance**

The gearbox bearing temperature, which is known from last chapter to be better avoided in order to increase the detectability, is separately examined in this section to demonstrate again the potential degradation in performance that can result. An extreme case is employed where the model only involves the cooling oil temperature and the bearing temperature and the data filtration here is only conducted with regards to these two involved variables, which differs from what have been applied previously. In this case the filtration picks up entries with positive oil temperature and bearing temperature and the refinement is based on the turbines operational data from the sub-group rather than the complete wind farm.

Figure 5-10 illustrates the validation results which demonstrate excellent model accuracy. However, the testing results for turbine T17 in Figure 5-11(a) also show good agreement between model estimations and observations even when the temperature peaks with apparent fault signatures, which lead to the failure in anomaly detection as shown in Figure 5-11(b). As has been mentioned in the previous chapter, this is because the gearbox bearing temperature shares a common causal relationship with the oil temperature with regards to gearbox failure and would accordingly carry some similar fault information, which will result in the ineffectiveness in anomaly detection. It can be therefore concluded that the gearbox bearing temperature should be excluded from the model inputs.

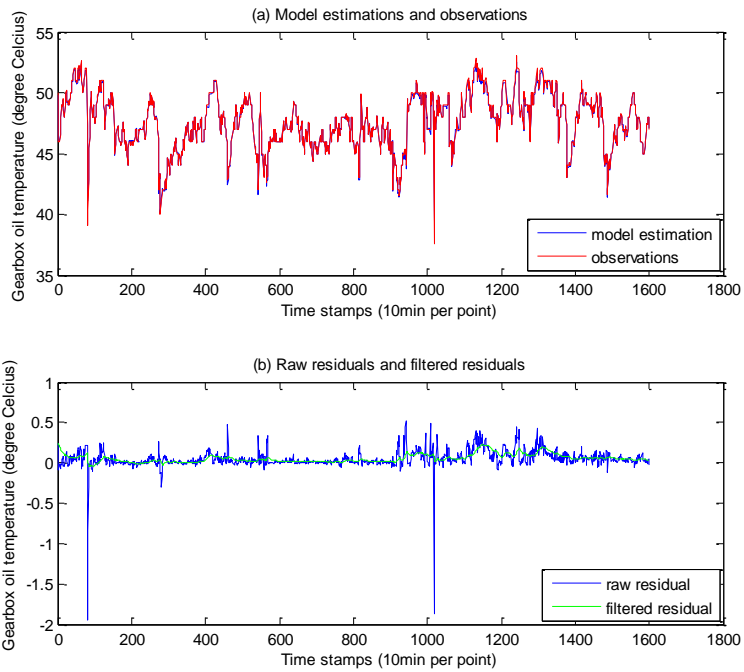


Figure 5-10: Validation results of T16 for standard spatial NSET with bearing temperature

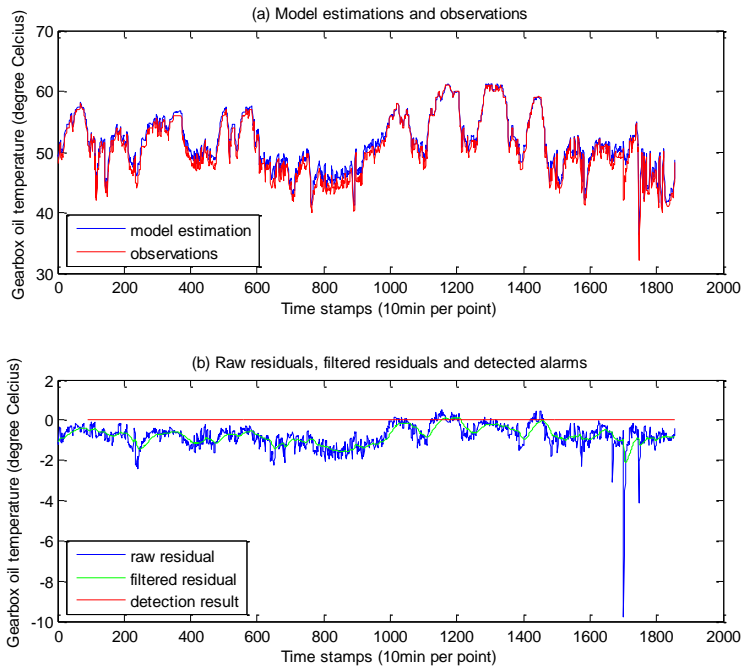


Figure 5-11: Testing results and anomaly detection of T17 for standard spatial NSET

### **5.2.3. Impact of normalised memory matrix and weighted parameters on model performance**

The performance for model with memory matrix normalised and variable weighted is investigated in this section using the same data as described in Section 5.2. The illustrations of the validation and testing results are included in Appendix II instead of being presented here due to their similarity in nature to those already presented earlier in this chapter, and the associated statistics of results can be found in Table 5-2. The normalised and weighted model shows significantly better accuracy than the standard model in the table and it is also capable of detecting the anomaly with sufficient time prior to the final failure in spite of the smaller detection ratio.

### **5.2.4. Discussion of the modified model in spatial NSET application**

The modified NSET model is believed to produce more reliable results than the standard model since the indicative variable, the gearbox cooling oil temperature in this case, of the turbine of interest is omitted from the estimation process for the weighting vector and the results are based on the measurements from valid sensors only. It was not preferred for the individual turbine analyses in last chapter due to the unsatisfactory performance resulting from insufficient input variables. The modified model is investigated here since the correlated variables from the surrounding turbines significantly increase the model's input size.

The implementation of the modified model is based on the normalised and weighted model with identical data usage as in the previous section. 17 variables are included in the model inputs since the oil temperature for the turbine of interest is absent from the input sets, and an optimal state number of 1017 is retained, resulting in a memory matrix size of  $17 \times 1017$ . The validation and testing results for the modified model are illustrated in Figure 5-12, Figure 5-13, Figure 5-14 and Figure 5-15, and the associated statistics are summarised in Table 5-2, together with those from other models under investigation.

It can be seen from both these figures and the table that the residual RMSs for the modified model are generally larger than the normalised matrix and weighted parameter model, particularly for the testing cases of T16 and T17. One potential reason for this is

the model auto-sensitivity, the value of which is calculated to be 0.88 for the normalised matrix and weighted parameter model, indicating the corresponding predicating residuals are generally underestimated by 88% and hence leading to smaller residual RMS values. Whereas the modified model has an auto-sensitivity value of 0 with regards to the oil temperature since this variable is absent from the model input sets, which is the ideal case according to the associated metric definition as introduced in Section 4.3.11 from last chapter. For this reason, the modified model with normalised memory matrix and weighted parameters, referred to as the modified spatial model, is used for further analyses.

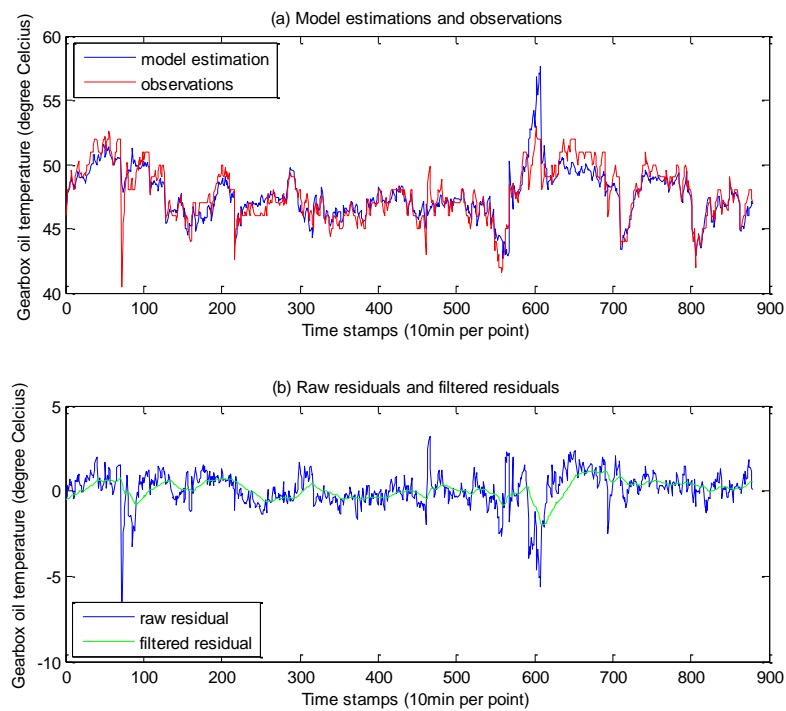


Figure 5-12: Validation results of T16 for modified spatial NSET

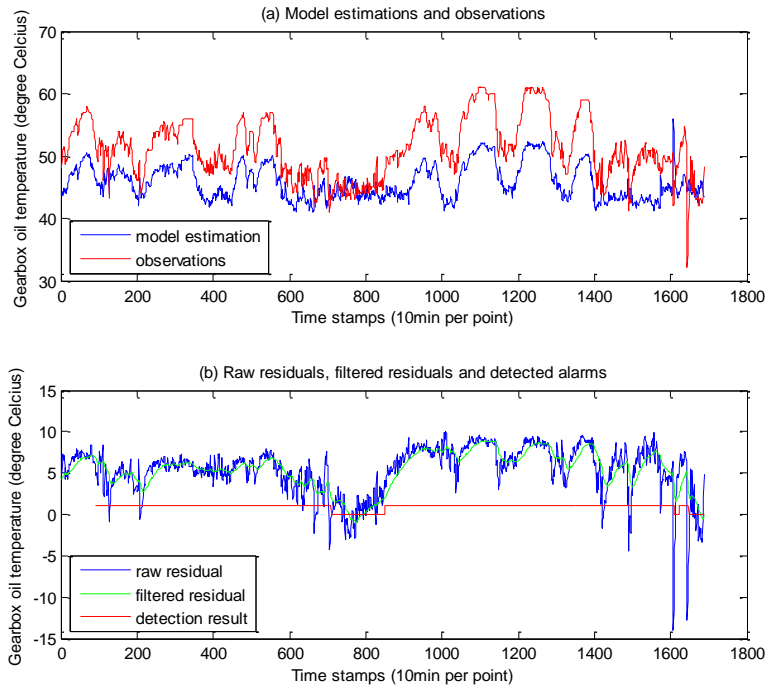


Figure 5-13: Testing results and anomaly detection of T17 for modified spatial NSET

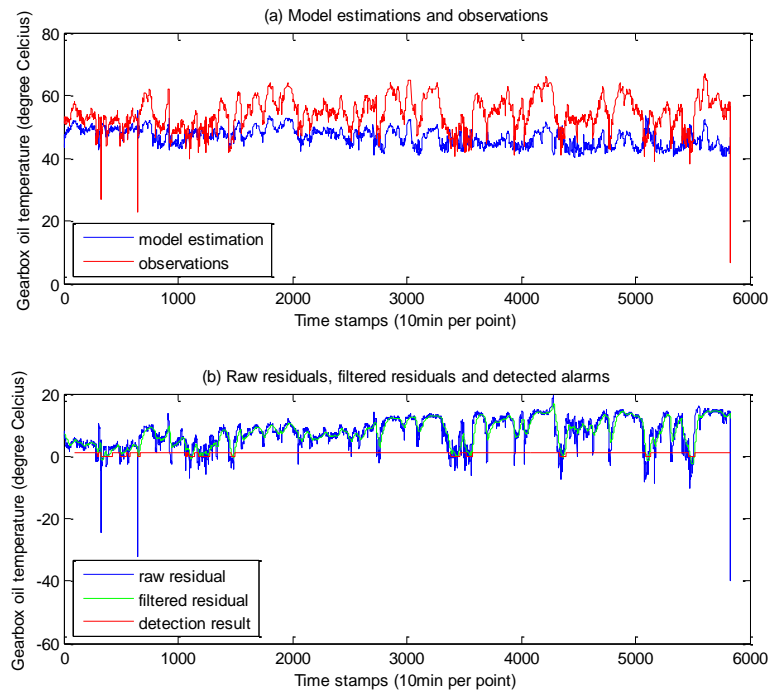


Figure 5-14: Testing results and anomaly detection of T16 for modified spatial NSET

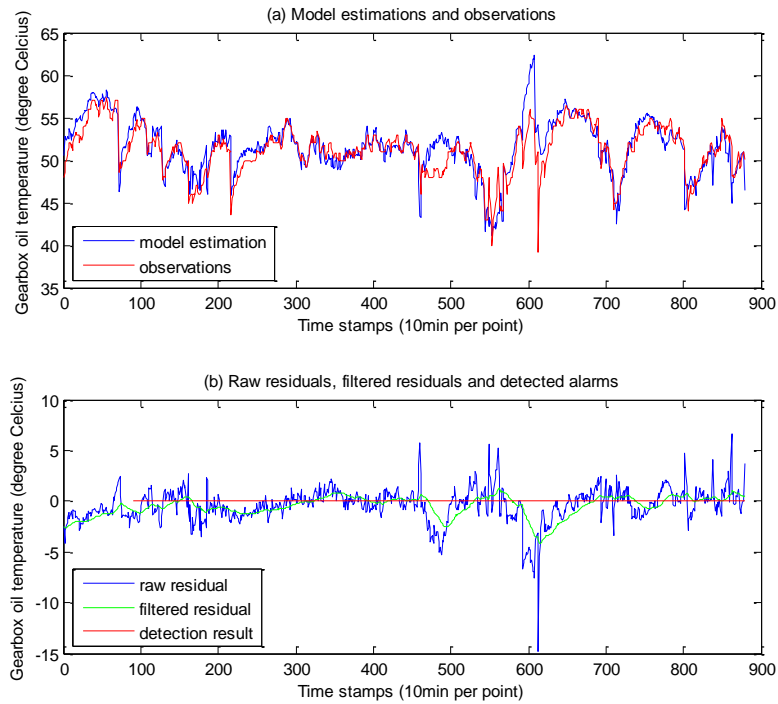


Figure 5-15: Testing results of healthy T14 for false alarm testing with modified spatial NSET

It should also be noticed that the training data comes from a period where the anomalous gearbox for turbines T16 and T17 had been replaced, i.e. the training and testing are based on different operational systems. As a consequence, the model would make prediction based on the training patterns that are learnt from the new system which might differ somewhat from the original one. This will obviously degrade the model accuracy and effectiveness, and hence should better be avoided, but this was not possible for the reason mentioned in Section 5.1.

		Validation: T16		Testing I: T17				Testing II: T16				Testing III: T14			
		Mean (°C)	RMS (°C)	Mean (°C)	RMS (°C)	RR	DR (%)	Mean (°C)	RMS (°C)	RR	DR (%)	Mean (°C)	RMS (°C)	RR	DR (%)
Oil temp + Power	Standard	0.866	1.551	4.636	5.439	3.51	75.1	7.007	7.855	5.06	87.1	1.415	2.067	1.33	0
Oil temp + Power + Nacelle temp	Standard	0.503	1.300	5.546	6.210	4.78	88.0	7.182	8.032	6.18	90.8	0.740	1.680	1.29	0
	Normalized & weighted parameters	-0.092	0.724	0.715	1.052	1.45	38.8	0.567	1.263	1.74	38.9	-0.248	0.926	1.28	0
	Modified	0.106	1.040	5.344	6.094	5.86	88.0	7.652	9.100	8.75	87.9	-0.424	1.725	1.66	0

Table 5-2: Effectiveness comparison for spatial models with different input combinations under standard and modified situations

### 5.3. Effect of sub-group size on model performance

The spatial modified NSET model shows satisfactory performance with 6 turbines in the sub-group. The effect of sub-group size on the model performance is investigated in this section based on the modified NSET model using turbine T16 again as the basis for sub-group selection. The correlation coefficients for wind speed between turbine T16 and the 17 available turbines in the wind farm are listed in descending order in Table 5-3. And the sub-group size is changed by varying the correlation threshold level.

Turbine No.	Correlation coefficient with T16	Turbine No.	Correlation coefficient with T16	Turbine No.	Correlation coefficient with T16
16	1.000	26	0.958	18	0.934
17	0.987	3	0.954	21	0.930
13	0.973	25	0.954	19	0.914
14	0.968	24	0.953	20	0.899
11	0.967	23	0.949	15	0.824
10	0.967	5	0.938		

Table 5-3: Correlation coefficients of wind speed between T16 and the available turbines in the wind farm

Figure 5-16 illustrates the relationship between the correlation coefficients and the associated (rescaled) geographical distance from turbine T16. It can be seen from this figure that the correlation level drops as the geographical distance increases in general with some exceptions such as turbine T15. Possible reasons for such point include the specific terrain roughness, land topology that are associated with the turbine and wake effects from the neighbouring turbines [46].

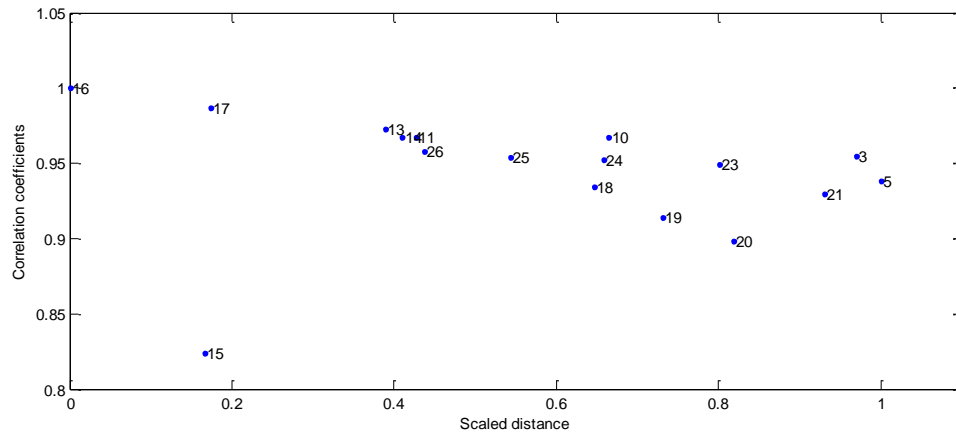


Figure 5-16: Spatial relationship for the available turbines in the wind farm with regards to turbine T16

The data usage for model validation and testing purpose here remains the same as described in Section 5.1, where the filtration of the operational data is conducted based upon these 17 available turbines within the wind farm. Four models with different sub-group size are investigated and compared here, including the one presented in last section and models with sub-group size of 10, 15 and 17 that covers all the turbines available in the wind farm. The corresponding matrix sizes of these models are kept around 1000 for a fair comparison.

The results are not presented here due to the consideration of space and also because they are similar in nature to those already presented. They can be found instead in Appendix III and the associated statistics are summarised in Table 5-4. Both the illustrations and the respective statistics in this case show little impact of the sub-group size on the model performance, which implies great potential to extend the spatial model to even larger wind farms so that modelling efforts can be saved without losing the model reliability. However, more available data need to be tested for the capability of extension of the spatial NSET model before any definite conclusions could be made since it is noted that the lowest correlation coefficient as listed in Table 5-3 is 0.82, which still exhibits a relatively high correlation level. Larger wind farms might be expected to have lower correlations and this would result in less accurate modelling.

Correlation Coefficient threshold	Sub-group size	Validation: T16		Testing I: T17				Testing II: T16				Testing III: T14			
		Mean (°C)	RMS (°C)	Mean (°C)	RMS (°C)	RR	DR (%)	Mean (°C)	RMS (°C)	RR	DR (%)	Mean (°C)	RMS (°C)	RR	DR (%)
0.96	6	0.106	1.040	5.344	6.094	5.86	88.0	7.652	9.100	8.75	87.9	-0.424	1.725	1.66	0
0.95	10	0.073	1.114	5.542	6.260	5.62	88.6	7.772	9.147	8.21	89.3	-0.430	1.765	1.58	0
0.90	15	0.079	1.129	5.372	6.197	5.49	88.1	7.870	9.190	8.14	89.9	-0.444	1.743	1.54	0
0.80	17	-0.053	1.185	5.667	6.554	5.53	88.2	7.997	9.266	7.82	91.1	-0.448	1.779	1.50	0

Table 5-4: Effectiveness comparison for the 3-inputs modified spatial model with different sub-group sizes

#### 5.4. Discussion of the model's capability of generalisation

The previous results are based on the models that are constructed on turbine T16 for the reason mentioned in Section 5.2. This section explores the model's capability of generalisation using other validating turbines within the largest available sub-group (comprising 17 turbines), which has been proved to be as effective as the models with any sub-group sizes.

In this case, the testing data remain the same as used for the 17-turbines sub-group in the previous section and the corresponding testing residuals are also identical with those for the 17-turbines sub-group as listed in Table 5-4 due to the identical memory matrix, based on which the model predictions are made. The only difference in this case is the validation result and hence the residual ratio, and the detection ratio changes as well since the associated hypothesis test is based on the maximal value of the validation result.

	Validation		Testing I: T17		Testing II: T16		Testing III: T14	
	Mean (°C)	RMS (°C)	RR	DR (%)	RR	DR (%)	RR	DR (%)
Sub-group based on T13	-0.716	2.366	2.77	80.6	3.92	83.5	0.75	0
Sub-group based on T10	-0.036	1.849	3.54	82.4	5.01	85.5	0.96	0
Sub-group based on T5	-1.166	2.259	2.90	87.1	4.10	89.0	0.79	0

Table 5-5: Effectiveness comparison for spatial models constructed based on different turbines with sub-group size of 17

Three random turbines are chosen for model validation: T5, T10 and T13, and the respective results of successful model application are listed in Table 5-5, which shows

only the RR and DR values since the Mean and RMS values remain the same due to the reasons mentioned above. It can be seen by comparing the statistics in Table 5-5 and those for the 17-turbines sub-group as shown in Table 5-4 that the impact of the validating turbine selection for the same sub-group on the model performance is insignificant, implying the model's ability to generalise and the effort saving potential for wind farm level condition monitoring.

## **5.5. Limitations of the spatial application of the NSET model**

The previous two sections have shown excellent capability of extension and generalisation for the spatial NSET model. However there are also some potential issues associated with the model due to the inclusion of large number of turbines and they are discussed in this section.

Firstly, the data filtration is based on all the candidates within the sub-group, which would result in failure of anomaly detection if the faulty data from the turbine of interest happens to coincide with the invalid data from another turbine in the sub-group. Even though a crude data refinement has been applied to remove the turbines that contain significant numbers of invalid entries as has been shown in Section 5.1, the possibility still exist, and the associated chance increases as the sub-group extends.

Another worry is the effect of the anomalous data on the model estimations for other healthy turbines. An example using the 6-turbines sub-group as described in Section 5.2 is illustrated in Figure 5-17, which shows the testing results for the healthy turbine T14 based on the anomalous T17 using the identical testing period (in testing case I) prior to its final gearbox failure. The high values of model prediction for T14 are due to the impact from the anomalous data, which results in the deteriorated model accuracy and reduced testing residuals. This will become a serious issue in the cases where there are more than one anomalous turbines in the selected sub-group. The model estimation for the faulty turbine would be affected in a similar manner by the anomalous data from other faulty turbines and the corresponding reduced testing residuals will lead to false

negatives in the worst case scenario. Attention is therefore required in spatial NSET applications with large numbers of turbines in the selected sub-group.

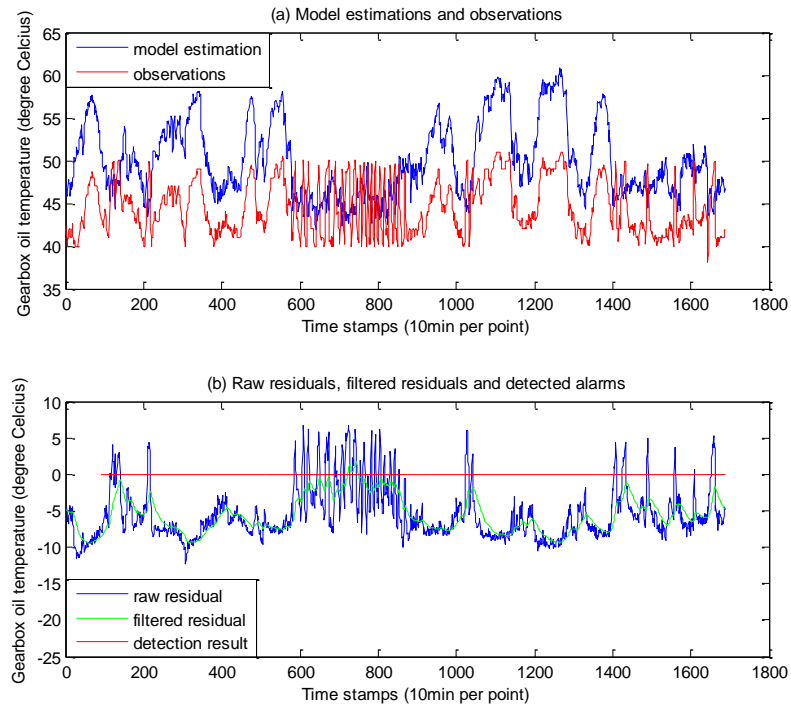


Figure 5-17: Testing results of the modified spatial NSET for healthy T14 based on the anomalous T17 in testing case I

## 5.6. Comparison between the spatial and individual turbine NSET model

It can be seen by comparing Table 5-2 and Table 4-7 from last chapter that the individual turbine NSET model significantly outperforms the spatial model in terms of model accuracy for different auto-associative forms (i.e. so called standard forms of the NSET model, including normalised and weighted). With regards to the modified model, which theoretically provides more reliable model predictions, the spatial NSET overcomes the limitation of insufficient variables faced by the individual NSET modelling by effectively employing the variables from the surrounding turbines and hence providing promising results. Besides, the spatial NSET also beats the individual

model in terms of effort saving. However, the feasibility of the spatial model implementation largely depends upon the data quality for the reasons mentioned in the previous section. Therefore no definite conclusions can be achieved as to which model is superior since they both have their advantages and limitations on performance, which in a way provides flexibility for model selection that are based on the data quality and availability.

## **5.7. Chapter summary**

The effectiveness of the spatial NSET model with oil temperature, power output and nacelle temperature is shown in this chapter, out of which the normalised matrix and weighted parameter model performs the best. A reasonable state number value of around 1000 is selected for the sub-groups with different sizes based on the compromise between model accuracy and computational complexity. The modified spatial NSET model brings further confidence to the model's reliability by omitting the indicative variable of the turbine of interest from the estimation process for the weighting vector, which in effect results in a model with an auto-sensitivity of zero. The little impact of sub-group size on model performance demonstrates the model's capability of extension and the performance of models validated with different turbines shows little variations, indicating the model's ability to generalise and more importantly significant amount of efforts would be saved by wind farm based condition monitoring without losing model effectiveness.

However, more case studies are required before widely applying the spatial NSET model for entire wind farm condition monitoring. Besides, failures of anomaly detection could be caused by either predictions based on faulty period of anomalous turbines or inclusion of too many turbines with poor data quality in the sub-group such that the data containing anomalous information are likely to be removed in the filtration process due to invalid entries in other turbine candidates.

## 6. Conclusions and future works

Promising SCADA data based algorithms for robust fault detection have been presented in this thesis with emphasis on the NSET technique for model estimation for both key components of individual wind turbines and also for groups of wind turbines. This modelling is complemented by a comparison of operational wind turbine power curves derived in a real time manner with a reference power curve, in order to identify anomalous behaviour. In contrast to previous NSET implementations, comparisons make use of a rigorous statistical comparison. Turbine gearbox and generator anomaly detection case studies, and a turbine yaw misalignment example, are utilised to demonstrate the effectiveness of the NSET algorithm and the proposed power curve based method. The main research contributions of this thesis and potential future work to improve the methods will be presented and discussed in the following sections.

### 6.1. Conclusions

The main research contributions presented in this thesis are listed below:

- For the power curve comparison method
  - A Copulas based outlier rejection method is demonstrated that can be used to clean up the reference power curve. This significantly improves the precision of the resulting reference curve and thus increases the sensitivity and reliability of subsequent anomaly detection, allowing earlier fault identification.
  - A real-time power curve tracking method is developed to identify any statistically significant deviation, using an appropriate hypothesis test, from the reference power curve on a bin by bin basis. This is demonstrated to identify certain faults in a timely manner.
- For the NSET technique
  - The optimal memory matrix size is determined as a compromise between model accuracy and computational complexity.

- The utility of additional null and maximal state vectors in the memory matrix is justified by showing improvement to NSET model performance.
  - The impact on model performance of re-scaling the memory matrix to normalise the parameter range of all variables to  $[0, 1]$  is investigated and demonstrated to significantly improve the model accuracy.
  - Adjustment of variables' weighting in the distance norm (conventionally the Euclidean norm) with NSET to reflect the relative importance of the model variables is shown to improve model accuracy.
  - The potential to extend the NSET model based on individual turbines to a multi-machine application is explored, and the effectiveness of such a spatially derived model has been demonstrated. Sub-group size is found to have little impact on model performance and the models validated with different turbines also show little variation in performance, allowing this approach to be applied to whole wind farms, thereby massively reducing computational effort without significant loss of model effectiveness.
  - The modified spatial NSET model brings further confidence to the model's reliability by omitting the indicative variable for the turbine of interest from the estimation process for the weighting vector, which in effect results in a model with an auto-sensitivity of zero.
- Both the power curve based fault detection and the NSET approach to anomaly detection have been implemented in a statistically rigorous manner through application of the Welch hypothesis test, which reduces the likelihood of false alarm and adds confidence in the condition monitoring methods.

## **6.2. Future works**

The robustness of the NSET technique in producing accurate and reliable model estimations allows for timely detection of system incipient anomaly, thus adding value to the condition monitoring of wind turbines and increase its cost-effectiveness. However, the applications presented in this thesis highlight the conflict between NSET

model accuracy and detection sensitivity, which is due to the auto-associated character of NSET models.

Another crucial aspect of condition monitoring algorithm development is the trade-off between the required detection sensitivity and the false alarm rate. Particularly for offshore wind turbines, false alarms can be costly in terms of unnecessary down time and maintenance actions undertaken that are actually not required. Turbine access offshore is costly and trips may be wasted if they have resulted from false alarms. The relationship between how far in advance the anomaly can be identified and the corresponding false alarm rates is not well understood and a good understanding of this relationship will merit further study in order to facilitate improved decision making for turbine repair and maintenance scheduling.

The autoregressive input (or the time lagged input variable) does not improve the performance of NSET model in the presented gearbox case study. One reason for this could be the data filtration that removes invalid measurements, resulting in an incomplete time series that would result in unwanted time varying changes to lag time, thus degrading the model. However, the use of a suitably time-lagged variable could be beneficial especially in cases where there are intrinsic time delays in the system, for example due to thermal mass, and this area deserves to be investigated in further research.

In addition, it has been realised that future work needed to investigate the NSET model's resistance to false alarms should be based on normally operating turbines with high values of the indicative variable (such as the gearbox oil temperature in the condition monitoring of turbine gearbox). Such data was not available at the time of writing of this PhD thesis.

The NSET approach should be extended to include data from additional components and subsystems, and could perhaps incorporate data from other sensors, in particular vibration sensors and oil particle counters, and in this manner approach the ideal of a fully holistic condition monitoring system. Also, much work remains to be done to

extend the framework of power curve based anomaly detection to cover further turbine sub-systems, or even individual components (including measurement instruments) faults, thus eventually allowing a comprehensive fault logic to be developed that would provide a powerful tool to wind farm operators.

Lastly, the tuning of key parameters, such as the significance level in the Welch's t test, should be based on more extensive operational data from field trials to improve algorithm performance and verify the capability of the NSET model and power curve tracking methods for condition monitoring. Such data, with documented false alarm rates and successful fault identification performance statistics, would allow the economic value of such condition monitoring systems to be determined.

# Appendix I

This appendix shows the validation and testing results of NSET model under different situations (standard model, model with normalised matrix and weighted parameters) for individual turbine generator case study.

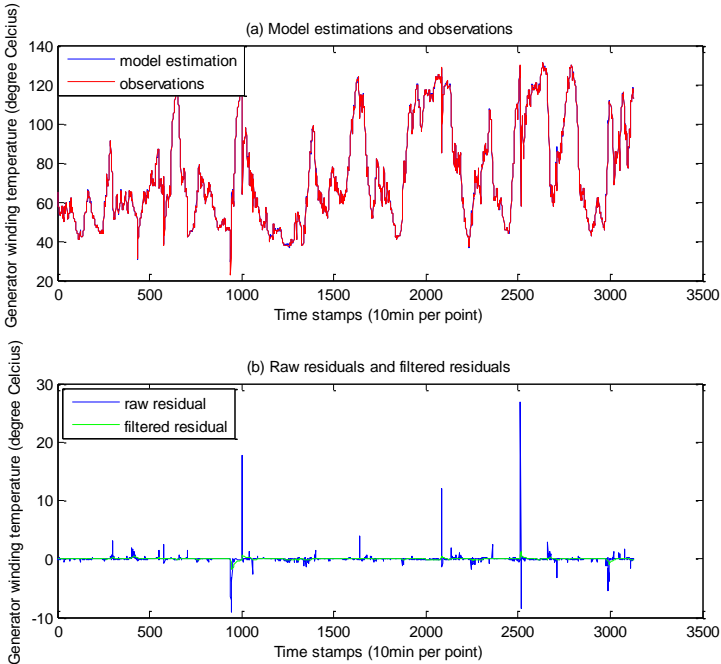


Figure 1: Validation results of standard NSET

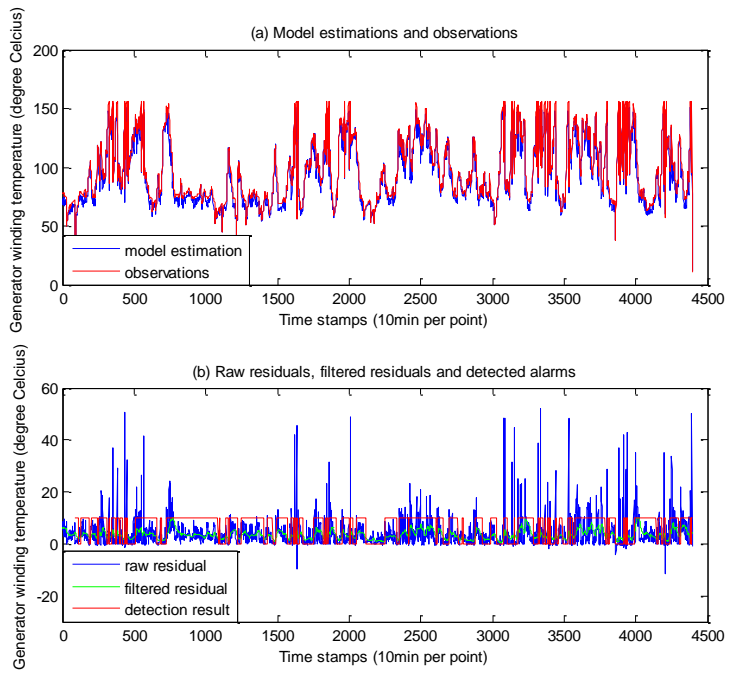


Figure 2: Testing results and anomaly detection of testing case I for standard NSET

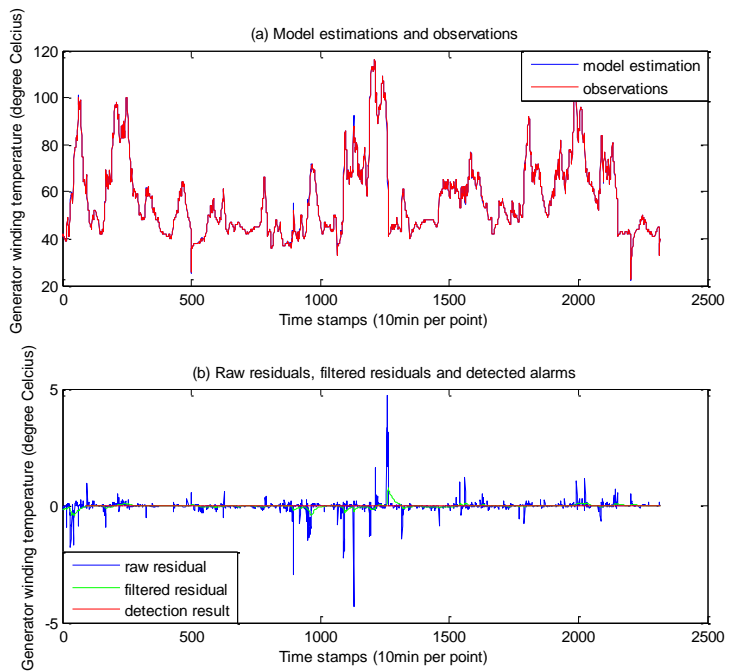


Figure 3: Testing results and false alarm investigation of testing case II for standard NSET

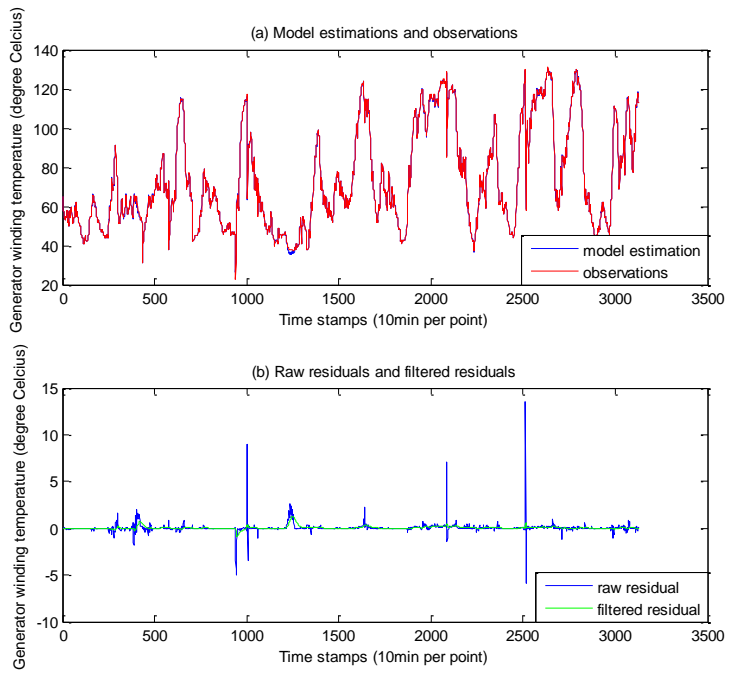


Figure 4: Validation results of normalised NSET

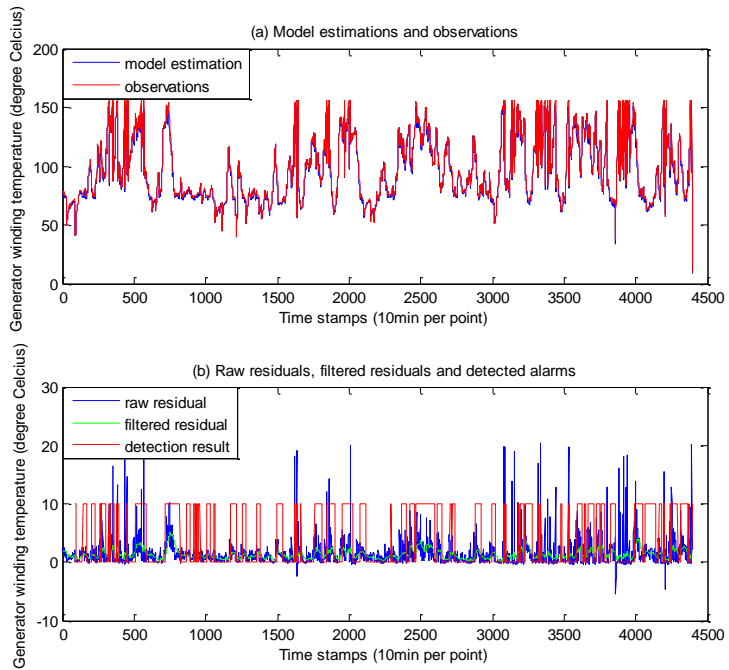


Figure 5: Testing results and anomaly detection of testing case I for normalised NSET

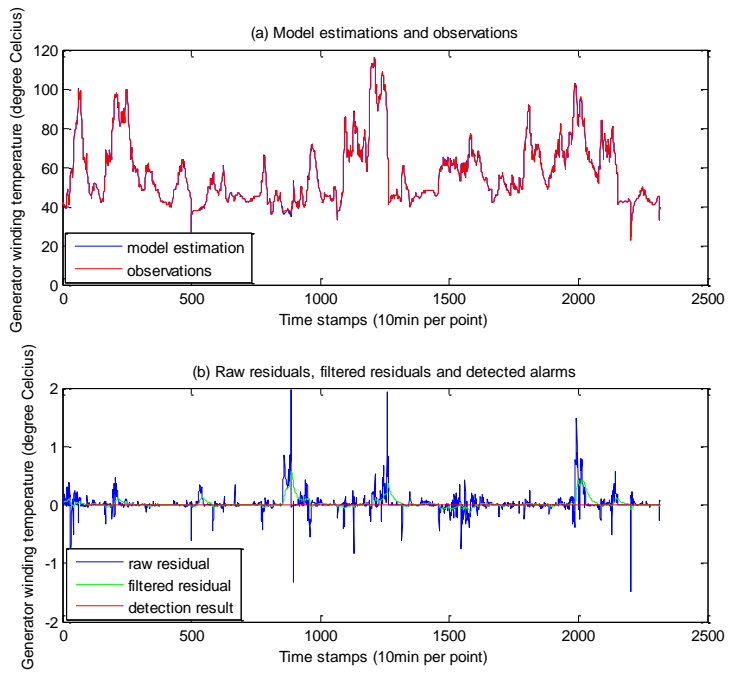


Figure 6: Testing results and false alarm investigation of testing case II for normalised NSET

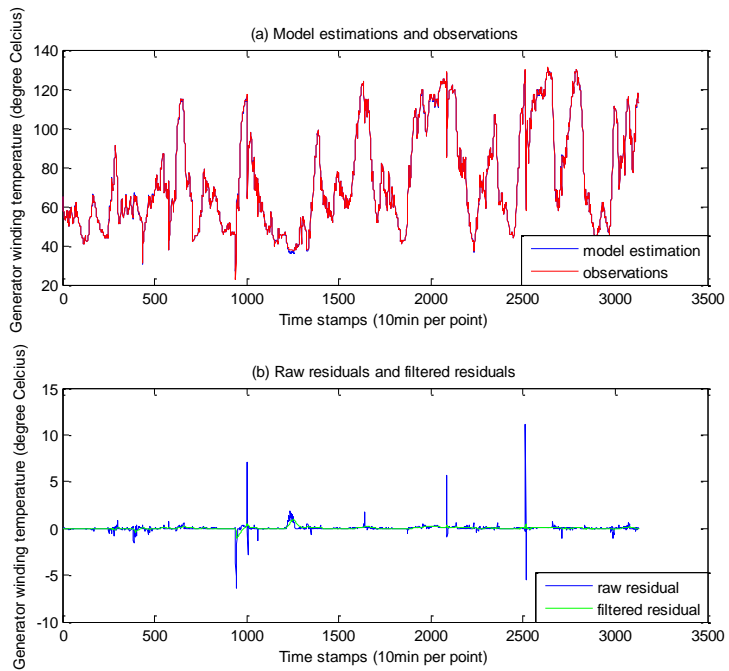


Figure 7: Validation results of normalised NSET with weighted variables

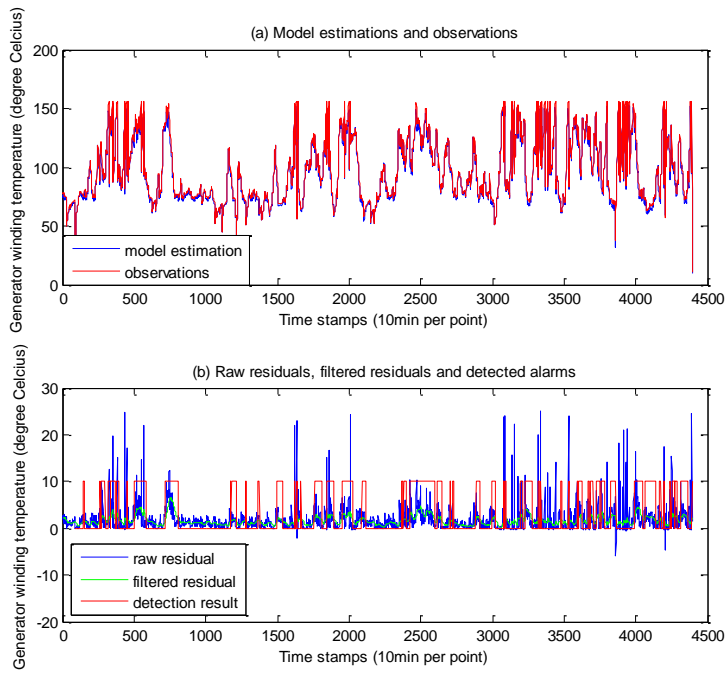


Figure 8: Testing results and anomaly detection of testing case I for normalised NSET with weighted variables

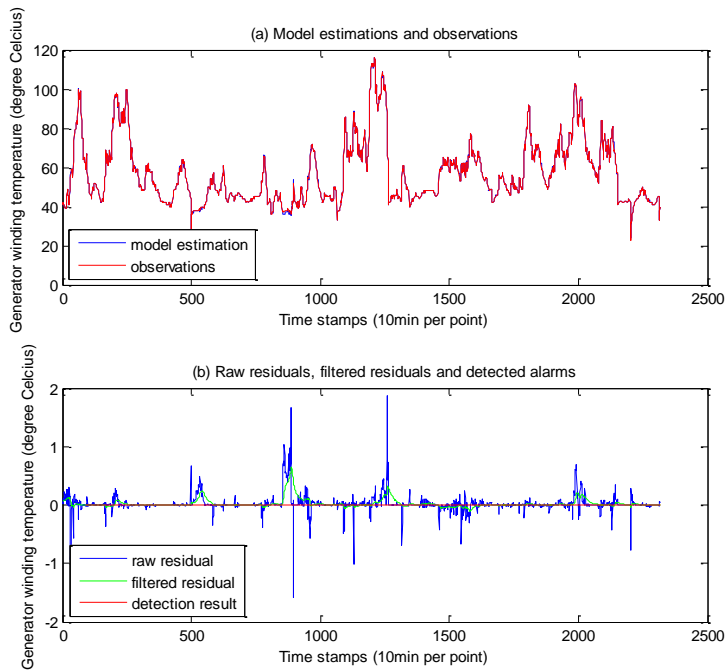


Figure 9: Testing results and false alarm investigation of testing case II for normalised NSET with weighted variables

# Appendix II

This appendix shows the validation and testing results of spatial NSET model with normalised matrix and weighted parameters for gearbox case study within 6-turbine sub-group.

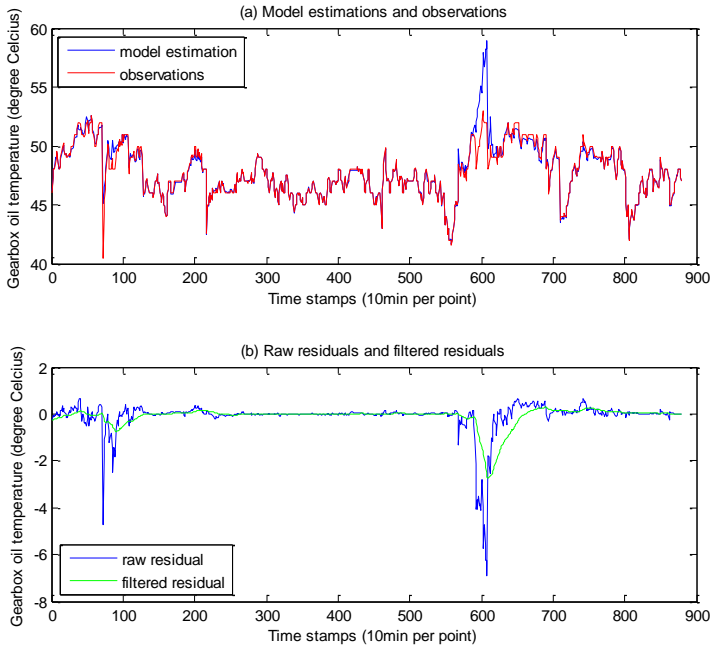


Figure 10: Validation results of T16 for spatial NSET model with normalised matrix and weighted parameter

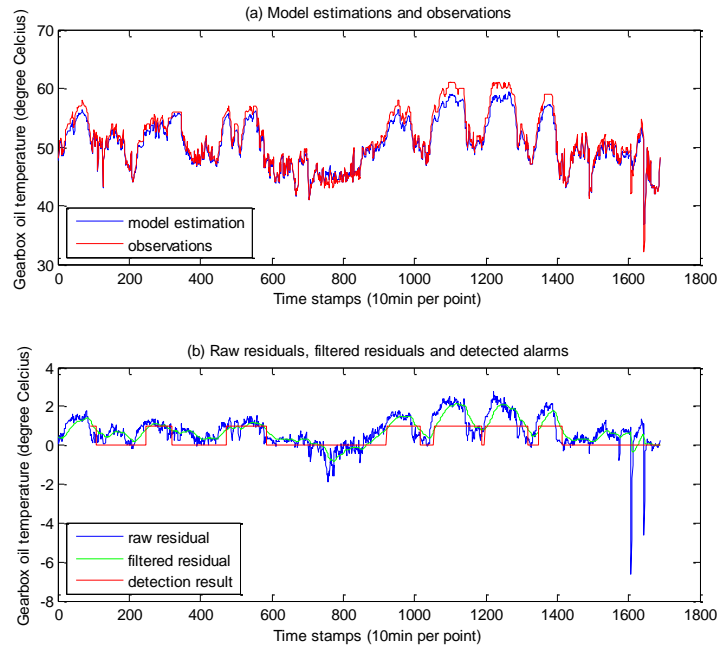


Figure 11: Testing results and anomaly detection of T17 for spatial NSET model with normalised matrix and weighted parameter

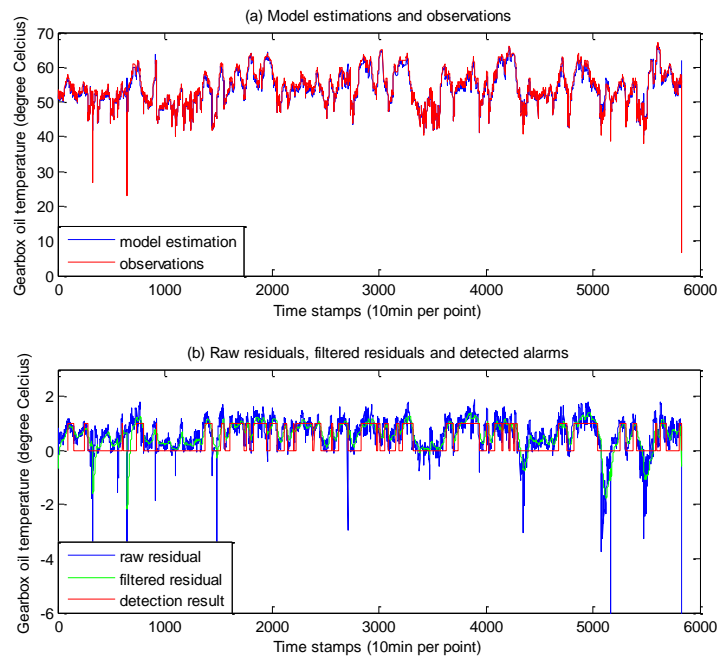


Figure 12: Testing results and anomaly detection of T16 for spatial NSET model with normalised matrix and weighted parameter

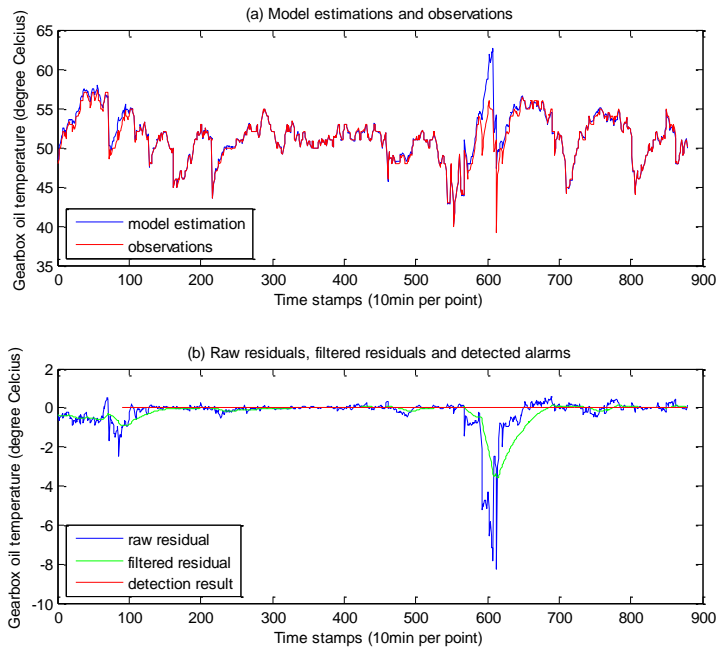


Figure 13: Testing results of healthy T14 for false alarm testing with spatial NSET model with normalised matrix and weighted parameter

# Appendix III

This appendix shows the validation and testing results of modified spatial NSET model with different sub-group sizes.

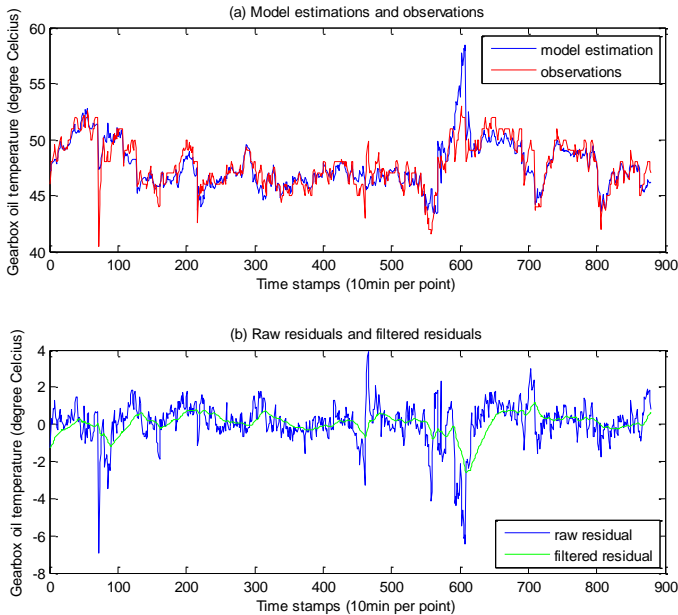


Figure 14: Validation results of T16 for modified spatial NSET with sub-group size of

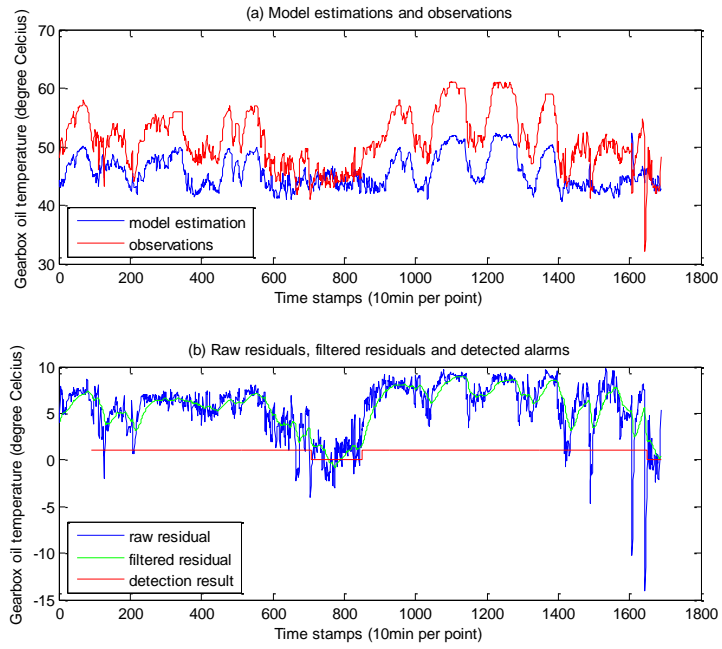


Figure 15: Testing results and anomaly detection of T17 for modified spatial NSET with sub-group size of 10

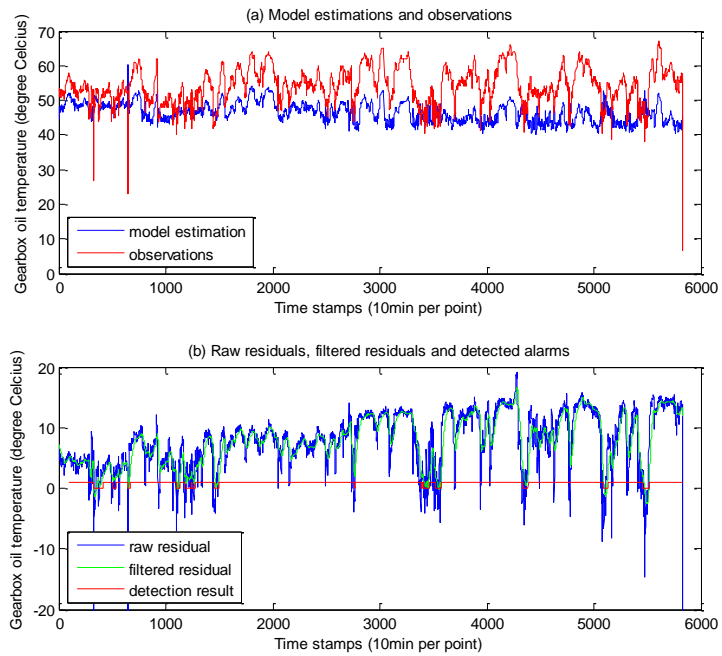


Figure 16: Testing results and anomaly detection of T16 for modified spatial NSET with sub-group size of 10

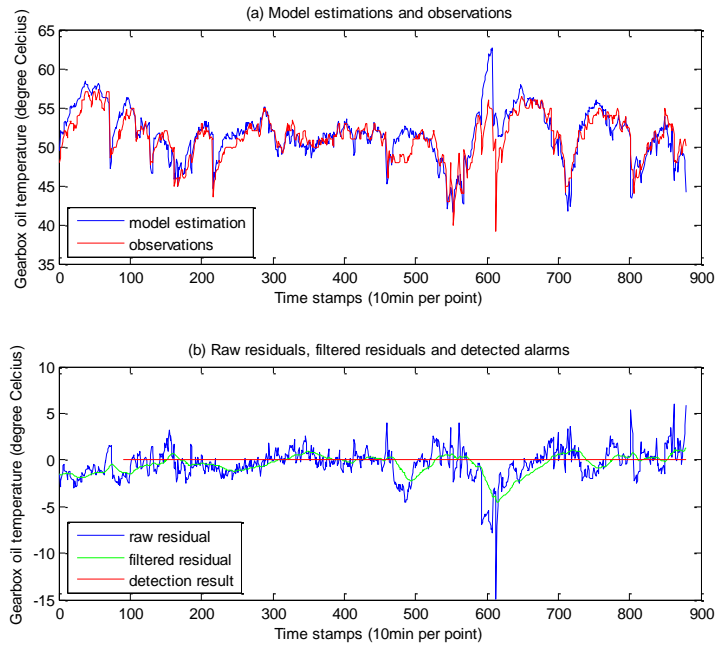


Figure 17: Testing results of healthy T14 for false alarm testing with modified spatial NSET with sub-group size of 10

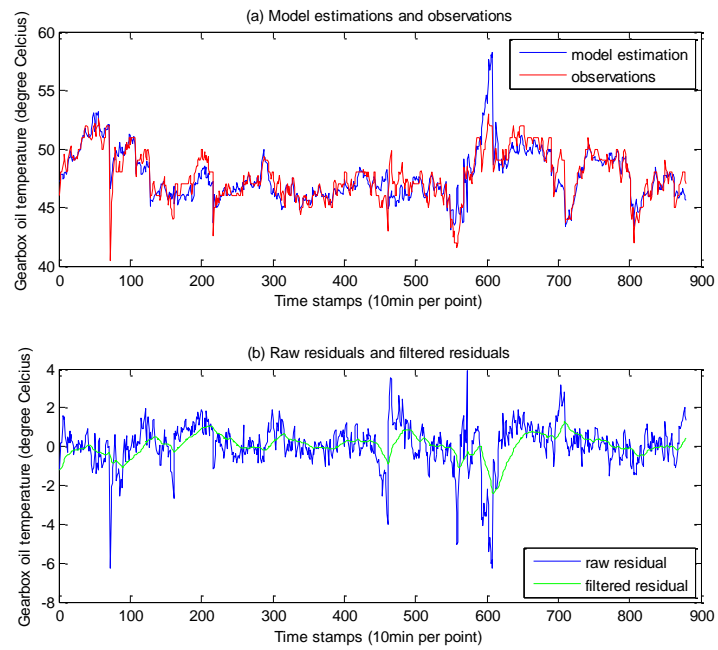


Figure 18: Validation results of T16 for modified spatial NSET with sub-group size of

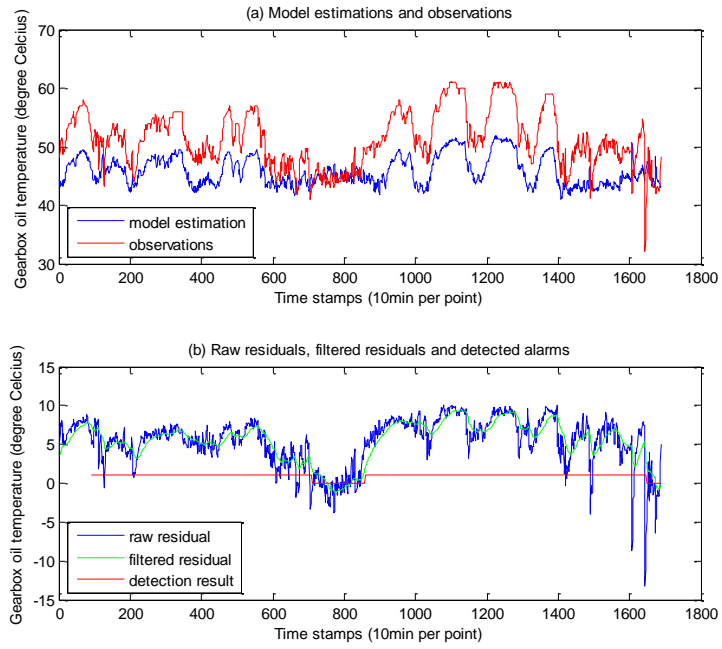


Figure 19: Testing results and anomaly detection of T17 for modified spatial NSET with sub-group size of 15

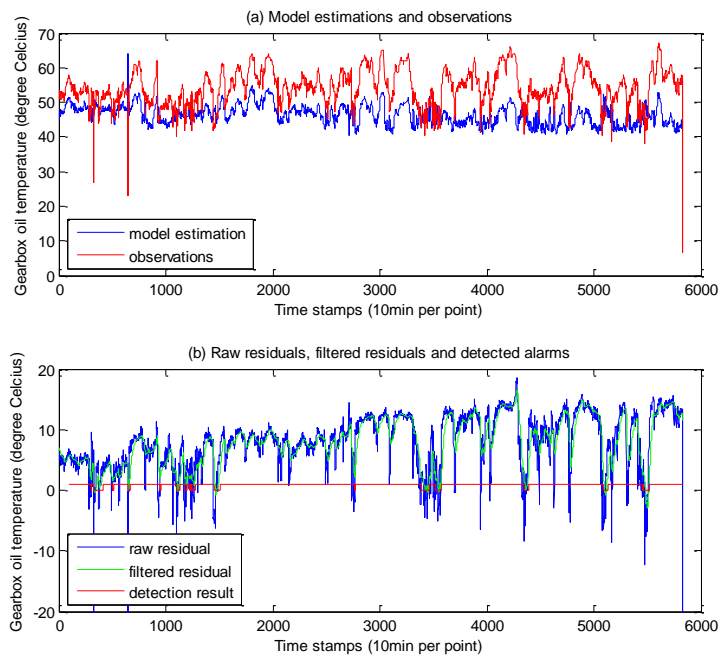


Figure 20: Testing results and anomaly detection of T16 for modified spatial NSET with sub-group size of 15

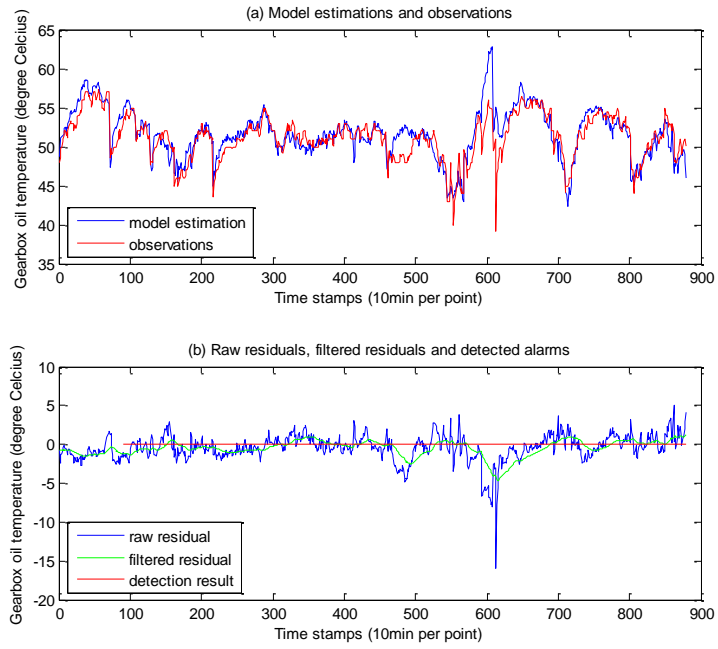


Figure 21: Testing results of healthy T14 for false alarm testing with modified spatial NSET with sub-group size of 15

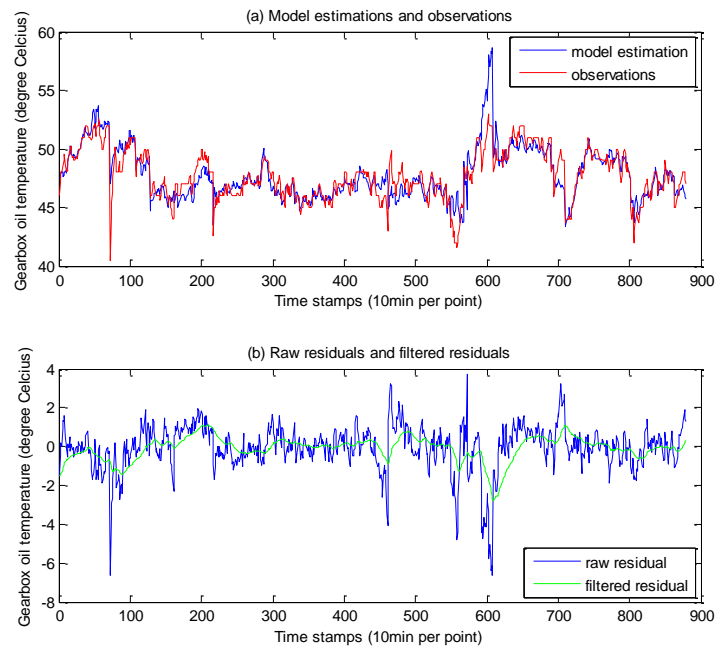


Figure 22: Validation results of T16 for modified spatial NSET with sub-group size of

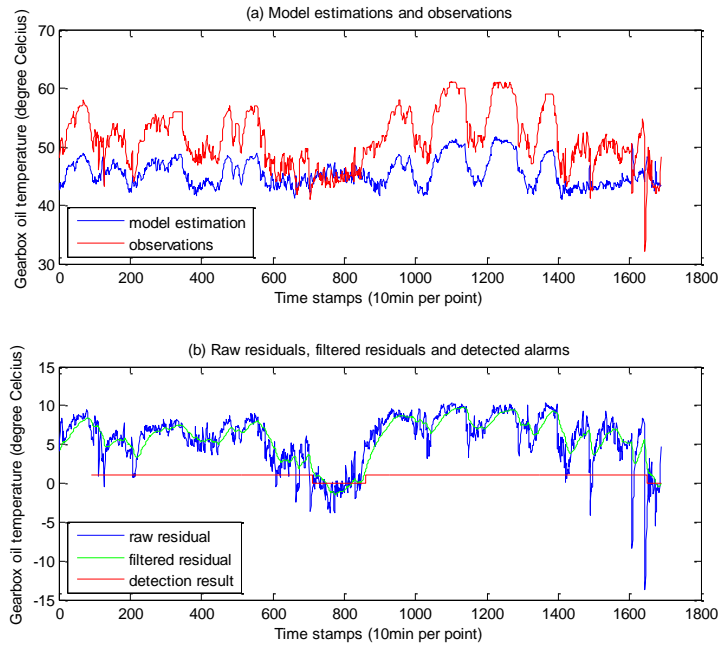


Figure 23: Testing results and anomaly detection of T17 for modified spatial NSET with sub-group size of 17

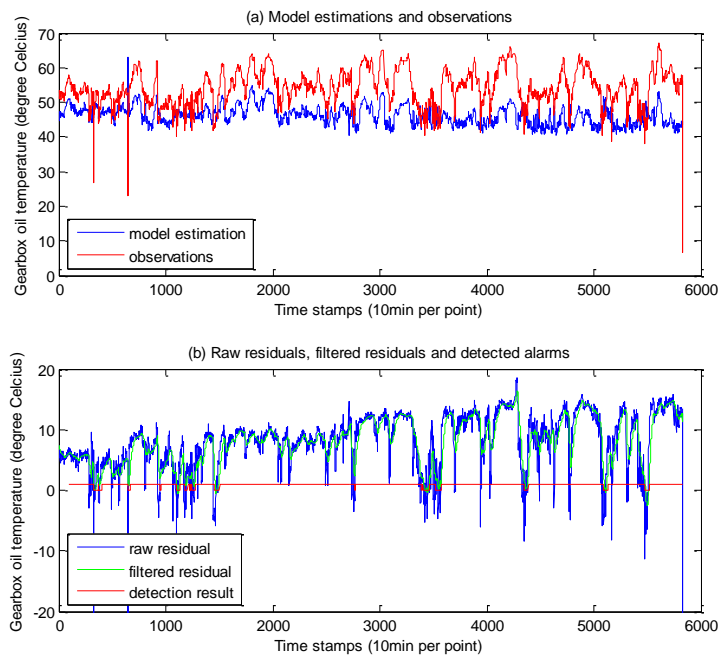


Figure 24: Testing results and anomaly detection of T16 for modified spatial NSET with sub-group size of 17

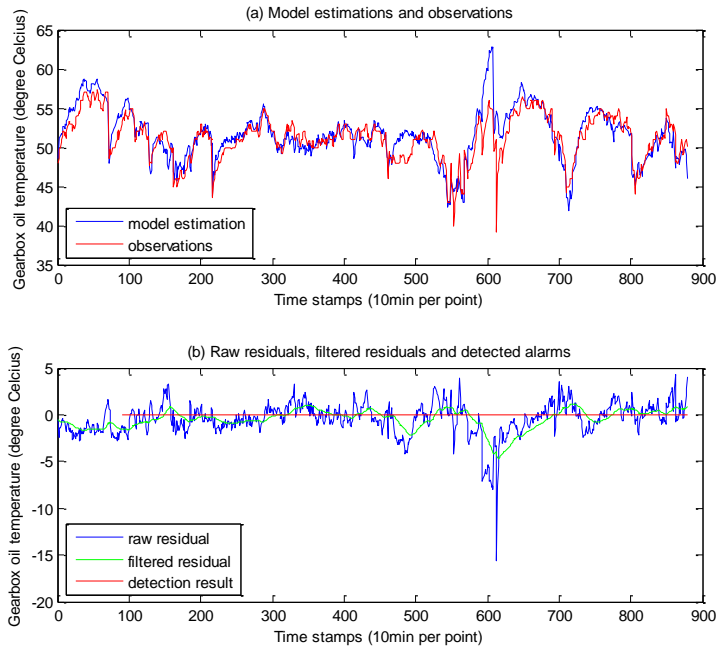


Figure 25: Testing results of healthy T14 for false alarm testing with modified spatial NSET with sub-group size of 17